Università degli Studi di Catania

Dottorato di Ricerca Internazionale in Ingegneria dei Sistemi

XXVIII Ciclo

Felice Maiorca

Innovative Electromechanical Transduction Mechanisms for Piezoelectric Energy harvesting from Vibration: Toward Micro and Nano Electro-Mechanical Systems.

Ph.D. Thesis

Coordinator: Prof. Ing. Luigi Fortuna

Tutor: Prof. Ing. Salvatore Baglio

December 2015

To life!

Abstract

Vibration energy harvesting is one the hottest topics
addressed by a big part of the scientific community. A lot
of transduction mechanisms have been investigated and
designed, based mechanical systems and transduction
principles in order to recover energy coming from
environmental vibrations. In this work, innovative
transduction mechanisms will be described, suitable to
harvesting energy from weak random vibrations, to
rectifying and multiplying voltages avoiding the use of
classic solutions based on diodes. Innovative devices will
be introduced, based on nonlinear mechanical systems and
piezoelectric transducers; analytical models will be
provided and simulation results will be shown. Laboratory
prototypes and experiments will be also described.
Comparisons between simulations and experiments results
will be provided in order to demonstrate the goodness of
the proposed approaches. Finally, MEMS technologies
suitable with piezoelectric energy harvesting, together
with a very simple micro scale prototype, will be

introduced   as   encouraging   elements   for   future
miniaturization   of   the   devices.

Contents

Introduction

One of the main goal of the scientific community is to obtain electric power by exploiting innovative strategies and physical principles in order to satisfy specifications such as a lower environmental impact and a lower cost at equal efficiency, in order to improve the quality of life of the individual and society as a whole. In recent decades the development of new consumer electronic devices (smart phones, tablets, notebooks, smart watches, etc.) has exponentially increased and this phenomenon has made people easier to carry out everyday tasks. Even in industrial and telecommunications, the progresses of electronics have had an important role in terms of simplification of complex systems, increasing the microchips power, reducing the amount of cables for sensors networks (today wireless sensors networks are widespread), etc. In biomedical applications, the improvement of electronics and the miniaturization of the devices have allowed to use sensors and actuators smaller and smaller, used to better diagnosis and to better treat

various types of diseases. A source of energy (electric network or batteries) is always needed in order to guarantee good performances of the electronics devices. The electric network causes strong limitations due sockets and cables; traditional batteries have a finite duration and the rechargeable ones don't solve the problem because of the dependence from the electric network. Finally, the disposal of batteries is critical for environmental protection: despite batteries are special waste, unfortunately, no one usually treats them as such, with negative consequences for health. Energetic issues also involve companies, especially in industrial where electronic equipment are placed everywhere in the plants: in this case, the replacement of batteries can be also difficult for the safety operators. Furthermore, in these cases a reduction of energy consumption can be translated in a significantly growing of earnings.

Energy harvesting is a branch of the science that studies the possibility of collecting energy from alternative sources, making it available for low power electronic devices, in order to extend the batteries life or, ideally, to

avoid their employment. An energy harvesting general processes can be summarized as follows: the first step consists in identifying a clean alternative energy source; the second consists in finding strategies useful to convert it in electric power. Finally, custom devices have to be designed in order to provide electric energy to low power electronic devices. As regards the first step, the world has to be observed critically and physical phenomena have to be studied in order to identify energy sources. Environment is full of mechanical vibrations, usually considered undesired noise. The main characteristics of these signals are similar to the white noise: studies have shown that the most of the power content of environmental vibrations is limited in few hundred hertz in terms of band of frequencies. This power could be collected, stored and used. Once vibrations have been identified as energy source, the main issues to be considered in energy harvesting from vibrations are basically three: the mechanical system, useful to intercept and elastically respond to mechanical vibrations, the transduction mechanism, employed to transform

mechanical energy in electrical and, finally, the mechanism devoted to rectify and store the electrical energy.

A lot of papers can be found in literature where different approaches have been exploited in order to achieve the goal. The most of solutions are based on very simple oscillating systems, such as cantilever beams, as mechanically coupling; piezoelectric materials have been widely employed as best way to transform mechanical energy in electric and, usually, diodes bridges have been employed to rectify voltages. In recent decades, progresses in micro electro mechanical systems (MEMS) have induced researchers to miniaturize vibration energy harvesters, in order to obtain devices having a size comparable with the microelectronic devices. The main issues in the scaling process have been related to increase of the natural frequency of the oscillating systems and to the decrease of the piezoelectric output voltages (typically under the diode's threshold 0.7/0.8 V). This is a bad condition because very small voltages cannot be rectified by using "diodes-based" traditional strategies.

In this work both the mechanical oscillators and the rectifying issues have been addressed, in order to design vibration energy harvesters suitable to the MEMS fabrication. The most of the efforts have been focused on

- investigating nonlinear oscillating mechanical systems in order to replace the linear ones
- design voltage rectifiers based on fully mechanical switch, avoiding the use of diodes.

Innovative linear and nonlinear strategies and prototypes will be shown in details later in this work; they have been designed, developed, prototyped and tested in three years of research activity.

This work is organized in chapters in order to facilitate both the reading and the understanding of the main concepts.

In *Chapter 1* the state of the art in terms of energy harvesting will be discussed, focusing the attention on linear and nonlinear bistable mechanical systems;

transduction strategies and simple traditional voltage rectifiers will be also briefly introduced.

In *Chapter 2 and Chapter 3* new energy harvesters and rectifiers will be described; simulations and experimental results will be shown in order to highlight the goodness of the three years of research activity.

MEMS technologies potentially suitable to miniaturize the developed devices will be introduced in C*hapter 4*, together with two examples. Finally *Conclusions and future trends* will be discussed.

Chapter 1

Energy harvesting: state of the art

Energy harvesting is one of the hottest topics that focus the scientific community's attentions. Many reasons can be discussed to justify the importance of this topic such as costs, environmental impact, safety, etc. Traditional energy production is characterized by the presence of pollutants due to the transformation processes of various substances, with terrible consequences for ambience and human race. Clean energy has to be employed to preserve the planet's health. Nature provides a lot of alternative sources to be exploited in order to obtain clean electrical energy, such as solar [1], wind [2], ocean waves [3], thermal [4], etc. Both in civil and in industrial solar and wind are widely employed and very good results have been obtained in terms of produced energy and pollution reduction. Consumer electronics is also involved in energy consumption and pollutions, especially in the last decades due to the boom of smart phones, tablet, wearable devices, etc. It is easy to note that solutions useful in industrial and

7

civil are usually not suitable to consumer electronics: firstly consumer devices are characterized by very small dimensions and very low power consumption as respect to industrial or civil plants, so it is very difficult to apply solar or wind as energy source, for example. Secondly, consumer electronics devices are usually portable, so batteries are needed in order to guarantee good performances. Likewise, nowadays wireless sensors networks (WSN) are widespread thanks to the improvements in electronics and telecommunications [5]. WSN are very good solutions when the encumbrance of traditional signal and power cables is a strong constrain for the whole of the system. WSN are widely employed in industrial to monitor plants, buildings, machines, processes, etc., and also in civil to implement home automation, to collect and to transfer large sets of measurement data from several points thus realizing distributed measurement systems that require batteries [6] [7]. The main limitation of wireless autonomous nodes is due to the limited battery life time: people have to periodically replace or recharge batteries and this task

could be unsafe when devices are placed in critical positions, for example. Finally, small electronic devices, sensors and actuators, are also employed in bio-medicine and bio-engineering [**8**], for diagnosis and treatment of disorders and diseases, for drugs delivery and so on; the heart bypass is probably the most famous. Modern electro medical devices are often integrated with applications, smart phone and tablet so that the whole of system can help people's goodness [**9**] [**10**]. Even in these cases, battery limited lifetime is a strong limitation and it may be serious inconvenience for the patients. It is easy to understand that batteries are the biggest limitation in electronics for both the limited lifetime and the big dimensions; rechargeable batteries don't solve the problems because of the dependence from the net. Batteries are also special waste and special treatments are needed to dispose of them [**11**], but people usually don't care, with general negative consequences for health and for ambient. As introduced at the beginning, energy harvesting is the branch of science that deals the individuation of alternative sources and strategies useful to

obtain electrical energy [**12**]. Environmental energy sources are abundant and have different characteristics, so that energy harvesting can be divided in two sections, macro and micro energy harvesting, according to the dimension of the devices and to the electric power generated: these characteristics make different energy harvesters suitable to different applications. Macro-energy harvesting includes big dimension systems, such as solar and wind plants; big dimension usually corresponds to big energy (MW), so that macro-energy harvesting is usually employed both in industrial and in domestic. Similarly, micro energy harvesting is referred to very small devices and very small voltages and power (<mW), suitable to micro and nano electronic devices (sensors, actuators, etc.) characterized by very low power consumption: suitable energy sources have to be investigated, such as mechanical vibrations [**13**]. Mechanical vibrations can be considered as a possible power source suitable to micro energy harvesting systems [**14**]. Vibrations are uncontrolled oscillations that effect the entire environment with characteristics of band limited white noise (few

hundred hertz). Vibration energy harvesting has focused the attention of a very large part of scientific community and very interesting results can be found in literature. In fact, unlike sun or wind, vibrations are always present, rich of energy and abundant in ambient. Several solutions have been developed in order to recover energy from environmental vibrations; once fixed the vibrational input, a lot of conversion mechanisms have been explored and various efficiencies have been detected in relation to the conversion strategy [**15**]. In general, a vibration energy harvester is composed of three main blocks: the first is a mechanical structure, to sense and carry mechanical energy, the second is a transduction mechanism, to convert mechanical energy to sense and carry mechanical energy, the second is a transduction mechanism, to convert mechanical energy to electrical energy, and the third block is devoted to adapt voltage signals to the load or to the end user. The mechanical structure is usually a mechanical oscillator that moves in response to external vibrational input; the transduction mechanism, that provides to transform mechanical energy in electric, can be
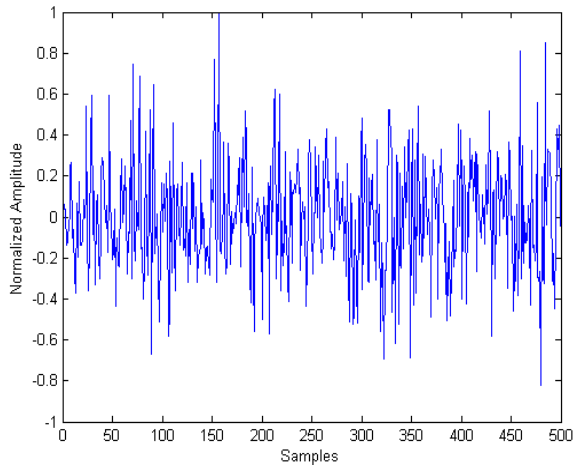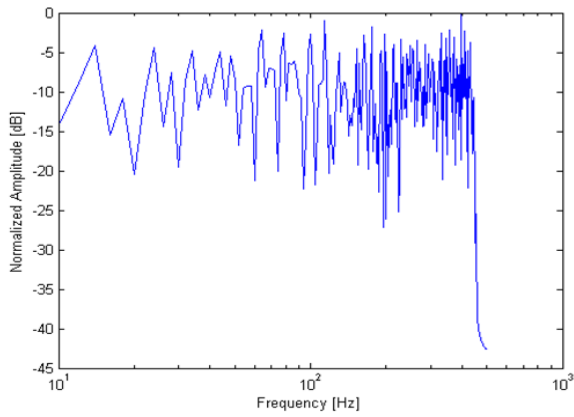
Fig. 1 - Example of band limited white noise.

Fig. 2 - Frequency spectrum of the signal in Fig.1.

Fig. 3 - General schema for vibration energy harvesting.

electrostatic [**16**], electromagnetic [**17**] or piezoelectric [**18**], while the energy management block can be composed of voltage rectifiers and a components for energy storage. In literature a lot of papers can be easily found, where vibration energy harvesters based on electrostatic or electromagnetic transduction strategies are investigated. However, a lot of scientist have focused the attention on transduction strategies based on oscillating mechanical structures (linear and nonlinear) and piezoelectric materials [**12**]. Environmental vibrational noise has to be coupled with a mechanical structure that oscillates in response to external forces; as consequence, the piezoelectric element deforms, allowing the conversion of energy from mechanical to electrical. Finally, the energy harvested has to be managed and stored for the future use [**19**].

1.1. Oscillating structures

As introduced, one of the fundamental components in an energy harvesting system is the mechanical system that elastically responds to external vibrations. A lot of mechanical structures have been designed, studied, tested and proposed by the scientific community, as it can be found in literature. The mechanical oscillating structures for vibration energy harvesting can be divided in two main classes: linear and nonlinear. Linear structures are easy to implement: a simple cantilever beam represents a good example. The main limitation of linear systems is due to the resonant behavior: if the frequency of the external input is very close to the mechanical resonance (strictly related to the material and the geometric characteristics), the system provides very good performances otherwise, the most of the mechanical input energy is lost and the efficiency drastically decreased. This is the most common case especially when environmental vibrations are considered as mechanical energy source: in fact, environmental vibrations have a wide spectrum (usually

14

limited to few hundred hertz) and only the energy related to a very small range of frequency (around the mechanical resonance of the linear system) can be harvested. The most of the energy is lost. Furthermore, the miniaturization of devices implies the increase of the mechanical resonance frequency so it is very difficult to obtain a good coupling between the vibrational source and the mechanical oscillating system. On the contrary, nonlinear systems are more difficult to study and to implement as respect to the linear ones, but they show very interesting characteristics in terms of wide band frequency response, so they are very suitable to be employed in vibration energy harvesting, especially in the real cases when the input frequency of vibration is random or unknown. The simplest nonlinear mechanical systems are the bi-stable systems: they have two stable and one unstable equilibrium point, with a double-well potential function. Bi-stable systems have a wide band frequency response and this characteristic make them suitable for energy harvesting from random vibrations. Details and references of linear and nonlinear
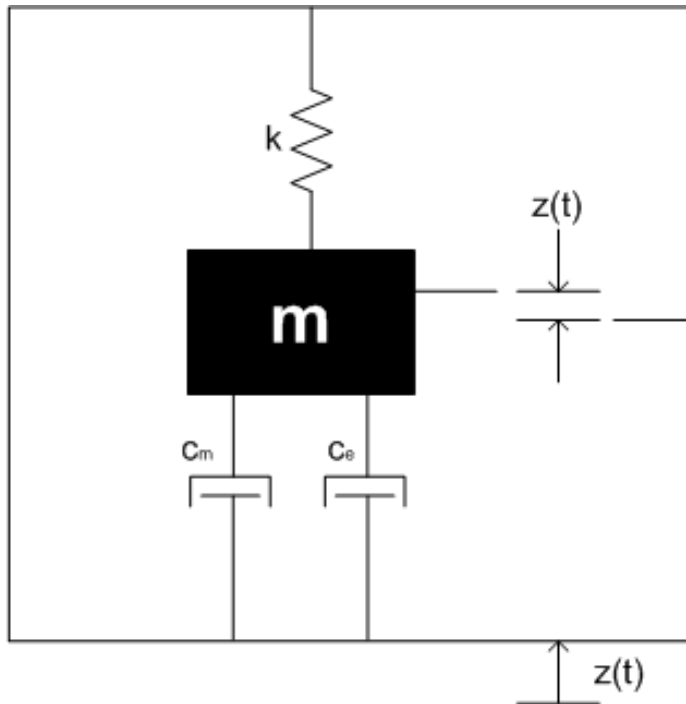
Fig. 4 - Schematization of a mass spring damper system

bi-stable systems will be provided in the next two paragraph.

1.1.1 Linear oscillating structures

Linear oscillator is the simplest mechanical structure employed in vibration energy harvesting. As known, it can be easily modeled as a typical second order mass spring damper system (Fig. 4). Referring the Fig. 4, a mass *m* is connected with a spring having *k* elastic constant, c_m and c_e take into account of the energy losses due to friction, electric phenomena due to transduction, etc.

y(t) is the external vibrational input and *z(t)* is the displacement of the mass due to *y(t)*. The system can be described using a second order equation as follows:

$$m\ddot{z} + d\dot{z} + kz = -m\ddot{y} \tag{1.1}$$

For a sinusoidal input like $y(t) = Y \sin(\omega t)$, the solution can be expressed as follows:

$$z(t) = \frac{\omega^2}{\sqrt{\left(\frac{k}{m} - \omega^2\right)^2 + \left(\frac{(c_m + c_e)\omega}{m}\right)^2}} Y \sin(\omega t - \varphi) \tag{1.2}$$

Where $\varphi = arctan\left(\frac{(c_m + c_e)\omega}{k - \omega^2 m}\right)$ and $\omega_n = \sqrt{\frac{k}{m}}$ .The amount of power extracted from the mechanical coupling system, equal to the power that the system is able to convert into electricity, can be expressed as
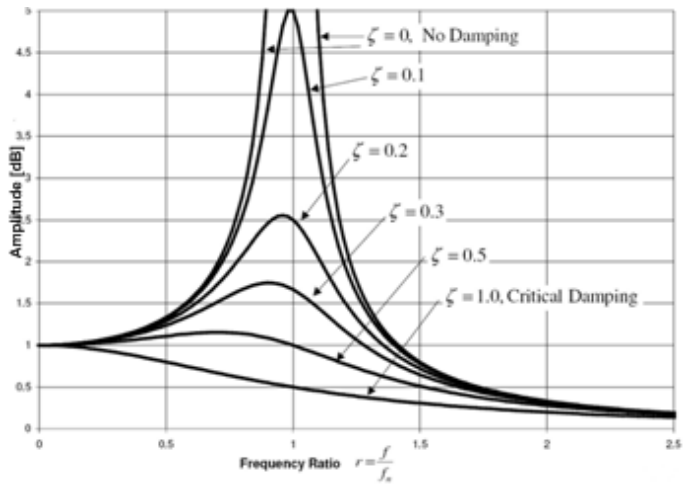
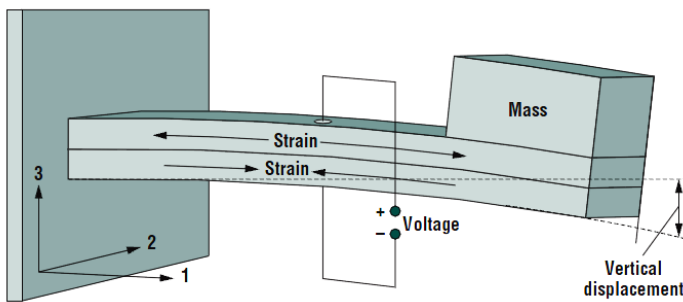**Fig. 5 - Normalized frequency spectrum of a linear structure for different values of the damping coefficient**

Fig. 6 - Piezoelectric linear cantilever beam with proof mass on the free tip.

$$P = \frac{1}{2} c_e \dot{z}^2 \tag{1.3}$$

The module of P is

$$|P| = \frac{m \zeta_e \omega_n \omega^2 \left(\frac{\omega}{\omega_n}\right)^3 Y^2}{\left(2\zeta_T \frac{\omega}{\omega_n}\right)^2 + \left(1 - \left(\frac{\omega}{\omega_n}\right)^2\right)^2} \tag{1.4}$$

where $\zeta_e = \frac{c_e}{2m\omega_n}$ is the electrical damping, $\zeta_T = \zeta_e + \zeta_m = \frac{c_e}{2m\omega_n} + \frac{c_m}{2m\omega_n}$ is the total damping that includes the mechanical, too.

When the frequency of the input signal is equal to the natural frequency of the mechanical system, the maximum electrical output power is produced:

$$|P| = \frac{m \zeta_e \omega^3 Y^2}{4\zeta_T^2} \tag{1.5}$$

If $A = \omega^2 Y$, then $|P| = \frac{m \zeta_e A^2}{4\omega\zeta_T^2}$ \hfill (1.6)

So, the output power is directly proportional to the mass and inversely proportional to the frequency and the damping. Since ζ_e depends on the employed transduction mechanism, it is very important to good design the mechanical system. Furthermore, the mechanical damping coefficient ζ_m has to be minimized in order to increase the
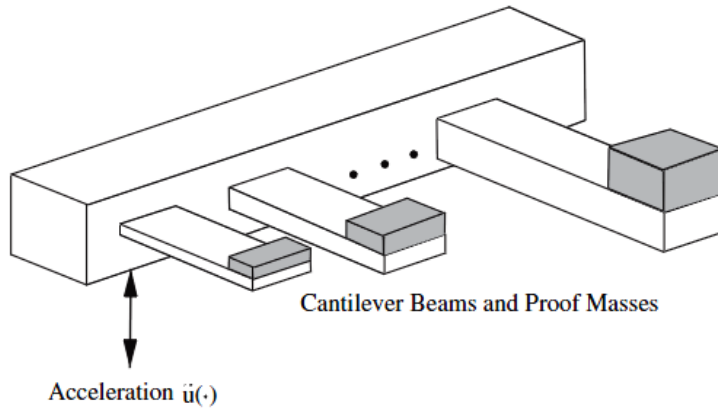
19

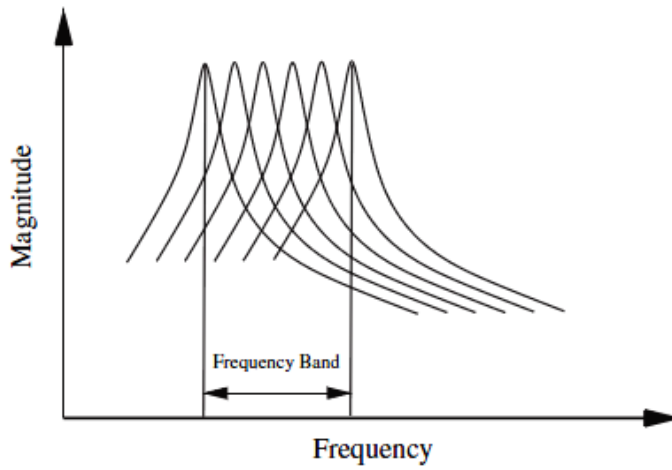**Fig. 7 - Shahruz's mechanical band-pass filter schematization**

Fig. 8 - General frequency response of a system as in Fig. 7

quality factor

$$Q = \frac{1}{2\zeta_m} \tag{1.7}$$

If ζ_m increases, the quality factor Q and the gain decrease a lot, while the band has a very low increase (Fig. 5). The system should have a large mass.

In general, linear systems are easy to study, design and realize; for example, cantilever beam is the simplest linear system both for macro and micro scale prototyping. The biggest limitation of linear systems is related to the frequency selectivity: as discussed above, the maximum power output is obtained when the frequency of the external input is very close (ideally equal) to the natural frequency of the mechanical system while the energy related to all the other frequencies is lost. Usually, the environmental vibration frequency cannot be predicted and it is not easy to design and realize a priori mechanical structures having a suitable natural frequency: this is the biggest issue of the linear mechanical oscillators. In literature, several solutions can be found having as main goal to overcome this limitation.
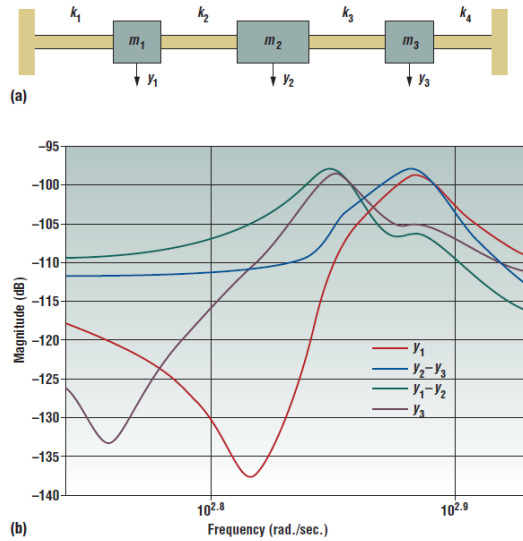
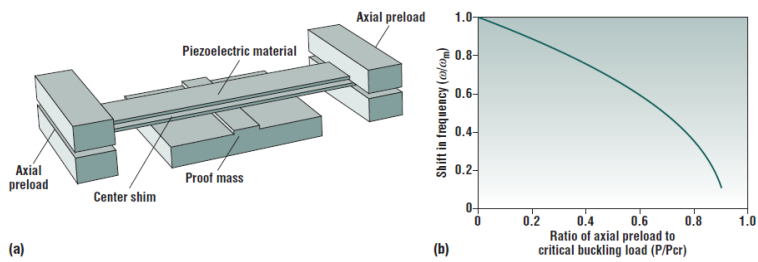**Fig. 9 - Roundy's solution schematization and simulations results.**

Fig. 10 - Mossi's solution schematization

For example, SM Shahruz [20] has designed a big device composed of an array of cantilever with different masses, geometries and, in consequence, different natural frequencies (Fig. 7 and Fig. 8). The whole of the device, also called mechanical band pass filter, was able to work wideband but it was characterized by very big dimension and costs, both in macro and in micros scale.

In [21] Roundy has investigated a solution based on the connection of *N* linear mass spring damper systems (Fig. 9). At least one of the mass spring damper systems resonates and spectra overlap in this configuration. Simulations results are shown in Fig. 9.

Tuning the resonance frequency is another way to overcome the linear system limitations: tuning can be active or passive [22]. Active tuning is not convenient in terms of power, as Roundy e Zhang have shown in 2005 [23]. As regards passive tuning, in 2005 Mossi has proposed a solution based on the variation of the axial preload (Fig. 10) in order to obtain a resonance frequency variation in a cantilever beam [24].
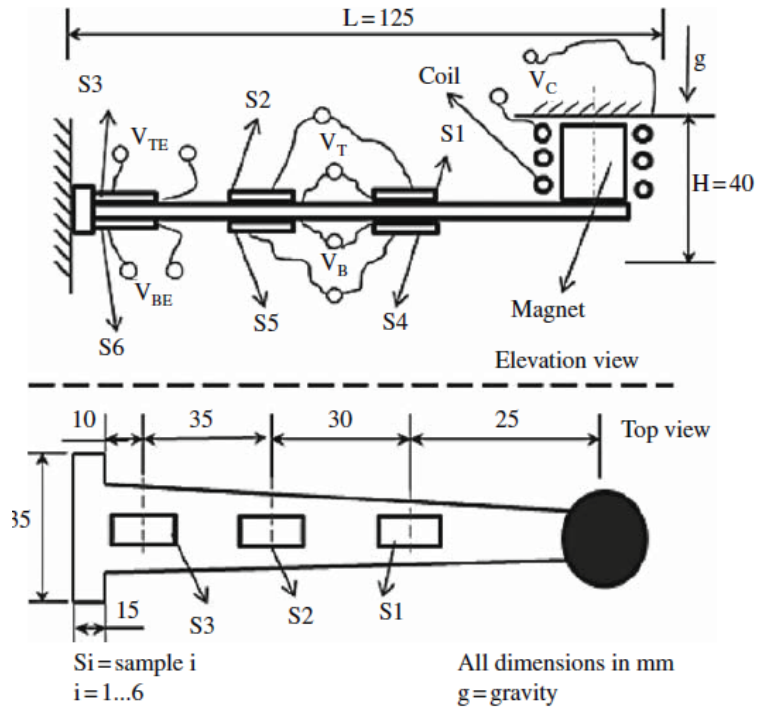
Fig. 11 - Tadesse's solution schematization.

In 2009 Tadesse proposed a solution based on a linear cantilever beam and two transduction mechanism at the same time (piezoelectric and electromagnetic) in order to increase the energy harvested [25]. Piezoelectric transduction was implemented by placing a piezoelectric layer in the maximum deformation area of the cantilever, while electromagnetic was obtained by using permanent magnet and coils (Fig. 11). Summarizing, in the last years both experiments and simulation have demonstrated that linear systems do not provide good performance in terms of vibration energy harvesting in the most of real scenarios. These are the main reasons why scientific community has focused the attention on nonlinear systems.
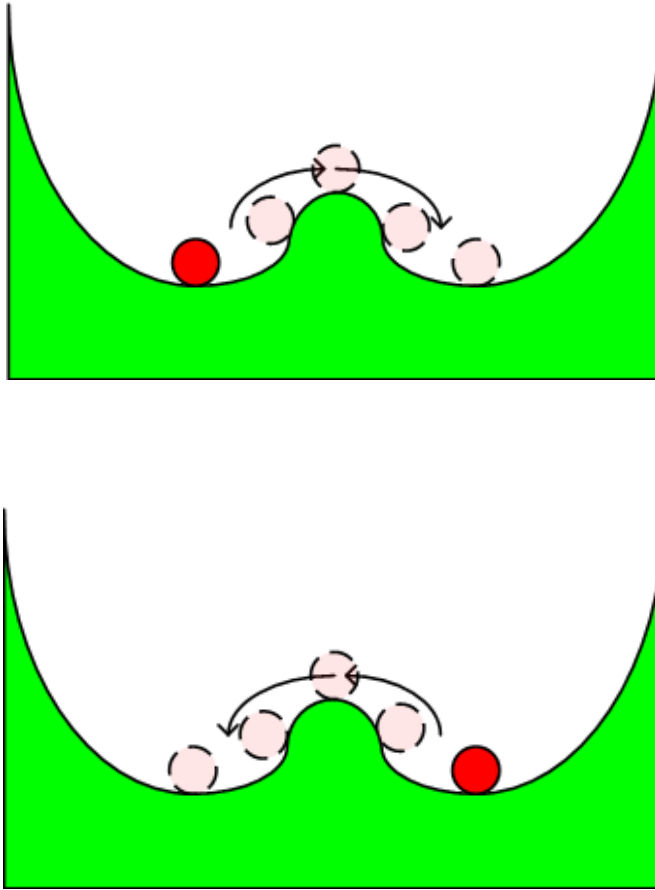
Fig. 12 - Bistable behavior.

1.1.2. Nonlinear oscillating structures

Nonlinear systems show good performances in environmental vibration energy harvesting, especially in terms of frequency response. Unlike linear systems, nonlinears have a large band frequency suitable with environmental random vibrations having a spectrum of few hundred hertz. In particular, scientific community has focused the attention on nonlinear bistable mechanical systems for energy harvesting applications. Bistable systems have two stable and one unstable equilibrium states and a double-well potential (Fig. 12). At rest the system lies in one of the two stable states; when a weak external perturbation occurs the system oscillates around the stable state instead, when the perturbation's energy is larger than the potential threshold, the system overcomes it and reach the other stable equilibrium state [26]. The simplest way to analytically model the bistability [27] [28] is a fourth-degree polynomial as follows:

$$U(x) = -\alpha x^2 + \beta x^4, \qquad\qquad (1.8)$$
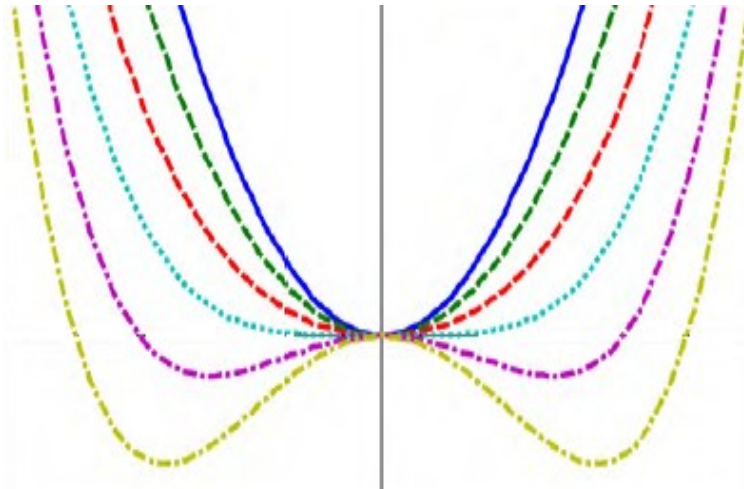
with $\alpha > 0, \beta > 0$ (Fig. 13).

27

Fig. 13 - Some *U(x)* shapes, changing α, β values.
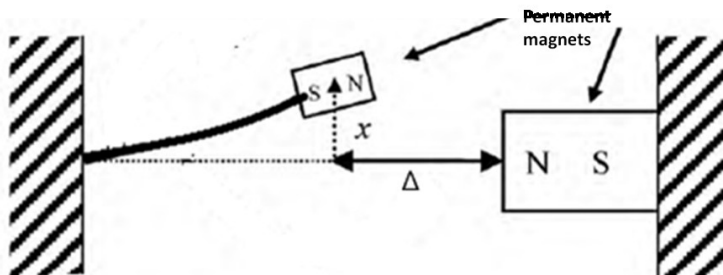

Fig. 14 - Example of magnetically induced bistable behavior.

In mechanical oscillating systems bistability can be obtained both mechanically and by introducing different kind of forces, for example magnetic force.

Consider a cantilever beam with a permanent magnet at the free tip and place it in front of a second fixed permanent magnet in opposite polarization [**29**] [**30**]: the potential of the whole of the system is double-well and a repulsive force due to the magnets pushes the free tip toward a stable equilibrium point (Fig. 14).

If an external force occurs, sufficient to overcome the potential threshold, the free tip of the cantilever moves to the other stable equilibrium point.

The distance between the two stable equilibrium point and the potential threshold are related to the magnetic force, to the distance between magnets and to the equivalent stiffness of the cantilever beam.

In Fig. 15 both linear and nonlinear behaviors are shown.

In Fig. 16 spectra are shown in the two cases just introduced, showing that the nonlinear system can be better employed in environmental vibration energy harvesting applications.
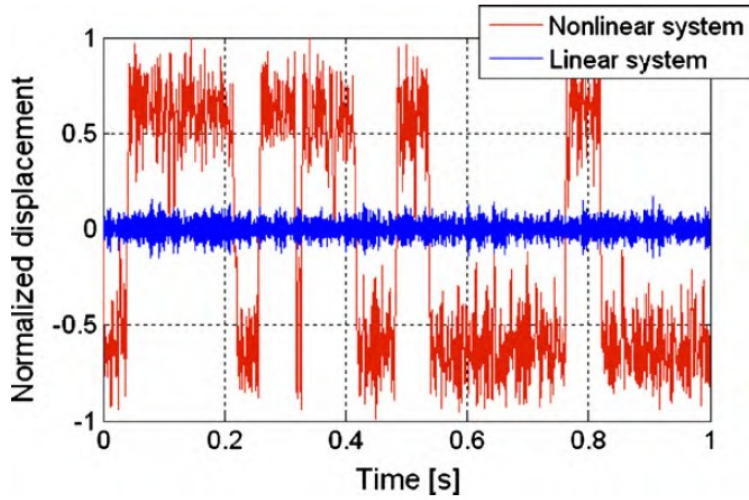
Fig. 15 - Linear and nonlinear (bistable) time domain behaviors (normalized).
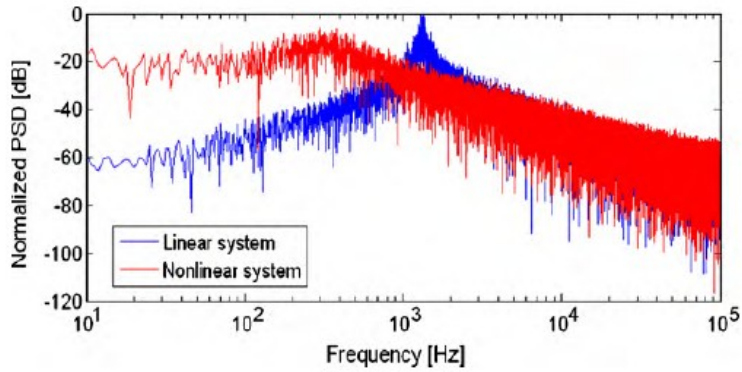

Fig. 16 - Linear and nonlinear (bistable) systems frequency spectra (normalized).

1.2. Transduction mechanisms

Transduction means conversion of any kind of energy in a different form. In engineering transduction also refers to the conversion of signals, and a transducers is a particular device that implements this function. According to the input and output signals, electro-mechanical, electro-optical, etc., a transducer can be defined. Usually, in electric and electronic systems, the output of a transducer is voltage or current. As regards vibration energy harvesting, the focus is on devices with mechanical input and electrical output. In vibration energy harvesting applications three main classes of transducers can be identified, according to the transduction principle: electrostatic, electromagnetic and piezoelectric.

1.2.1. Electrostatic transduction

Electrostatic transduction mechanism is based on the variation of a capacitor's capacitance due to the relative displacement of the plates. For example, consider the capacitance of a two parallel plane plates capacitor
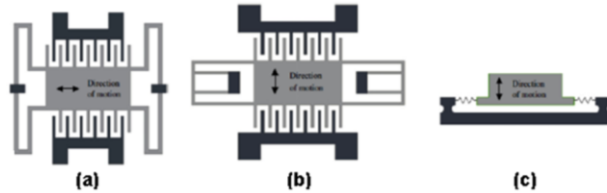
Fig. 17 - Examples of electrostatic transduction mechanisms in MEMS.
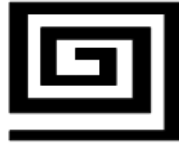
Fig. 18 - Example of planar coil layout in MEMS.

$$C = \varepsilon\frac{A}{d} = \frac{Q}{V} \qquad\qquad (1.9)$$

where ε is the permittivity of the dielectric, d is the distance between the plates, Q is the charge and V is the electric potential difference and A is the area of the single plate. The energy stored can be expressed as

$$E = \frac{1}{2}QV = \frac{1}{2}CV^2 = \frac{1}{2}\frac{Q^2}{C} \qquad\qquad (1.10)$$

The interaction force between the plates, when there is a relative motion, can be expressed as energy's first

32

derivatives with respect to the displacement while the recovered energy can be expressed as work done against the electrostatic force; energy can be expressed in two ways: as increasing voltage, when capacitance decreases and the charge is constant, or as a flow charge when capacitance decreases and the voltage is constant. In general, electrostatic transduction is widespread in MEMS (**Errore. L'origine riferimento non è stata trovata.**), especially in interdigitated configurations, because of the advantages due to the scaling. The main issues of the electrostatic transducers are related to the needs to be power supplied and to the small output voltages and currents.

1.2.2. Electromagnetic transduction

The electromagnetic transducers are based on the Faraday-Neumann-Lenz principle

$$V = -N\frac{d\Phi}{dt} \tag{1.11}$$

where N is the number of the coil's turns, Φ represents the flux concatenated with the single coil, V is the induced

electromotive force. The flux can be expressed as a function of the magnetic field B and area A_i of each coil

$$\Phi = \sum_{i=1}^{N} \int B \cdot dA \qquad (1.12)$$

(the integral is extended to each A_i), so the output energy is proportional to the number of coils, to the magnetic field B and to the relative velocity between the parts of the system. In integrated technology and in MEMS, robust transducers can be fabricated, based on planar coils (**Errore. L'origine riferimento non è stata trovata.**) and permanent magnets that provide the constant magnetic field; very high currents and small voltages can be easily obtained by using this transduction strategy. However in general, planar coils and permanent magnets could be negative affect the performances of the integrated systems as a whole.

1.2.3. Piezoelectric transduction

Some materials exhibit a potential difference when a deformation occurs and vice versa deform when an

electric filed is applied: this capacity is defined piezoelectricity and materials are called piezoelectrics.

The piezoelectric effect is due to the displacement of electric charges in response to the related deformation of the material: because of the pressure, the electric charges move to the ends of the material so a piezoelectric current can be read by connecting two conductors with the ends (copper wires, for example) and by closing the circuit. Vice versa, the material expands or contracts in response by applying a potential difference.

A lot of piezoelectric materials can be found in nature, such as quartz and galena; in energy harvesting application the piezoelectric ceramics (in particular the Lead Zirconate Titanate, better known as PZT) play a very important role.

The elementary cell of PZT crystal is shown in Fig. 20.

Lead atoms are placed at the corners of the unit cell and the atoms of oxygen to the centers of the faces. Above the Curie temperature, the lattice is cubic and consists of oxygen octahedrons regularly arranged with an ion titanium or zirconium at the center. Below the Curie
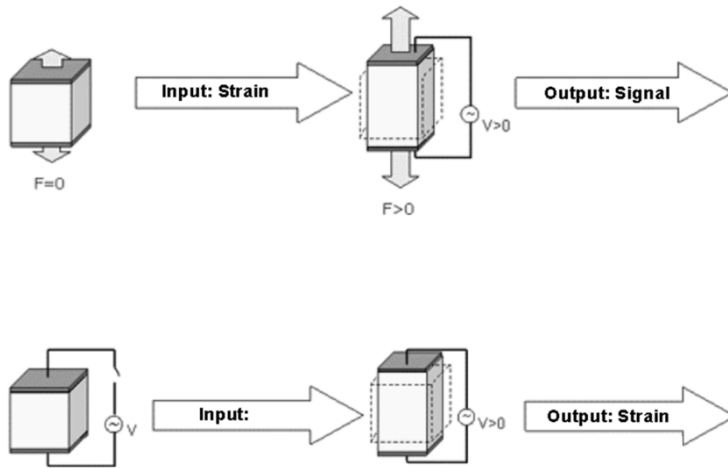
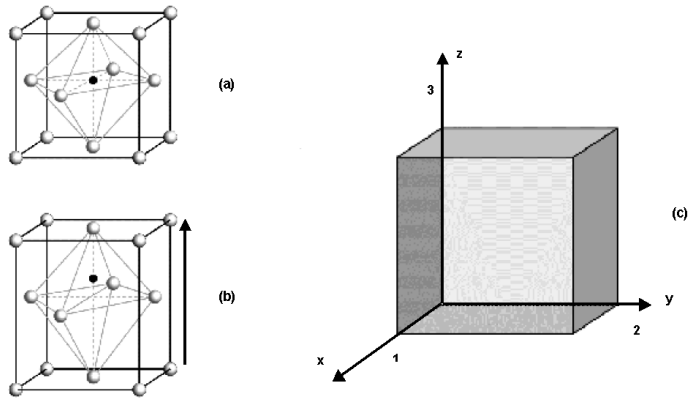**Fig. 19 - Direct and inverse piezoelectric effects.**

Fig. 20 - Elementary cell of PZT crystal: (a) unpolarized, (b) polarized, (c) directions and reference system.

36
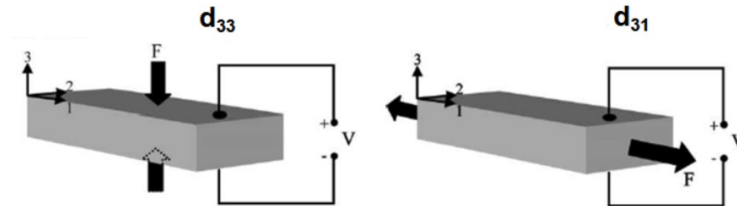
Fig. 21 - *d₃₃* and *d₃₁* working principles.

temperature, the lattice structure is reordered in a mixture of tetragonal and rhombohedral crystals and the ion titanium or zirconium moves from the center position to one of the permitted directions.

Because of this phase transformation with atomic displacements of about 0.1 Å, it takes place a separation of charge that produces an electric dipole with a single axis of symmetry. Generally, the behavior of piezoelectric materials is strongly anisotropic. The characteristic parameters of this kind of material are the piezoelectric constants d_{ij} [C / N] and the coupling factors k_{ij} (the subscripts *i* and *j* can assume values *1,2* or *3* and represent the axes *x, y* and **z** of a Cartesian orthogonal reference system integral with the crystal of material, Fig. 20).

37

Piezoelectric constants are defined as ratio between the short circuit density charge in the i direction and the applied stress in the j direction. Piezoelectric materials can work in bending mode and in compression mode; in both cases the most common configurations are d_{33} and d_{31}.

Coupling factors are also defined as ratio between the output electrical energy in i direction and the input mechanical energy in j direction and give information about the conversion efficiency.

An useful way to analytically model the piezoelectric transduction is the following:

$$\dot{V} = k_{pzt}\dot{s} - \Gamma V \qquad (1.13)$$

Where V and $\dot{V}$ are the piezoelectric output voltage and its first derivate, $\dot{s}$ is the first derivate of the strain, k_{pzt} takes into account of both the geometrical and the intrinsic characteristics of the piezoelectric layer and, finally, Γ is elated to the time constant of the whole of the considered system (including the load).

Chapter 2
Nonlinear bistable energy harvesters

In this chapter innovative solutions for vibration energy harvesting, developed during three years of research activity, are presented. All the systems are based on cantilever beams that oscillate in response to external vibrations; the nonlinear behavior has been always induced by using permanent magnets placed on the cantilevers' tips in repulsive configuration, in order to obtain the double-well potential. Piezoelectric transduction strategy has been used, when considerations in terms of voltages and power produced have been carried out.

Important results of the research activity have been obtained step by step in the three last years. The starting point was the study of a simple bistable mechanical system composed of two magnetically coupled cantilevers, in order to evaluate characteristics in terms of dynamics and frequency response when random vibrational input, emulating the environmental noise, occurs. A macro-scale

laboratory prototype have been fabricated and experiments have been carried out; at the same time, an analytical model has been obtained by studying the physical phenomena involved and by introducing some approximations. Simulations have been carried out and compared with experimental results, confirming the goodness of the proposed approach. The geometry of the prototype have been designed looking to possibility of down scaling the system in the future exploiting MEMS technologies, so magnets have been placed in repulsive configuration with parallel magnetization: this will be more clear by reading forward in this chapter. The preliminary results have encouraged to deeply study the phenomena and to enlarge the horizon by introducing the piezoelectric transduction mechanism, the possibility to harvest energy from vibrations coming from different directions, the possibility to create an array of nonlinear bistable cantilevers, and so on. A lot of prototypal devices have been studied, fabricated, modeled and tested, each one having a specific application context. After the introduction of the magnetically coupled dual cantilever, a

system composed of an array of four bistable cantilevers with different masses will be described as possible energy source for autonomous sensors nodes. Then, a general analytical model suitable to all the introduced systems will be provided together to a comparison in terms of performances and output power. After that, the analysis of a two dimensional energy harvester will be reported, useful to scavenge energy from vibrations in different directions and, finally, a tristable system will be introduced as a possible solution to decrease the potential barrier in several magnetically coupled nonlinear mechanical systems.

2.1. Magnetically coupled cantilevers with antiphase bistable behavior for kinetic energy harvesting

Several strategies have been proposed to address the issue of recovering energy from low-frequency and large-bandwidth vibrations [31]. Efficient solutions have been reported based on bistable oscillators [32] [30] where bistability is obtained by exploiting the repulsive force produced by two facing permanent magnets (see Fig. 22a):
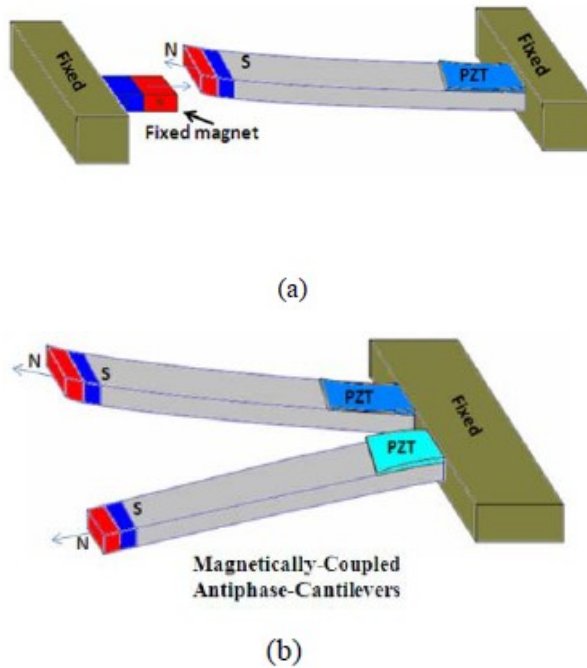
Fig. 22 - (a) Bistable mechanism, based on opposing magnets, tipically used to increase the bandwidth response of the harvester; (b) the device proposed based on Magnetically-Coupled Antiphase-Cantilevers.

one placed on the tip of a cantilever while the other is placed on the device frame. Implementations of this strategy on MEMS devices have been also presented [**30**] [**33**]. In view of fully integrated bistable MEMS harvesters it must be considered that the realization of very close

magnets having opposite orientations is challenging, it is then easier to work with a single orientation of magnetization. The approach presented here is based on the use of two parallel cantilevers each one carrying a magnet on its tip, the two magnets will have identical magnetization (see Fig. 22b). The device is excited by the inertial force *F(t)* coming from environmental vibrations that will act together with the nonlinear elastic force due to the magnetic interaction between the two cantilevers.

It results into a bistable behavior for each beam; moreover both cantilevers will behave in antiphase one respect to the other. The magnetically coupled system has been modeled considering two mass (*m*)-spring (*k*)-damper (*d*) equations. The magnetic interaction has been modeled via two nonlinear terms:

- $k_{nl} = \alpha - \beta x_i^2$, correlated with the displacement of the oscillator (x_i, *i = 1,2*);

- $k_{nlc} = \gamma - \delta(x_2 - x_1)^2$, that includes the relative displacement between the cantilevers.

Furthermore a magnetic damping coefficient (d_m) has been also considered:
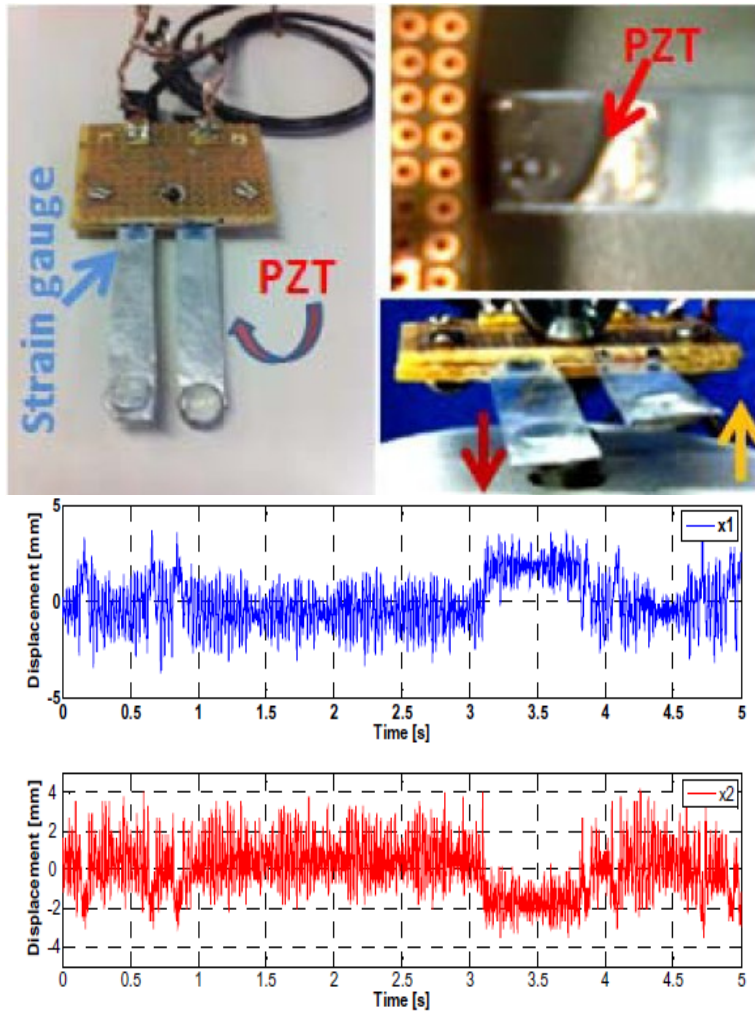
43

Fig. 23 - (a) The experimental prototype developed. (b) tip-displacement of both cantilevers.

$$\begin{cases} m\ddot{x}_1 = -d\dot{x}_1 - kx_1 + k_{nl}x_1 + k_{nlc}(x_2 - x_1) + d_m(\dot{x}_2 - \dot{x}_1) + F(t) \\ m\ddot{x}_2 = -d\dot{x}_2 - kx_2 + k_{nl}x_2 - k_{nlc}(x_2 - x_1) - d_m(\dot{x}_2 - \dot{x}_1) + F(t) \end{cases}$$

$$(2.1)$$

The shape of the two double-well potentials is related with the terms α, β, γ, δ estimated through measures.

The prototype (see Fig. 23a) used to validate the mechanical principle is composed of two aluminum beams having a length of 40mm and a width of 7.5mm. Two permanent magnets with parallel polarities have been used to create the two stables states as shown in on the right. Both magnetic structures have been fixed on the cantilever tips and the distance between the two beams has been fixed at 4mm. Two piezoceramic elements (see Fig. 23a) have been used as active material in order to harvest energy from known imposed vibrations and two strain gauges conditioned through Wheatstone bridge followed by a low-noise amplifier have been used to monitor the displacement of both structures.

The experimental setup consists of a board to support the Magnetically-Coupled Antiphase-Cantilevers; a shaker has
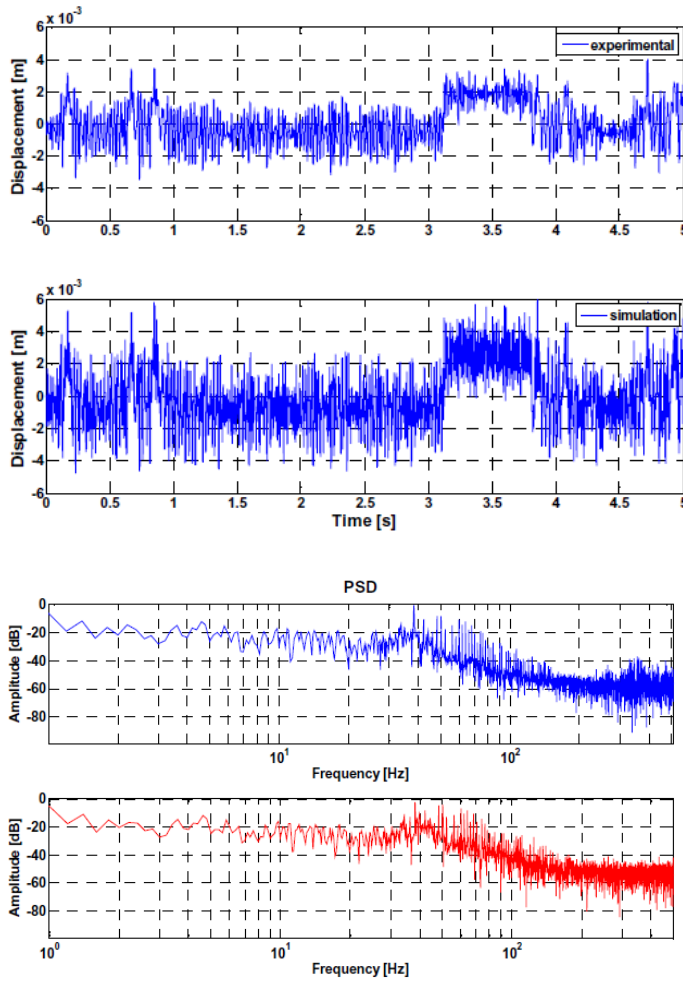
Fig. 24 - (a) Tip-displacement: experiment V$_s$ simulations; (b) spectral analysis, on the top the state-variable x_1 and on the bottom x_2.

been used as a vibration source driven by a Gaussian white noise generator (low-pass) filtered at 450Hz. Finally an accelerometer has been used as a feedback element. Fig. 23b shows the measured tip displacements in presence of an acceleration (rms) of about 5.8g, where the bistable and antiphase behaviors are evident. In Fig. 24a, the experimental signal has been compared with the model assuming two identical beams having a mass (*m*) of 0.82g and damping (*d*) of 0.0044Ns/m, both experimentally estimated. The linear elastic constant (*k* = 44 N/m) has been evaluated through the cantilever beam model.

The parameters α, β, γ, δ of the two nonlinear terms have been estimated through a fitting procedure (Nelder–Mead nonlinear algorithm). Fig. 24b shows the power spectrum: a wide band appears as consequence of the bistable dynamic.

An output power of about 3.5µW has been measured with a resistive load of 500kΩ for an acceleration (rms) of about 5.8g. Harvested energy is 2-times higher compared to a single beam nonlinear oscillator (Fig. 22a) and 10-times more compared to a linear system (single cantilever

in absence of magnetic coupling). Work is in progress toward optimization of the MEMS design and realization, moreover the proposed bistable antiphase behaviors is currently investigated for further exploitation in "fully mechanical MEMS rectifiers"

2.2. Multiple nonlinear oscillators

Several innovative strategies have been proposed in order to harvest energy from low-frequency, large-bandwidth and mixed signals (periodic and stochastic sources) [**32**]. An efficient solution has been proposed in [**34**] where two parallel cantilevers each one carrying a magnet on its tip and having identical magnetization have been used as energy harvester. This configuration improves bistable oscillators performed exploiting the repulsive force produced by two facing permanent magnets also in the perspective to carry out fully integrated bistable MEMS harvesters. The oscillator here proposed is suitable to scavenge energy from low level mixed signals with multiple piezoelectric elements to increase the power budget and in order to be tolerant to small frequency

fluctuation of the input source. The device is composed of multiple magnetically-coupled cantilevers having each one a double well potential energy function with different natural frequencies inside each stable state. This feature plays a key role, in fact a bistable oscillator has an energy barrier that should be exceeded in order to start the switching between one steady state to the other recovering the energy with a broad spectrum of response. In order to overcome the barrier, that typically is fixed and difficult to be tuned, a possible solution is to use vibrations mixed with periodic signals [**35**] [**36**] [**32**] as often provided in nature. In [**32**] authors demonstrate that it is possible to find an optimal mix of noise variance and amplitude of sinusoid in order to increase the performance of the harvester. Moreover also the frequency of the periodic signal can improve the efficiency especially when its value matches the system's natural frequency inside a single well than it does at other frequencies, thus a bigger displacement will be induced. The choice of different resonant frequencies here pursued implies that even in presence of frequency variations of the sinusoidal

component or its fluctuations the system will start to switch also in presence of small vibration level granting an improvement in overall conversion effectiveness. The system is composed of four beams, coupled through four permanent magnets in order to create the nonlinearity and four masses in order to induce four different natural frequencies inside each stable state. The analytical model can be described through the following second order equations [**34**]:

$$m_i \ddot{x}_i + d \dot{x}_i + k x_i - k_{nl} x_i + k_{nlc} (x_i - x_{i-1} - x_{i+1}) + d_m (\dot{x}_i - \dot{x}_{i-1} -$$

$$xi+1+dpztVi=F(t) \tag{2.2}$$

It represents a dynamical model of a nonlinear beam (i^{th}) having a mass m_i, spring k and damping d. The dotted terms represent the first derivative of the variables. The terms d_m and d_{pzt} are the magnetic damping and the piezoelectric damping respectively. V_i is the piezoelectric output voltage, while the noisily source and the sinusoidal bias are represented by *F(t)*. The two terms k_{nl} and k_{nlc} represent the nonlinear coupling correlated with the displacement (x_i) and with the relative displacement of each neighbor cantilever (x_{i-1} and x_{i+1}) respectively.

Both terms can be explained in the form:

- $k_{nl}=2A - 4Bx_i^2$
- $k_{nlc}=C - D(x_i - x_{i-1} - x_{i+1})^2$

where the terms *A*, *B*, *C* and *D* account for the double well potential shapes. The piezoelectric elements can be described through the following equation:

$$\dot{V}_i = k_{pzt}\dot{\bar{x}}_i - \frac{1}{\tau}V_i \qquad (2.3)$$

Where $\dot{V}_i$ is the first derivative of the ith piezoelectric output, while $\dot{\bar{x}}_i$ is the first derivative of the displacement of the piezoelectric element. τ is the time constant given by the product of the electric load R_{load} and the piezoelectric capacitance C_{pzt}, while K_{pzt} is correlated with the intrinsic properties of the piezoelectric film. The task to be accomplished within experiments is the analysis of the output voltage concerning each cantilever (assumed 4 coupled beams, *i=1...4*). Fig. 25 shows a schematization of the prototype. The system is composed of four aluminum beams (40mm x 9mm) each one having a mass of about 0.82g and damping of 0.0044kg/s. Both parameters have been estimated through experiments while an elastic
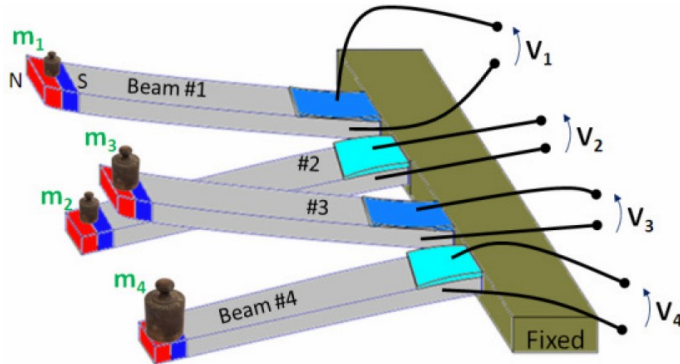
51

Fig. 25 - Schematization of the oscillators with four added masses.

constant (k) of 44kg/s^2 has been evaluated using the model of a clamped cantilever [**37**]. The damping effect of piezoelectric elements (d_{pzt}= 1e-007N/V, the magnetic damping (d_m= 1e-010kg/s) and the coefficients of the nonlinearity (A= 10N/m, B= 1056750N/m^3, C= -11.3513N/m, D= -3.9045e-004N/m^3) have been evaluated by using a fitting procedure (Nelder–Mead nonlinear algorithm [**34**]) between the model and the experimental data. Four elements of Lead Zirconate Titanate PbTiO$_3$, having a piezoelectric coefficient K_{pzt} of 1.13 109V/m have been fixed at the anchor of the cantilevers. The beams are magnetically coupled through four NdFeB

permanent magnets each fixed on the cantilever tip in repulsive force condition in order to create the two stables states. A natural frequency inside a single well of about 37Hz has been evaluated through the model [**37**]. In order to validate the principle several masses have been glued at the tip of each beam ($m_1 \sim 0.82$g, $m_2 \sim 0.88$g, $m_3 \sim 1.3$g and $m_4 \sim 2.5$g respectively). Fig. 26 shows the experimental setup that is composed of:

- a shaker (TIRA TV 50009) to impose mechanical vibrations

- a band-limited white noise generator to emulate the ambient vibrations (assumed limited at 450Hz)

- a sinusoidal generator to emulate the deterministic component

- a conditioning circuit able to sum both signals

- four piezoelectric elements (Lead Zirconate Titanate $PbTiO_3$) have been used in order to extract energy from external vibrations

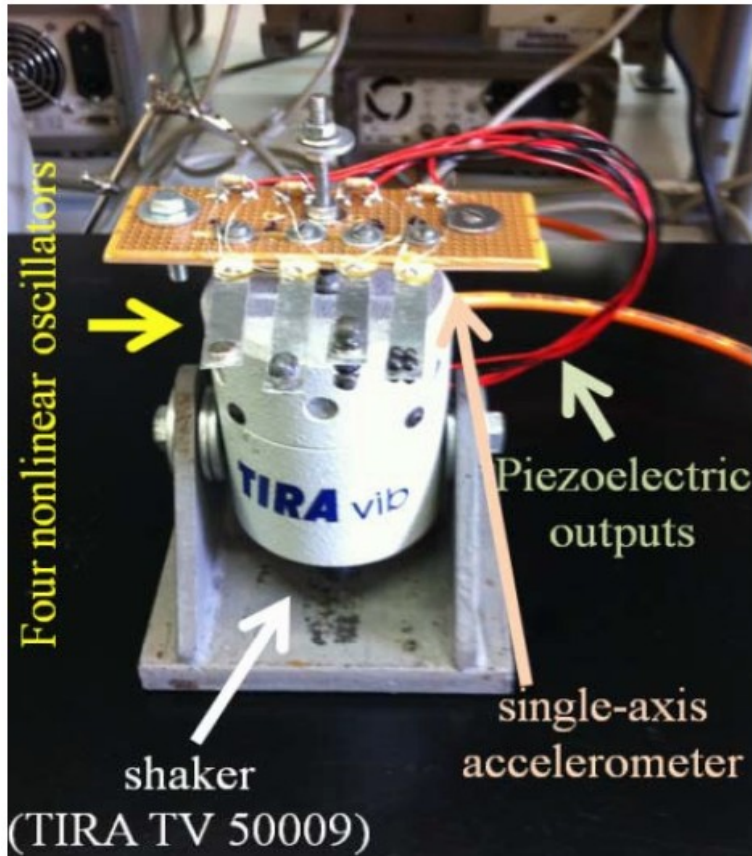- A single-axial accelerometer has been used as a feedback element.

53

Fig. 26 - fig2 - Experimental setup

A resistance of 330kΩ has been connected as resistive load (R_{load}), while an intrinsic piezoelectric capacitance (C_{pzt}) of about 1.2nF has been measured across each

piezoelectric. During measures a maximum voltage of about 2V has been detected. Fig. 27a shows the simulation results in absence of additive masses ($m_1 = m_2 = m_3 = m_4 = 0.82$g). The system has been excited through 7.5m/s^2 (rms) of random accelerations summed with a sinusoidal bias having frequencies less than 35Hz. This vibration level is not enough to start the switching and the excitation frequency of the sinusoid is far from the natural frequency of the linear region, consequently the system does not switch, so the beam will oscillate into a single well. Moreover in presence of additive masses ($m_1 = 0.82$g, $m_2 = 0.88$g, $m_3 = 1.3$g, $m_4 = 2.5$g) different values of natural frequencies are guarantee inside each single well. Exciting the system through 7.5m/s^2(rms) random accelerations summed with a sinusoidal bias in the range from 20Hz to 35Hz the system will start to switch between the two stable regions (see Fig. 27b) as consequence a wider spectrum is attended so more energy can be recovered.
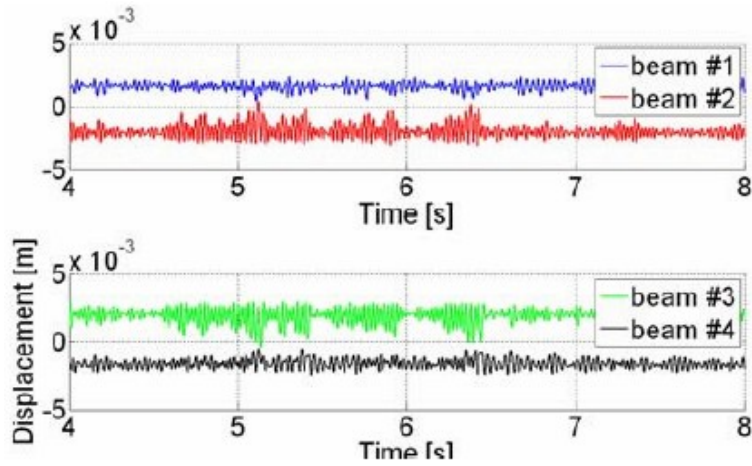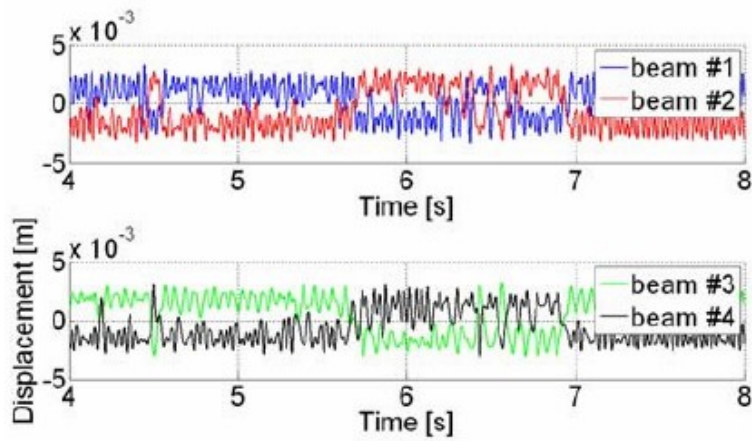
Fig. 27 - Simulation results: (a) tip displacement of the four beams in absence of additive masses and (b) in presence of additive masses. A distance of 4mm appears between the two stable states.

Fig. 28 shows the experimental results. In particular Fig. 28a shows the FFT of the voltage output (V_3) in absence of additive masses. The shaker has been driven by the two signals, combined through the conditioning circuit. An amplitude of about 7.5m/s^2 has been imposed while the periodic signal (sinusoid) has been fixed at about 37Hz. The spectrum evinces that the system oscillates inside a single well, in accordance with the theory. Fig. 28b shows the effect of the mass increment. The natural frequency of each system (linear region) will be different (f_1~37Hz, f_2~35Hz, f_3~29Hz and f_4~21Hz respectively) so in the mentioned range the system will oscillate and the movement of one beam will be propagated to the neighbor showing a wide band response. This characteristic is useful to recovery the vibration energy located at low frequency such kinetic sources available in the ambient or in the human body. The presented approach allows scavenging of energy from kinetic sources having: low level mixed signals, wide band response, multiple piezoelectric elements in order to extract more energy and tolerant to variation of the sinusoidal component.

57
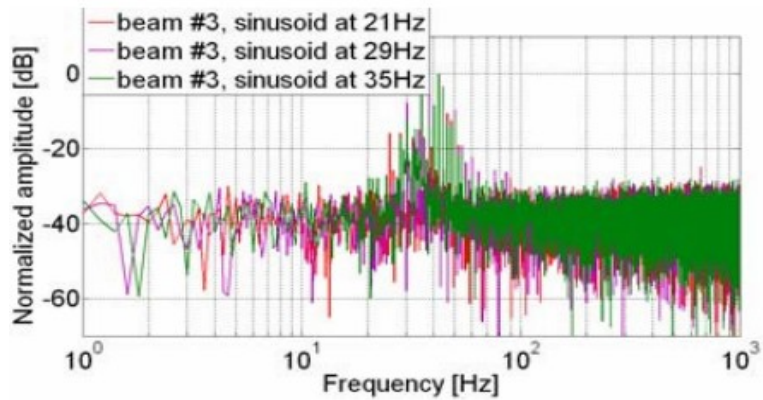
(a)
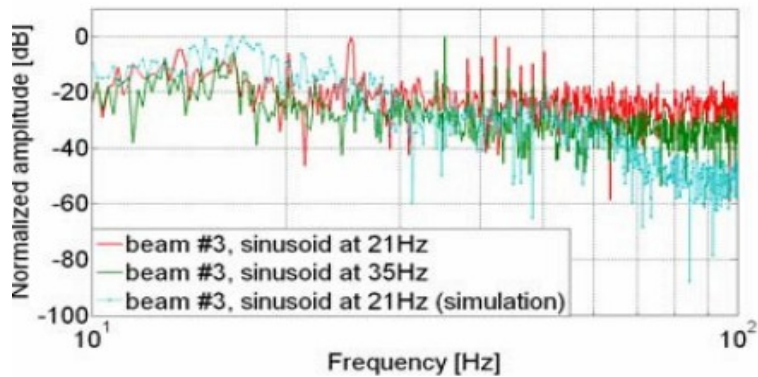
(b)

Fig. 28 - FFT of the output voltage (V_3). (a) without masses: in presence of vibrations and sinusoid (in the range 20-35Hz) having amplitude of about 7.5m/s^2. The natural frequency inside each well corresponds to f1~f2~f3~f4~37Hz, a linear response appears. (b) With additive masses: in presence of vibrations and sinusoid (in the range 20-35Hz) having amplitude of about 7.5m/s^2.

58

The experimental results show the suitability of the system to recovery energy from external vibrations. A maximum power of about 50µW has been evaluated through measures. An improvement in terms of bandwidth (wide), resolution (about 7m/s2), and power harvested (4-times more) compared with linear and nonlinear systems has been observed. Furthermore it is suitable to be integrated thanks to the parallel magnetization of the magnets. In this context, the work is in progress through the device fabrication based on MEMS technology.

2.3. Performance characterization of different nonlinear transduction mechanisms for piezoelectric energy harvesting

The three nonlinear oscillators here proposed and characterized are composed of multiple magnetically-coupled cantilevers having each one a double well potential energy function with different natural frequencies inside each single well. The nonlinear-transduction mechanisms have been assumed as coupled mass-spring-damper systems with a nonlinear response of the elastic term. Furthermore the proposed devices present several intriguing advantages such as: scavenging from low level signals (random and periodic), wide band response, multiple piezoelectric elements and simple fabrication on MEMS devices. The nonlinear transducers here proposed are: 1) nonlinear single beam, 2) magnetically coupled double beam, 3) four magnetically coupled beams. These devices have been previously studied [**30**], [**37**], [**38**], and here characterization and device performance will be exploited showing the suitability of the proposed mechanisms to sustain or to

supply autonomous nodes, wireless sensor networks, etc.

In this section, considerable effort will be concentrated towards investigation of dynamic model. It is based on analytical description of the device in two physical domains: mechanical and electrical, including the electromagnetic coupling related to permanent magnets located at the tip of each single-oscillator. The electromechanical architecture here presented is based on *N*-magnetically coupled beams (a reference is shown in Fig. 29) modeled as coupled second order nonlinear equations. This analytical approach has been previously addressed through oscillators in macro and micro-scale [**30**], [**37**], and here a brief overview of the model will be addressed including a more general modeling oriented for N magnetically-coupled oscillators. Each device has been considered as a cantilever beam having each one a NdFeB magnet at the tip. The magnetic interaction between the N beams provides repulsive forces obtaining the double well (bistable and nonlinear) behaviors in the oscillators. Mathematically, a system of N magnetically-coupled
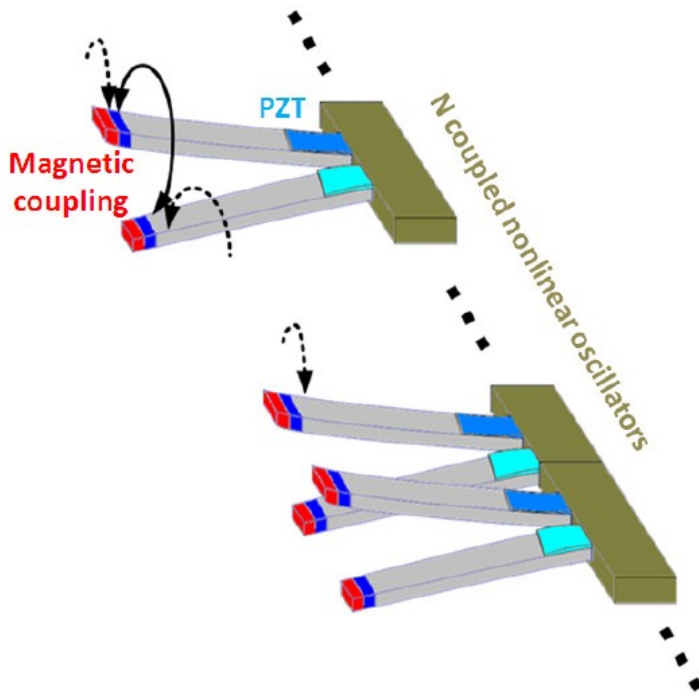
**Fig. 29 - Schematization of N nonlinear oscillators.**

oscillators can be modeled using second order nonlinear differential equations that can be written as follows [**38**]:

$$m_i \ddot{x}_i + d\dot{x}_i + kx_i - k_{nl}x_i + k_{nlc}(x_i - x_{i-1} - x_{i+1}) + d_m(\dot{x}_i - \dot{x}_{i-1} - \dot{x}_{i+1} + d_{pzt}V_i = F(t)$$ (2.4)

m_i, d_i and k_i are the mass, the damping coefficient and the spring constant of the ith beam, respectively. The terms $\dot{x}_i$ and $\ddot{x}_i$ are the first and the second derivate of the displacement x_i, while d_m and d_{pzt} take into account the magnetic damping effect and the piezoelectric damping due to voltage V_i (see Eq.2). $k_{nl}=2A$ - $4Bx_i^2$ and $k_{nlc}=C$ - $D(x_i$ - x_{i-1} - $x_{i+1})^2$ are used to represent the nonlinear coupling between the ith beam and its neighbors with displacement x_{i-1} and x_{i+1}; these terms are also related with the double well potential shape through the constants A, B, C and D. $F(t)$ is the external force that represents the vibrations that can be found in the environment.

Concerning the electrical modeling (PZT output), the following equation can be considered [**38**]:
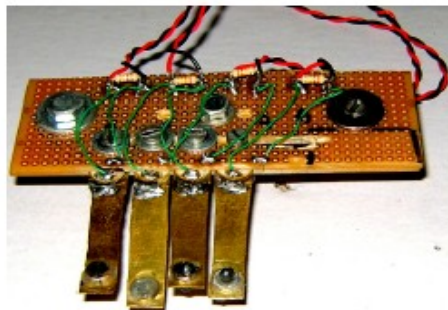
$$\dot{V}_i = k_{pzt}\dot{\bar{x}}_i - \frac{1}{\tau}V_i$$ (2.5)

63
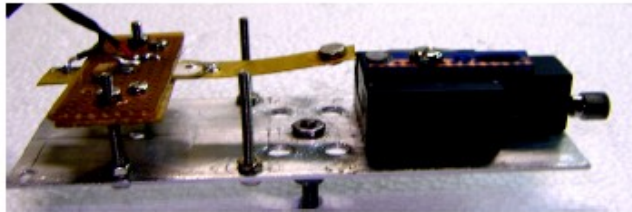
a
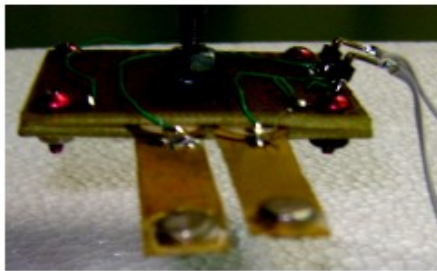
b

c

Fig. 30 - Prototypes of nonlinear transducers a) N = 1, b) N = 2, c) N = 4.

where $\dot{V}_i$ is the first derivate of the piezoelectric output voltage V_i of the ith beam, $\dot{\bar{x}}_i$ is the first derivate of the displacement of the piezoelectric element, τ is its time constant and k_{pzt} takes into account its intrinsic properties. The following three cases will be analyzed and will be considered in the characterization section:

1) Nonlinear single beam (see Fig. 30a):

The system is composed of a cantilever beam (N = 1, the two magnets present un-parallel polarization and one magnet is fixed), so $i = 1$, $x_{i-1} = x_0 = 0$ and $x_{i+1} = x_2 = 0$. The equation (2.4) of the analytical model will assume the following form:

$$m_1 \ddot{x}_1 + d\dot{x}_1 + kx_1 - k_{nl}x_1 + d_m\dot{x}_1 + d_{pzt}V_1 = F(t)$$

$$(2.6)$$

2) Magnetically coupled double beam (see Fig. 30b):

The oscillator includes two cantilever beams (N = 2, the magnets have parallel polarization).

For $i = 1$, $x_{i-1} = x_0 = 0$ and $x_{i+1} = x_2 \neq 0$

For $i = 2$, $x_{i-1} = x_1 \neq 0$ and $x_{i+1} = x_3 = 0$

Two equations derive from (2.4):

$$\begin{cases} m_1\ddot{x}_1 + d\dot{x}_1 + kx_1 - k_{nl}x_1 + k_{nlc}(x_1 - x_2) + d_m(\dot{x}_1 - \dot{x}_2) + d_{pzt}V_1 = F(t) \\ m_2\ddot{x}_2 + d\dot{x}_2 + kx_2 - k_{nl}x_2 + k_{nlc}(x_2 - x_1) + d_m(\dot{x}_2 - \dot{x}_1) + d_{pzt}V_2 = F(t) \end{cases}$$

$$(2.7)$$

3) Four magnetically coupled beams (see Fig. 30c):

four cantilever beams have been coupled (N = 4, the magnets present parallel polarization).

For $i = 1$, $x_{i-1} = x_0 = 0$ and $x_{i+1} = x_2 \neq 0$

For $i = 2$, $x_{i-1} = x_1 \neq 0$ and $x_{i+1} = x_3 = 0$

For $i = 3$, $x_{i-1} = x_2 \neq 0$ and $x_{i+1} = x_4 \neq 0$

For $i = 4$, $x_{i-1} = x_3 \neq 0$ and $x_{i+1} = x_5 = 0$

Four equations derive from (2.4):

$$m_1\ddot{x}_1 + d\dot{x}_1 + kx_1 - k_{nl}x_1 + k_{nlc}(x_1 - x_2) + d_m(\dot{x}_1 -$$
x2+dpztV1=Ft

$$m_2\ddot{x}_2 + d\dot{x}_2 + kx_2 - k_{nl}x_2 + k_{nlc}(x_2 - x_1 -$$
x3+dmx2−x1−x3+dpztV2=F(t)

$$m_3\ddot{x}_3 + d\dot{x}_3 + kx_3 - k_{nl}x_3 + k_{nlc}(x_3 - x_2 -$$
x4+dmx3−x2−x4+dpztV3=Ft

$$m_4\ddot{x}_4 + d\dot{x}_4 + kx_4 - k_{nl}x_4 + k_{nlc}(x_4 - x_3) + d_m(\dot{x}_4 -$$
$$\dot{x}_4) + d_{pzt}V_4 = F(t)$$

(2.8)

Experiments have been carried out and the oscillations have been induced through an inertial force *F(t)* applied by using a shaker. The system is composed of brass beams (40 mm x 9 mm) each one having a mass of about 8.2e-4kg. Each beam presents and poled monolithic piezoelectric material (Lead Zirconate Titanate PbTiO$_3$) located at the anchor that will be subjected to a longitudinal mechanical stress (3-1 mode) when oscillations occur. The experimental setup is composed of: a shaker (TIRA TV 5009) to impose mechanical vibrations, a signal generator in order to impose the energy
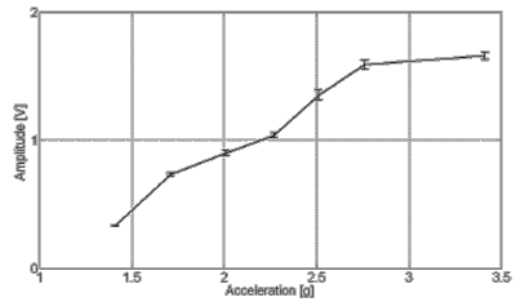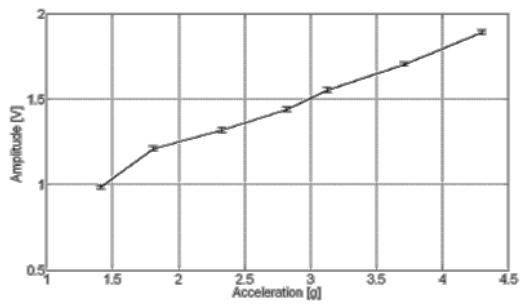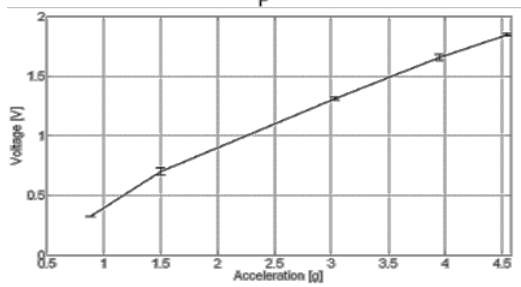
Fig. 31 - Calibration diagram of the three prototypes

sources, a feedback accelerometer to monitor the impressed vibrations.

The task to be accomplished within experiments is the analysis of the output voltage concerning each cantilever assuming three case studies (N = 1, N = 2, N = 4 respectively). The characterizations have been accomplished by using a resistive load across each PZT element of 330kΩ that represents the optimal load evaluated through experiments.

The experimental analysis of the device is represented by the calibration diagram reproducing the behavior of the PZT output voltage as a function of the vibration amplitude (Root Mean Square, RMS). Vibrations have been imposed through the shaker, considering acceleration between 0.88g and 4.5g. In order to emulate environmental source [30], Gaussian white noise limited at about 450 Hz has been used to excite each bistable beam. Fig. 31 shows the evolution of the output signal as function of the external vibrations. The slope variation that occurs at ~2.3g (case study N=1), ~1.8g (case study N=2) and at ~1.5g (case study N=4), represents the threshold
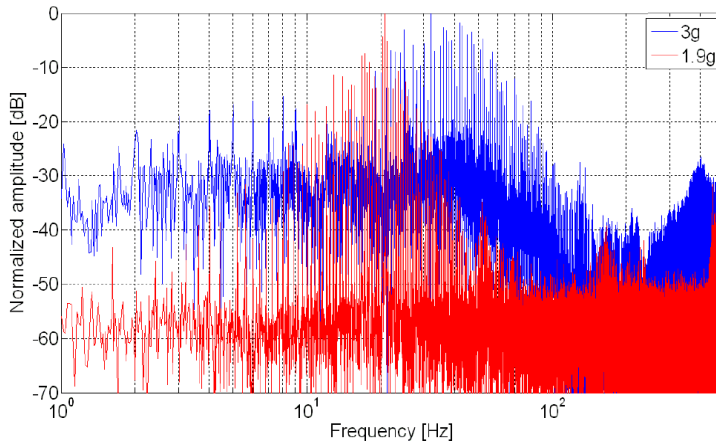
Fig. 32 - Output spectrum (N = 1) in linear condition (1.9g) and bistable condition (3g). The spectrum is normalized to its maximum value of amplitude.

(energy barrier) required to switch between one steady state to the other. Several strategies have been pursued to decrease the amplitude of the barrier in order to recovery energy from low-level ambient vibrations [**34**]. In this context the obtained results demonstrate that the architecture based on 4 coupled nonlinear transducers presents a decrement of the energy barrier amplitude with the advantage to collect energy from lower amplitudes of vibrations (starting from 1.5g) as respect the other two

architectures. This effect is related with the nonlinear term k_{nlc} presented in Eq.1 and its correlation with the displacement of the neighbor beams; increasing the number of the beams a more "flexible" structure is attended. This improvement is counterbalanced by a decrement of the PZT output voltage of each beam as consequence of the magnetic damping dm (see Eq.1) increment. The maximum power (RMS) obtained (considering a single beam response in presence of vibrations of about 2.5g) corresponds to ~5.5μW (case study N = 1 and N = 2), and ~4μW (case study N=4). The efficiency of a single beam corresponds to about 18.5% evaluated as output/input power. In terms of spectral analysis the threshold level is necessary to initiate bistable oscillations and to enlarge bandwidth as shown in Fig. 32 in the case study N = 1. With a lower level of vibration noise (< 2.3 g), the system oscillates inside a single well (linear response), losing the benefits of the nonlinearity (wide band of response).

Modeling of N different transducers has been performed and three systems have been studied and compared in

terms of calibration diagram, power budget, efficiency, spectral content. In particular the systems present a wider bandwidth of response in condition of bistable oscillation, that represents a suitable prerogative in order to recovery energy from ambient vibrations (that typically present a wide spectrum from few Hertz to hundred of Hertz). The coupled structure using $N = 4$ has the advantage to recovery energy about four times more as respect the single beam device ($N = 1$), but it presents performance degradation in terms of occupied area. Furthermore, in the perspective to integrate the device the parallel magnetization of the four coupled beams ($N = 4$) and double beam ($N = 2$) would be greatly preferable and simple to implement in micro and nano scale, as respect a single beam based on un-parallel magnetization. The work is in progress with a more exhaustive analysis of the devices based on more performant active materials and the downscaling process based on a PiezoMumps technology.

2.4. Two Dimensional Bistable Vibration Energy Harvester

Usually the vibrations energy harvesting are intrinsically focused on a single incoming direction (1D) of vibrations. It is worth noting that in order to generate maximum power from energy harvester, a good matching between sources and the harvesters in terms of vibration directions is also required. For this reasons, several approaches have been proposed where interesting solutions are investigated to approach the issue of multidimensional energy harvesters. In [39] authors present a two-dimensional linear oscillator having the two resonance frequencies at 370.5 Hz and 373.9 Hz. Both frequencies can be tuned of few Hz of deviation through fabrication techniques. In [40] a SOI-based integrated device has been presented. A capacitive transduction mechanism has been used in order to convert ultrasonic mechanical energy into electrical power. A linear response has been detected with resonance frequencies of 38,520 Hz and 38,725 Hz, harvested power of about 0.1nW and maximum peak-to-peak output voltage of 10mV.
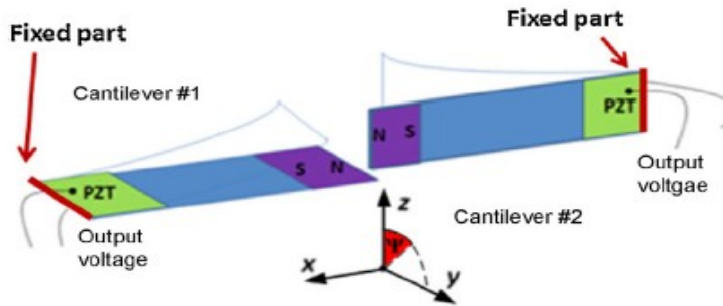
(a)
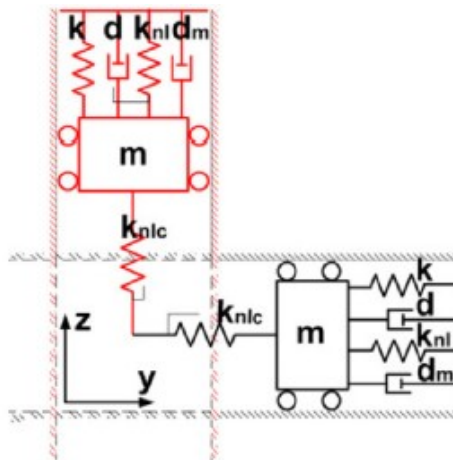
(b)

Fig. 33 - (a) Schematic principle of the two dimensional wide-band energy harvester and (b) physical model of the system assumed as two second order nonlinear equations.

In [**41**] authors propose a more efficient device having a piezoelectric (a bimorph lead zirconate titanate) output and a macro-scale proto-type. It is capable to generate the electricity from two-dimensional 60 Hz external sources generating a power of about 7.5 mW. Moreover also in bi-dimensional energy harvesters, if the environmental vibration frequency deviates from the harvester resonance, very little power can be extracted. In this work, the rich nonlinear behavior of two bistable beams with bonded piezoelectric patches for broadband

beams with bonded piezoelectric patches for broadband nonlinear energy harvesting is exploited. The bi-axial vibration energy harvester here proposed is composed of two magnetically coupled bistable beams, with piezoelectric output, capable to recovery energy even when the direction of ambient vibration is not aligned with the beam axes. The schematic principle is shown in Fig. 33a. Two cantilevers are used: one that deflects along the z direction, the other moving along y direction. Two neodymium permanent magnets have been placed on the two cantilever tips with opposite magnetization in order to

75

provide for repulsive force. As stated above, this device (thanks to the combined action of the two orthogonal cantilevers) allows for collecting energy from incoming vibrations whichever is their incoming direction on the y–z plane. Each cantilever will sense the component of the vibration along its sensing direction, therefore for generic vibrations on the y–z plane each one of the two cantilevers will respond to the projection of the kinetic energy along its own axis respectively. All the incoming energy is therefore collected. The presence of permanent magnets on the cantilever tip has been largely exploited in order to obtain bistable behaviors [**30**] [**42**] [**43**] and therefore to improve the device performances thanks to the enlargement of the power spectral density at lower frequencies. The presence of the two opposing magnets allows for obtaining a greater efficiency also for the issue of bidirectional energy harvesting; in fact the vibrations induced in one of the two beams are transmitted to the other cantilever through the magnetic coupling due to the couple of opposite magnets that are also responsible of the bistable behavior. Therefore each beam behaves in a

bistable way whichever is the direction of the incoming vibration thus resulting into a very efficient bi-directional energy scavenging. Fig. 33b shows the physical model that can be described through two magnetically coupled second order equations [**37**]. Each cantilever has been modeled by considering a mass *m*, spring *k* and damper *d*; a term that describes the magnetic coupling has been added to each equation. Referring to Fig. 33b, the variables y and z represent the tip displacement along both axes (*y* and *z* respectively). While $\dot{y}, \dot{z}$ and $\ddot{y}, \ddot{z}$ represent respectively the beam velocity and the beam acceleration along *y* and *z*-axis. The two terms k_{nl} and k_{nlc} represent the nonlinear coupling correlated with each displacement (*y* and *z*) and with relative displacement of each cantilever respectively. The terms d_m and d_{pzt} represent the magnetic damping and the piezoelectric damping effect respectively, while the noisy source (having a physical dimension of Newton) along *y* and *z*-axis is represented by n_y and n_z respectively:

$$\begin{cases} m\ddot{y} + d\dot{y} + ky - k_{nl}\,y - k_{nlc}\,(z-y) - d_m\,(\dot{z}-\dot{y}) + d_{pzt}\,V_y = n_y \\ m\ddot{z} + d\dot{z} + kz - k_{nl}\,z + k_{nlc}\,(z-y) + d_m\,(\dot{z}-\dot{y}) + d_{pzt}\,V_z = n_z \\ \qquad\qquad \dot{V}_y = k_{pzt}\,\dot{\bar{y}} - \Omega V_y \\ \qquad\qquad \dot{V}_z = k_{pzt}\,\dot{\bar{z}} - \Omega V_z \end{cases}$$

$$(2.9)$$

The terms k_{nl} and k_{nlc}, that represent the nonlinear force due to the presence of magnets, can be explained in the form:

- $k_{nl} = 2\alpha - 4\beta\delta^2$, correlated with the displacement of the beam oscillation along y-axis ($\delta = y$) or z-axis ($\delta = z$).

- $k_{nlc} = \gamma - \delta(z-y)^2$, including the relative displacement between the cantilever beams.

where the terms α, β, γ and δ account for the double well potential shapes. The last two equations account for the piezoelectric transduction: the terms V_y and V_z represent the piezoelectric output voltage for each active material (hypothesized lead zirconate titanate), $\dot{V}_y$ and $\dot{V}_z$ are the first derivates of the voltages, while $\dot{\bar{z}}$ and $\dot{\bar{y}}$ are the first derivate of the displacement (along both axes) of the piezoelectric elements evaluated by applying the

Tab. 1 - Coefficients details.

Name	*Value*	*Units of measurement*	*Information*
m	0.00082	kg	Proof mass
k	44	N/m	Linear elastic constant
d	0.0044	Ns/m	Damping coefficient
α	22.96	N/m	Nonlinear elastic constant
β	1542700	N/m^3	Nonlinear elastic constant
γ	-16.6277	N/m	Nonlinear coupling
δ	$-5.9681 \cdot 10^{-4}$	N/m^3	Nonlinear coupling
d_m	$1 \cdot 10^{-10}$	kg/s	Magnetic damping
d_{pzt}	$1 \cdot 10^{-9}$	N/V	Piezoelectric damping
k_{pzt}	$1.129 \cdot 10^9$	V/m	Piezoelectric constant
Ω	113.23	s^{-1}	Inverse of the time constant

Castigliano's theorem. Ω is the inverse of the time constant given by the product of the electric load R_L and the piezoelectric capacitance C_{pzt}, while K_{pzt} is correlated with the intrinsic properties of the piezoelectric film. The prototype **is composed of two aluminum beams having a length of 40 mm and a width of 9 mm. Two cylindrical permanent magnets (NdFeB, having a diameter of 7 mm and height of 4 mm) with opposite polarities have**

 summarizes the coefficient and the unit of measurement.

The prototype is composed of two aluminum beams having a length of 40 mm and a width of 9 mm. Two cylindrical permanent magnets (NdFeB, having a diameter of 7 mm and height of 4 mm) with opposite polarities have
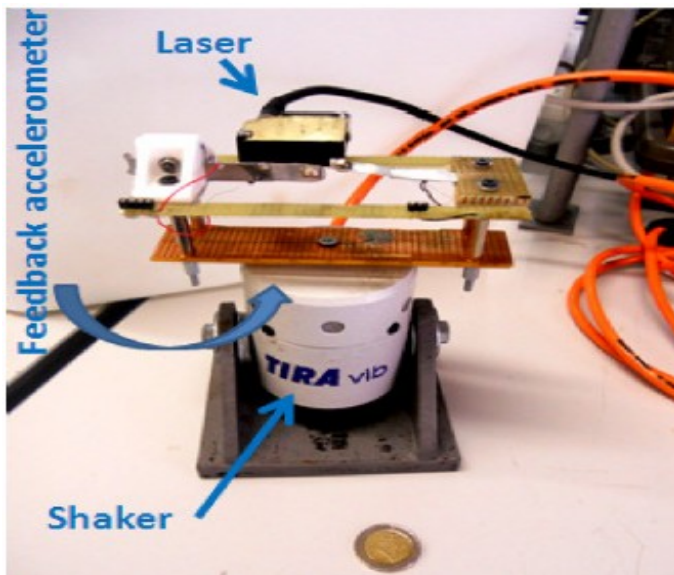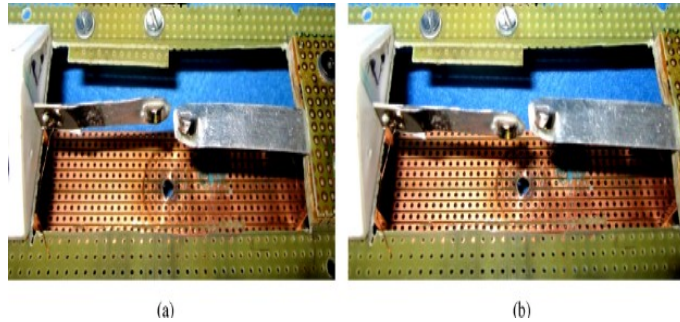

Fig. 34 - Experimental setup.

Fig. 35 - Prototype.

been used to induce two stable positions. Both magnets have been placed on the cantilever tips, one over each cantilever, separated by a 4 mm gap and with identical magnetic orientation. The magnetic induction generated by a single magnet corresponds to about 7mT. The experimental setup (see Fig. 34 - Experimental setup.) includes a shaker (TIRA TV 50009) to impose mechanical vibrations, a band limited white noise generator to emulate the ambient vibrations (assumed limited at 450 Hz), a laser distance sensor to monitor the mechanical displacement. Piezoelectric elements (lead zirconate titanate PbTiO3) have been placed on each cantilever in order to extract

energy from external vibrations. Furthermore a three-axial accelerometer has been used as a feedback element. Fig. 35 shows the proposed device that is composed of two cantilever beams: one deflects along the z direction and the other one oscillates along y direction. The cantilevers are magnetically coupled by two permanent magnets with opposite magnetization placed on their tip to provide repulsive force thus inducing the desired bistable behavior. Fig. 35a and b show the first stable state and the second stable state of the structure respectively.

Each cantilever will sense the component of the vibration along its sensing direction, the magnetic force will induce displacement into the other cantilever; the resulting system will therefore allow for collecting energy from incoming vibrations in any two directions on the y–z plane.

The system has been simulated by considering a mass (m) of a single beam (assumed located at the tip) having a value of 0.00082 kg and the damping coefficient (d) corresponding to 0.0044 Ns/m. Both characteristics have been experimentally estimated, while the elastic constant ($k = 44$ N/m) has been evaluated using the single-

beam model [**44**]. The coefficients α, β, γ, δ, d_m and d_{pzt} have been evaluated by using a fitting procedure (Nelder–Mead nonlinear algorithm [**45**]) between the model and the experimental data. The optimization process consists of minimizing a functional that represents the root mean square of residuals between the observed beam displacement and the predicted one [**46**]. Eq. (2.10) shows the model.

$$
\begin{cases}
0.00082\ddot{y} + 0.0044\dot{y} + 44y - k_{nl}y - k_{nlc}(z-y) - 10^{-10}(\dot{z}-\dot{y}) + \\
\qquad +10^{-9}V_y = n_y \\
0.00082\ddot{z} + 0.0044\dot{z} + 44z - k_{nl}z + k_{nlc}(z-y) + 10^{-10}(\dot{z}-\dot{y}) + \\
\qquad +10^{-9}V_z = n_z \\
\dot{V}_y = 1.129 \cdot 10^9\,\ddot{y} - 113.23V_y \\
\dot{V}_z = 1.129 \cdot 10^9\ddot{z} - 113.23V_z
\end{cases}
$$

$$(2.10)$$

The terms k_{nl} and k_{nlc}, can be explained in the form:

- $k_{nl} = 2 \cdot 24.96 - 4 \cdot 1542700\delta^2$, correlated with the displacement of the beam oscillation along y-axis ($\delta = y$) or z-axis ($\delta = z$).
- $k_{nlc} = -16.6277 - 5.9681e^{-4}(z-y)^2$.

Simulations have been performed by using Matlab Simulink and Dormand-Prince solver [**47**]. Several rotation angles of the structure (Ψ) and several analyses in

83

terms of tip displacement, output voltages, and power budget have been conducted. A stochastic source having amplitude (standard deviation, std) starting from 60 m/s2 has been imposed. This range of vibration represents an emulation of the common vibration level that the ambient offers (e.g. wind induced vibrations [**48**]). Fig. 36a shows simulation results assuming a rotation angle $\Psi = 45°$. The figure evinces the beam displacement and the PZT output
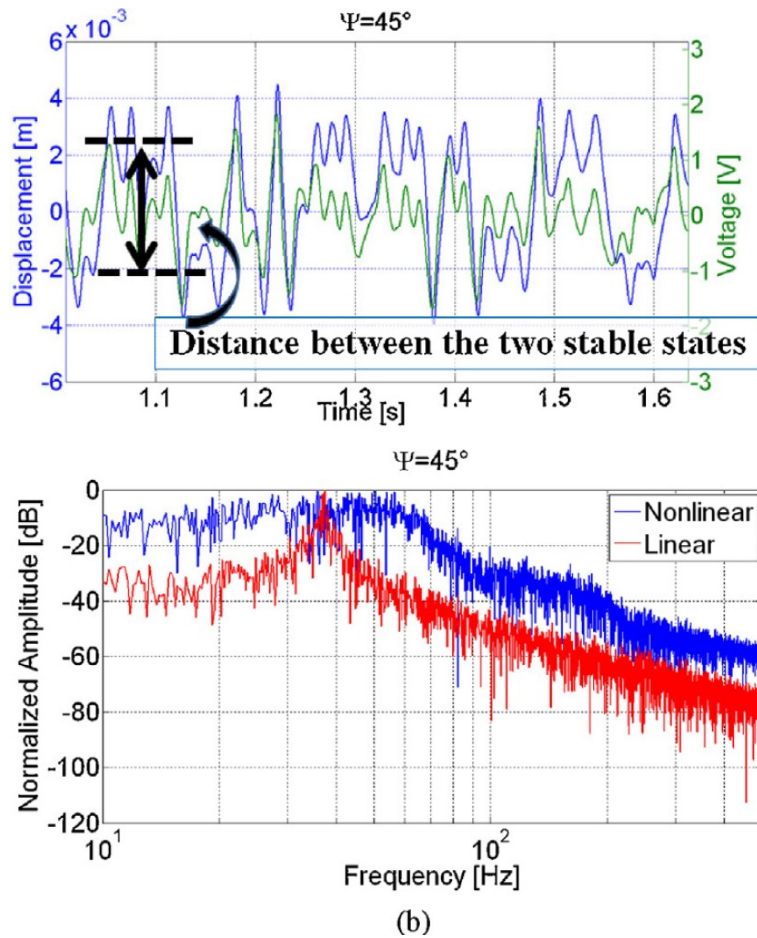
Fig. 36 - (a) Beam displacement and PZT output assuming Ψ = 45°in presence of Gaussian white noise (having a bandwidth of 0–450 Hz) and (b) displacement spectrum (linear vs. nonlinear condition). The peak around 40 Hz represents the inner-well resonant frequency.
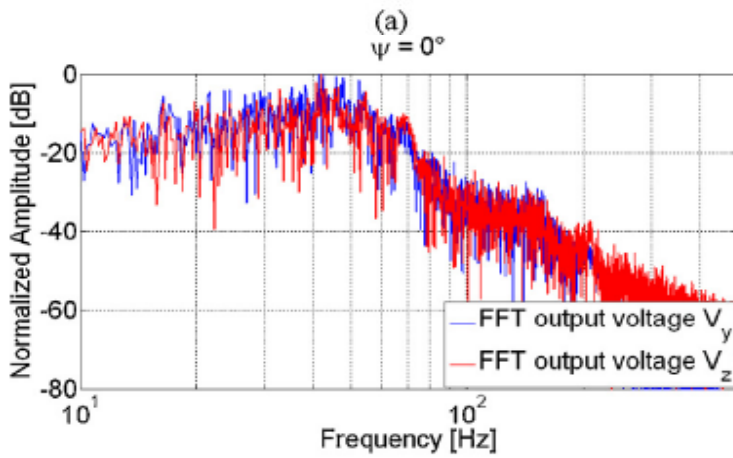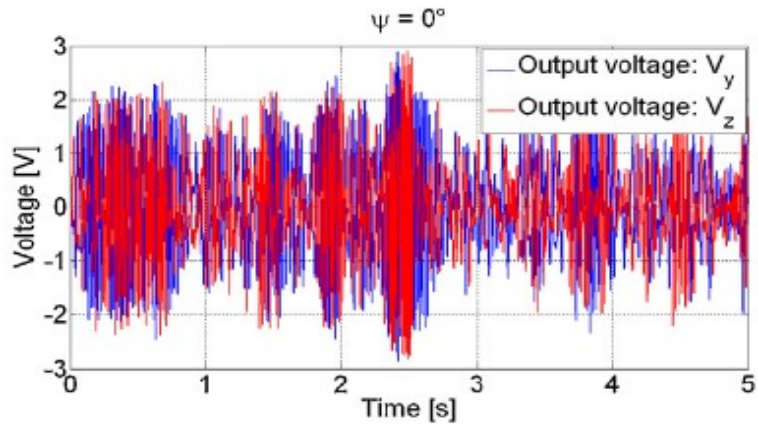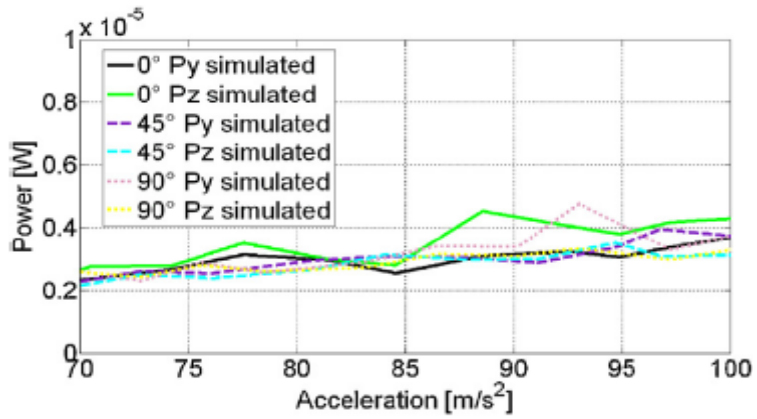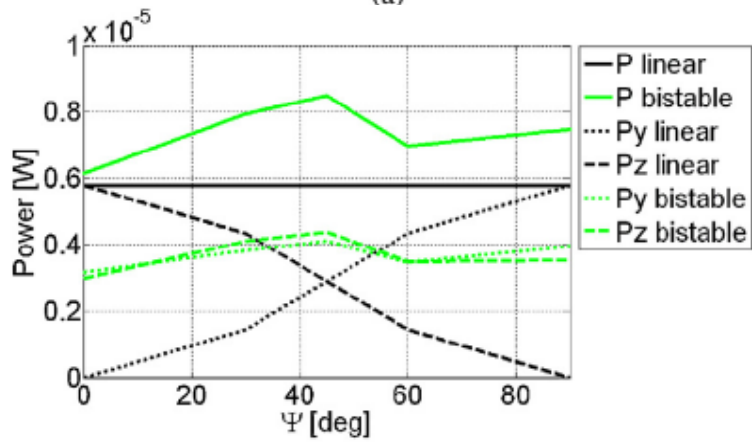
Fig. 37 - (a) Output voltage evolution of each piezoelectric transducer and (b) FFT of both signals.

(a)

(b)

Fig. 38 - (a) Power output of both PZTs assuming a resistive load (R$_L$) of 330 kΩ and (b) power output of the cantilever beam sensible to the y and z-axis assuming an accelerationof 95 m/s^2.

that evolves between its two stable regions as consequence of a noisily acceleration source (Gaussian white noise) having an amplitude (std) of 95 m/s2. Fig. 36b shows the FFT of the displacement compared with a linear case (assuming absence of magnetic coupling). Fig. 37 shows the output voltage of both piezoelectric elements and the FFT assuming a rotation angle $\Psi = 0°$.

Both figures show the improvement of the nonlinearity in terms of displacement, and in terms of spectral response that appear enlarged as respect a "classical" linear case [49]. A maximum voltage of about 5 V has been detected assuming a purely resistive load (R_L) of 330kΩ that represents the optimal resistive load for the piezo considered in this experiment. In order to validate the capability of the system to recovery energy even when the direction of ambient vibration is not aligned with the beam axes, several analyses in terms of rotation angle have been conducted. Fig. 38a shows the power harvested for three values of rotation angle as function of external accelerations. The graph shows an increment of power for both piezoelectric elements also in presence of several
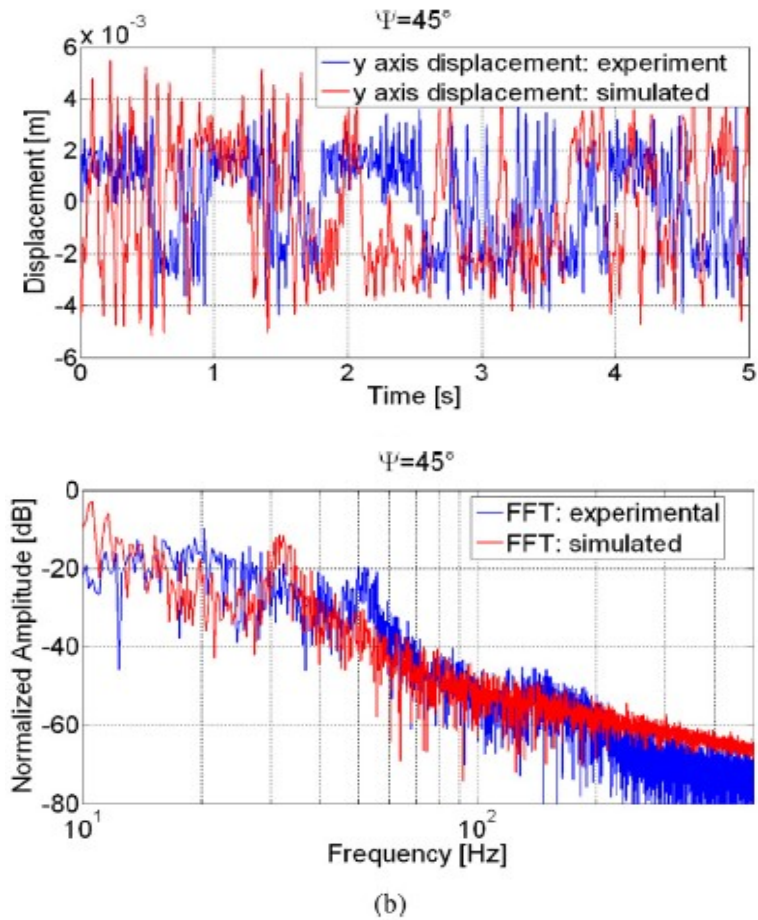
rotations of the structure. In other words the vibration impressed along the z-axis of the beam induces the movement to the y-axis of the other cantilever and vice versa, obtaining two bistable systems able to recovery energy coming from different directions. As represented in Fig. 38b, the total power output in linear condition, i.e. in absence of magnetic coupling, presents a constant evolution as function of Ψ in the range of 0–90°; while poor performances are obtained in the proximity of 0° and 90° for each single beam respectively. It is worth noting that the nonlinear system evinces its suitability showing an improvement not only in terms of wider bandwidth as respect the linear case [30] (see Fig. 36b) but also in terms of power extracted (see Fig. 38b).

Fig. 39 shows the experimental results obtained in the case of vibration level of about 95 m/s^2. The acceleration is imposed along the z direction, it can be observed as the two cantilevers are both vibrating, due to the magnetic coupling.

The results are in accordance with the mathematical model of the system and its simulations thus demonstrating the

(a)
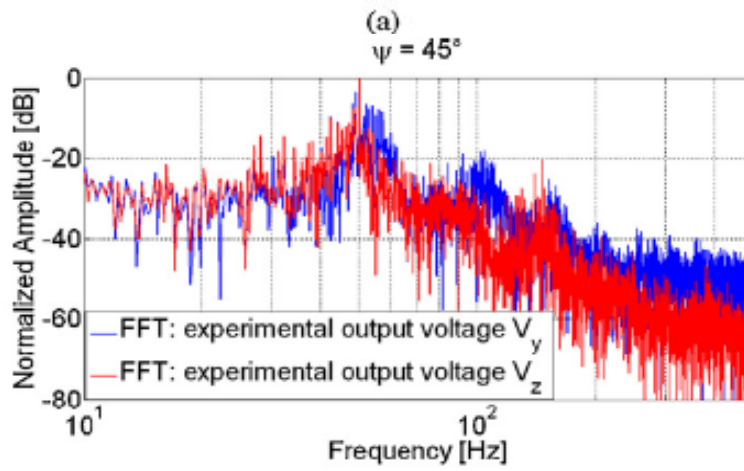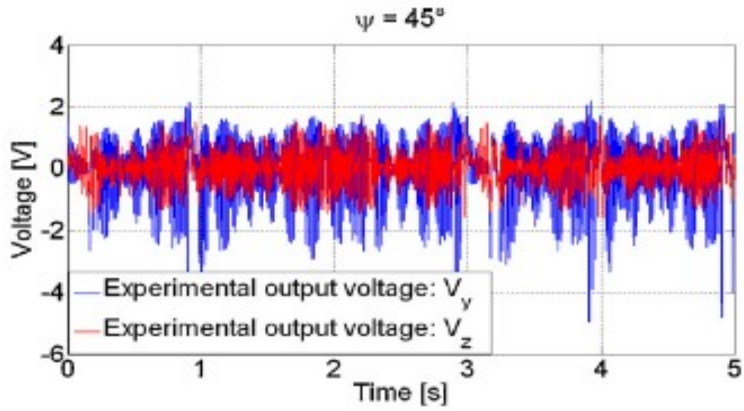
(b)
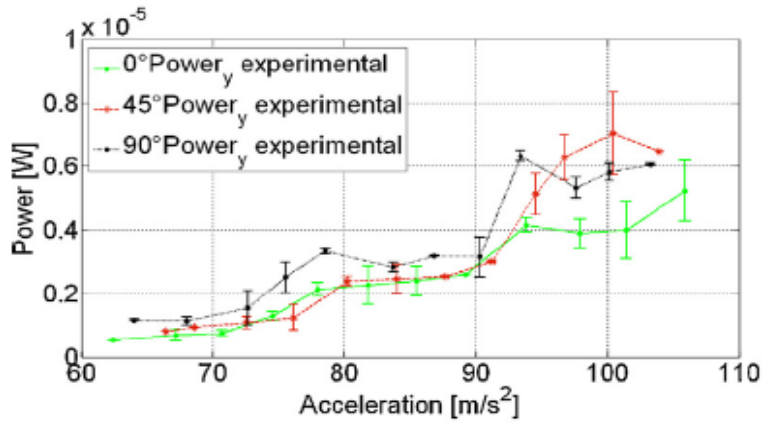
(c)
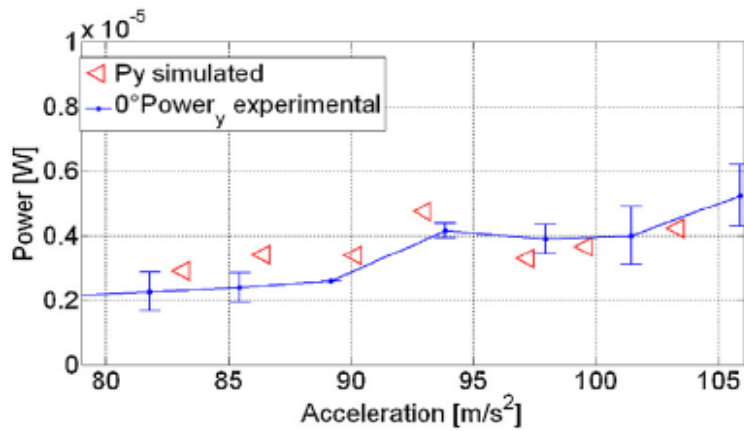
(d)

Fig. 40 - (a) Measured output voltage of each piezoelectric element, and FFT of both signals (b). (c) Measured power output of the cantilever #2 in presence of a resistive load(R_L) of 330 kΩ. (d) Comparison between experiments and simulations in presence of an acceleration of about 95 m/s^{2}and $\Psi = 0\circ$.

suitability of the proposed novel approach, furthermore a minimum acceleration amplitude (necessary to induce the switching mechanism) of about 60 m/s^2 has been experimentally detected. However it should be noticed how this acceleration value is strictly related to the actual implementation of the experimental prototype presented here; a different optimal realization can certainly address lower minimum acceleration values. In particular Fig. 40a and b shows the piezoelectric element output for both vibrating systems, detecting a variation of about 4.5V with a resistive load (R_L) of 330 kΩ and capacitance C_{pzt} of about 1.2nF. The vibrations induced through the shaker in the *z*-axis beam are transmitted to the *y*-axis beam (or vice versa) obtaining two bi-stable behaviors. As a consequence a wide spectrum appears thus resulting into a very efficient energy scavenging. Fig. 40c shows the measured power harvested for three values of rotation angle (0°, 45° and 90° respectively) as function of external accelerations.

The graph shows an increment of power for both piezoelectric elements also in presence of several rotation

of the structure. Furthermore Fig. 40d shows a comparison between experiment and simulation showing good agreement with the theoretical considerations. Summarizing, the experimental results show the suitability of the system to recovery energy from vibration coming from different directions. A maximum power of about 5.6μW (rms) has been detected for each beam with optimal load of about 330kΩ for incoming accelerations however oriented in the y–z plane, even in the case of very disadvantageous orientations. An improvement in terms of overall power harvested by the coupled bi-directional bistable elements compared with the linear system has been therefore observed. The analytical model of the system has been proposed whose parameters have been experimentally identified taking into account the prototype developed. The approach proposed here allows exploiting the benefit of bistable energy harvesters in 2D: each of the two beams will behave bistable and therefore will produce electrical energy from low frequency vibrations; whichever will be the direction of the incoming vibrations both cantilevers will vibrate with the same behaviors due

to the magnetic coupling. As it has been shown, this result into an improvement of the overall power harvested with respect to a bi-dimensional linear harvester.

Work is in progress toward the validation of this principle applied to a couple of micromachined cantilever beams, based on Silicon On Insulator (SOI) technology, both magnetically coupled through micro magnets realized by using neodymium alloy magnetic powder.

2.5. Tristable systems: a possible solution to increase the resolution of magnetically coupled nonlinear energy harvesters

Bistable piezoelectric devices are very good solutions to harvest energy from environmental vibrations, as described in previous paragraphs. This family of electromechanical systems is able to provide a large band frequency response and it can be suitable to be fabricated in MEMS technologies, under several conditions. However, it should be noted that this family of system presents an energy barrier that must be exceeded in order to start the switching between the two stable states obtaining the attended spectral response. Unfortunately the barrier is very often difficult to decrease, to overcome or to tune. A recent solution has been proposed in [**34**] where the external vibrations have been mixed with a time-periodic excitation to decrease the threshold level necessary to switch between stable states. Unfortunately often both the sources are not available together. The solution here described improves previous works focusing the attention on a tri-stable nonlinear oscillator composed
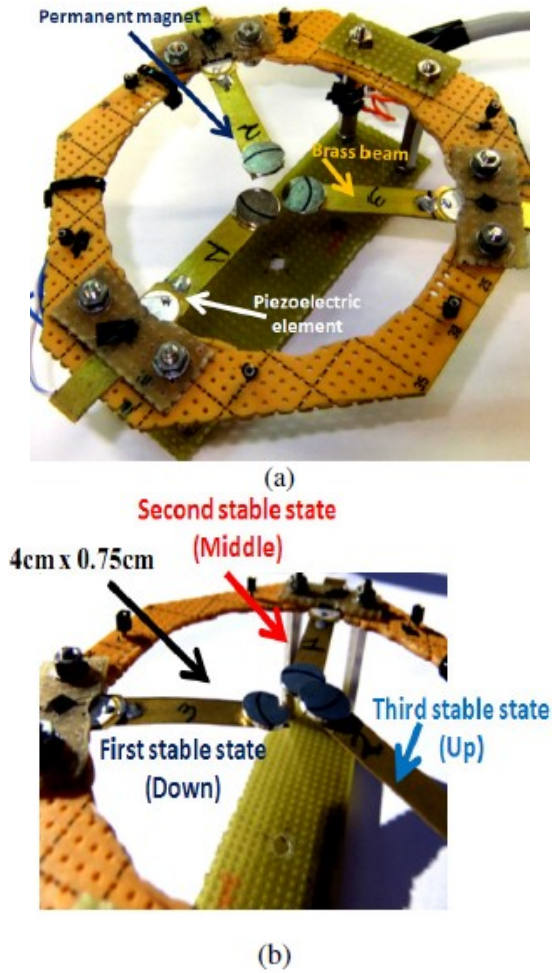
Fig. 41 - Experimental prototype: (a) magneticallycoupled cantilevers having piezoceramic elements used as active materials. (b) Zoom of the device in a stable condition.

of three magnetically coupled PZT-beams. The proposed structure presents several intriguing features such as:

- compact (three beams)
- suitable to be integrated (parallel magnetization facilitates the microfabrication process)
- higher resolution
- wider spectral response

In Fig. 41 a tri-stable oscillator is shown; it is composed of three magnetically coupled beams having each one a permanent magnet placed at the tip in order to realize the desired tri-stable potential energy function.

The magnetic dipoles are all equally aligned along the axis orthogonal to the support with identical magnetization. Piezoceramic transduction is considered. Each beam has been modeled as second-order system having a potential energy function *U(x)* as presented in equation 1.

$$U(x) = \alpha x^2 + \beta x^4 + \gamma x^6 \hspace{3cm} (2.11)$$

where x denotes the beam displacement and the terms α, β, γ relate the shape of the potential function. Fig. 42 shows a
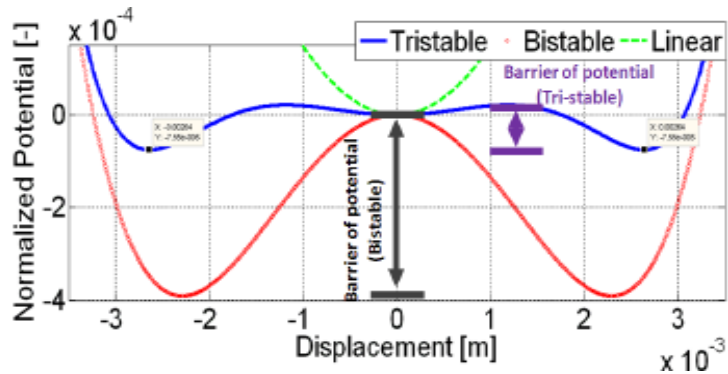
Fig. 42 - Simulation result: potential energy function comparison. 1) parabolic energy function ($U(x) = \alpha x^2$), 2) double-well energy function ($U(x) = \alpha x^2 + \beta x^4$), 3) tri-stable potential ($U(x) = \alpha x^2 + \beta x^4 + \gamma x^6$.
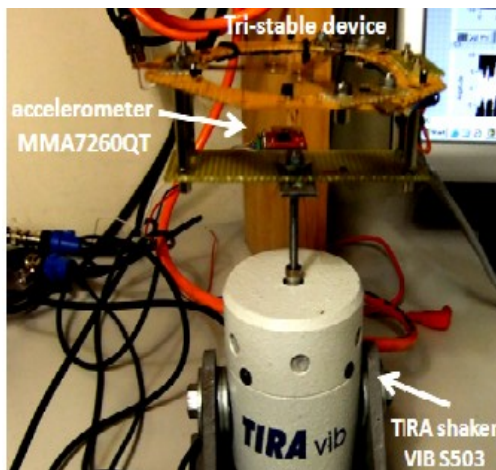

Fig. 43 - Experimental setup.

Tab. 2 - Cantilevers' parameters.

Name	Value	Units of measurement
m	0.0005	kg
l	0.04	m
w	0.0075	m
t	$200 \cdot 10^{-6}$	m

comparison of a linear, bistable (both realized removing one and two beams respectively from the structure presented in Fig. 41) and tristable device respectively. A decrement in terms of barrier amplitude has been detected as respect a classical bistable behavior, as consequence a resolution improvement is expected. The prototype is composed of three aluminum beams having a length of 40mm and a width of 7.5mm and placed at 120°. A permanent magnet has been placed on the free tip of each cantilever with a suitable polarization in order to couple the beams. Each single cantilever has an inertial mass m, length l, width w and thickness t, as summarized in Tab. 2. A piezoelectric transducer (Lead Zirconate Titanate) has been fixed at the anchor of the cantilevers, in order to maximize the output voltage.
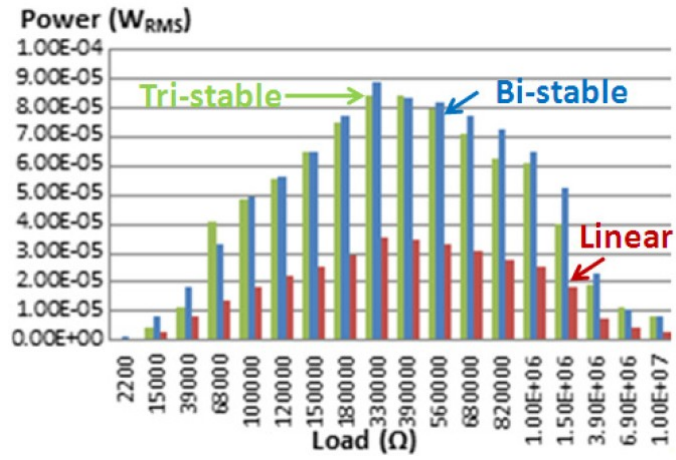
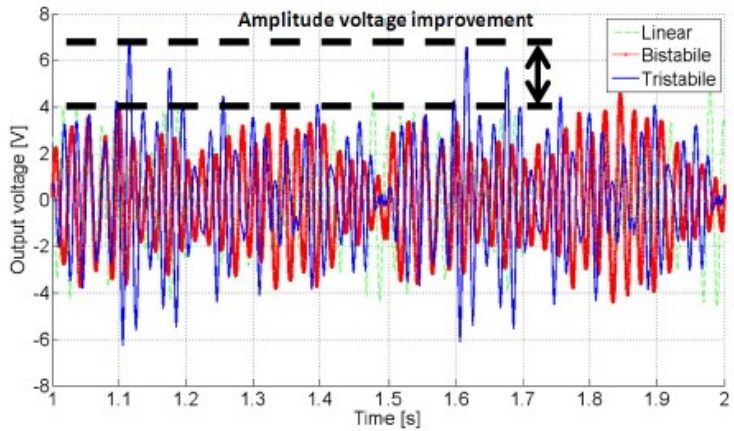**Fig. 44 - Piezoelectric output power as function of resistive loads.**

Fig. 45 - Experimental results.

101

The setup (see Fig. 43) is composed of:

- a shaker TIRA VIB S503 with an amplifier TIRA BAA60

- a signal generator Hp 3312OA, used to emulate the external vibrations

- an accelerometer MMA7260QT used as feedback element.

A preliminary campaign of measurement has been carried out in order to establish the optimum resistive suitable to achieve the maximum electric power transfer in linear, in bistable and tristable case respectively. To achieve this goal, 18 values of resistive load have been investigated and the corresponding electric power has been calculated, using a random noisy acceleration of about 3.8g Root-Mean-Square (RMS). Experiments demonstrate that the maximum power transfer occurs using a resistive load of about 330 kΩ see Fig. 44). Fig. 45 shows the piezoceramic output voltage in presence of an acceleration of ~1.5g (RMS). In this condition the tri-stable system oscillates between its stable regions and higher voltage amplitude appears as respect the bistable and linear cases.
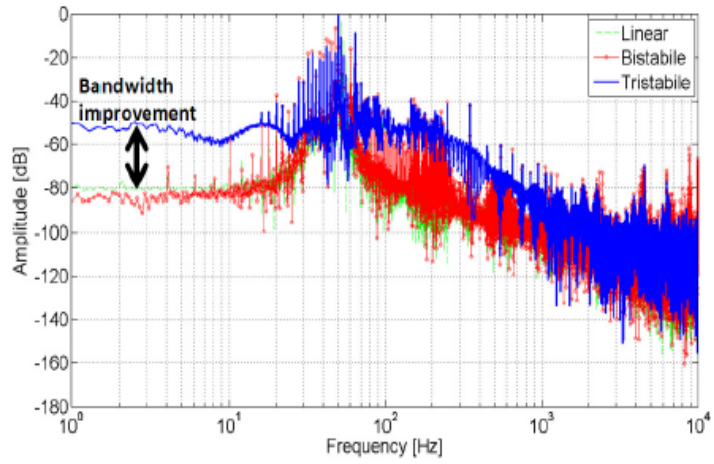
(a)
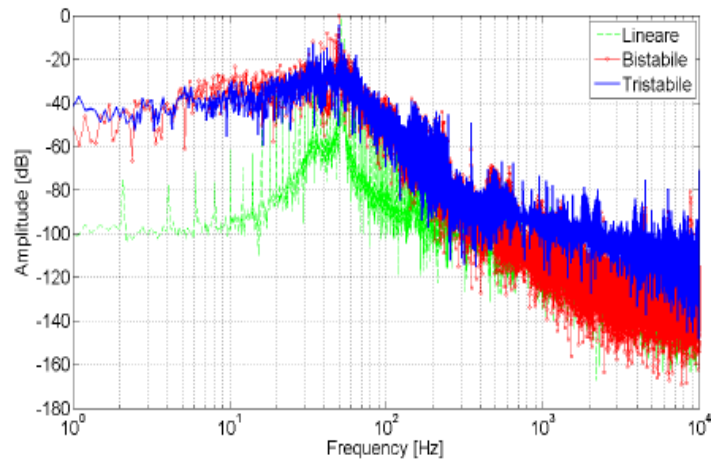
(b)

Fig. 46 - Spectral response.

103

Fig. 46 shows the spectral responses. In presence of vibration level of ~1.5g only the tri-stable system start the oscillation. While the bistable switches from ~2.7g of vibration level. An improvement in terms of resolution has been detected in presence of tri-stable behaviors and it has been estimated to ~0.8g.

The system (composed of three coupled PZT disposed at 120°) improves previous works presenting several interesting features such as: 1) compact device, 2) high performances in terms of resolution, 3) suitable to be realized in MEMS technology, 4) wide band of response. The validation of this principle with integrated prototypes will be conducted in the future.

Chapter 3.

"Vibration-driven" rectifiers based on mechanical switches.

Energy harvesting has become a very important research and development subject in recent years, with particular emphasis on its impact on the development and deployment of wireless and self-powered systems [50]; this emphasis has lead to the investigation of different kinds of energy sources (solar, thermal, biochemical, etc.) together with strategies to scavenge energy from these renewable sources [12]. Among the numerous potential energy sources, vibrations are widespread and, generally, rich of energy; hence there have been numerous engineering efforts to exploit them for electric power generation [51]. The simplest vibration energy harvesting solutions are based on inertial mass-spring-damper systems (i.e. cantilever beams with suspended proof masses) coupled to different transduction technologies e.g. piezoelectric [18], electromagnetic [17] or electrostatic

[**16**]; among these choices, the piezoelectric transduction approach has been found, to date, to exhibit better performance than the others [**12**].

The most restrictive limitation of linear mass-spring-damper solutions is the necessity of tuning the mechanical resonance frequency to the frequency of the incoming vibrational signal in order to produce optimal performance. However, environmental vibrations have a wide frequency spectrum [**52**] usually with a strong random component. This severely reduces the efficiency of the linear transduction mechanism. These shortcomings have been addressed by developing nonlinear energy harvesters. In [**53**] an analysis on the role of nonlinearity and the importance of vibrational sources description has been carried out. In particular, solutions based on bistable, non-resonant, oscillating systems have been proposed [**29**] [**54**] [**32**] [**30**] that use magnetic repulsive forces to induce bistable behavior in vibrating cantilevers.

Of course, in any reasonable energy harvester, the electrical energy harvested needs to be stored. One of the more common storage technologies is underpinned by a

diode bridge rectifier; this technique works efficiently only when the AC voltage produced by the piezo electric transducers exceeds the diode threshold.

However, micro and nano power harvesters are frequently required to provide energy to autonomous devices developed in MEMS and NEMS technologies without losing the scaling advantages. Reducing the harvester size inevitably corresponds to a reduction in the output voltage amplitude to a value below the diode threshold. Moreover, the incoming signal used for energy scavenging is often weak and distributed over a wide frequency spectrum at low frequencies; the resulting output voltage is usually below the minimum value necessary to pass the diode threshold and cannot be rectified and stored.

Many techniques have been proposed to overcome the above limitations [**55**] [**56**] [**57**] [**58**] however most of these use a synchronized approach so that their performances in the presence of random wideband excitations leave much to be desired. In some energy harvesting applications, a combination of synchronized techniques and active diodes has been explored [**59**] [**60**]

[**61**] [**62**], but these approaches have the same voltage threshold and power consumption limits due to the use of active elements. In [**63**], the authors propose a mechanical switch solution forced by thermal actuation, while in [**64**] the switch is driven by an electrostatic force. In [**65**] [**66**] [**67**] an inertial force is used to control the switch. The issue of collecting and storing energy from weak and random vibrations has been addressed in [**68**] wherein the authors have introduced a new solution based on the interaction between a switch, driven by the external vibrations, and an inductor.

In this chapter new solutions, aimed at harvesting energy from vibrations (typically occurring in a low frequency band and having a significant random component), rectifying and multiplying the generated voltage and storing the energy, are proposed; the systems have been modeled and an experimental prototypes have been developed and tested.

3.1. Diode-less Mechanical H-Bridge Rectifier for "Zero Threshold" Vibration Energy Harvesters

The solution here proposed is based on the use of two parallel cantilever beams that oscillate in response to a mechanical input. Each cantilever carries a permanent magnet, which also acts as a proof mass, on its free tip. A piezoelectric layer couples the fixed ends of the cantilevers producing a voltage output in response to the strain induced by the external vibrations. The magnets are placed on the cantilever with the same magnetic orientation so that the beam tips repel one another, thereby inducing bistable behavior [37].

The switching mechanism is realized via two conductive pads on both sides of each cantilever and a pair of conductive stoppers orthogonal to the plane of the cantilevers; they are in the close proximity but not in contact with the cantilevers. Both the pads, of each cantilever, are connected with the bottom plate of the piezoelectric transducer through a conductive line. Fig. 47 schematizes the layout.
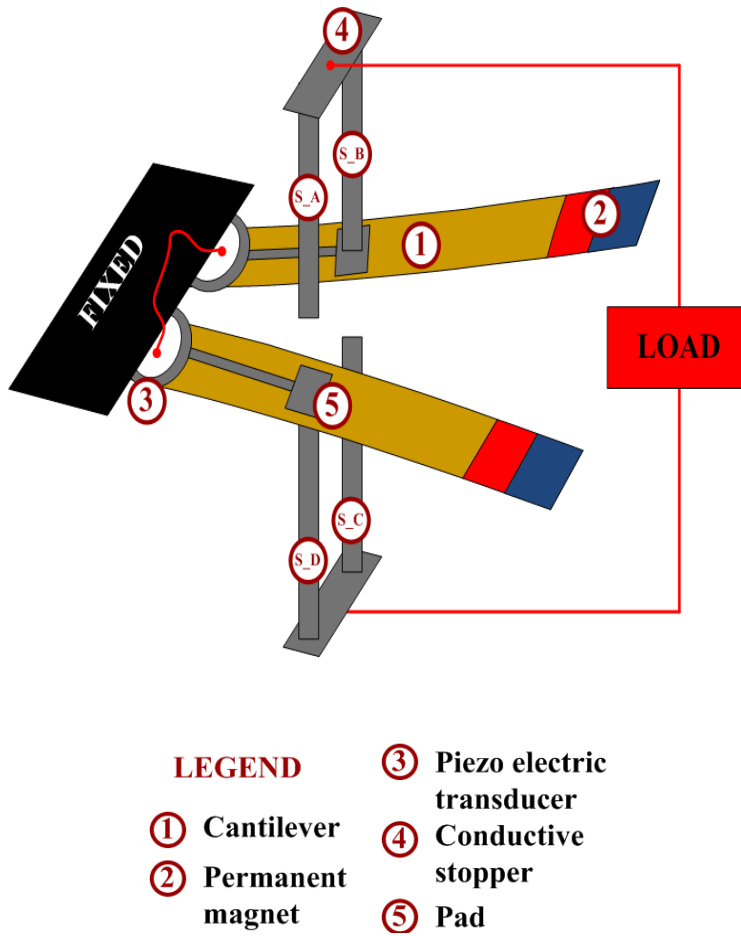
LEGEND

① Cantilever
② Permanent magnet
③ Piezo electric transducer
④ Conductive stopper
⑤ Pad

Fig. 47 - Schematic representation of the bistable mechanical switching system.

The magnets induce bistable behavior: each cantilever has two equilibrium states, UP and DOWN. If one beam is in an equilibrium state (e.g. UP), the other one is forced into the other one (e.g. DOWN), and vice versa. The two beams are, therefore, always in an anti-phase configuration. Four electrical contacts have been realized: two on the top surface of the cantilevers (S_A and S_B), and two on the bottom surfaces (S_C and S_D). The system can be, therefore, schematized as a voltage generator comprising the two piezoelectric elements, which are connected to the load via the four switches.

In the absence of external vibrations all the switches are open and the whole system is in equilibrium with the beams pushed apart; each beam occupies one of the two stable states. In the presence of an external vibrational input with an amplitude larger (this is necessary in order to have switching events between the stable states) than the threshold of the bistable system, the beams exchange their respective equilibrium states and, due to their inertia, touch the two stoppers thus closing the corresponding switches. Specifically, either the couplet [S_A, S_C] or
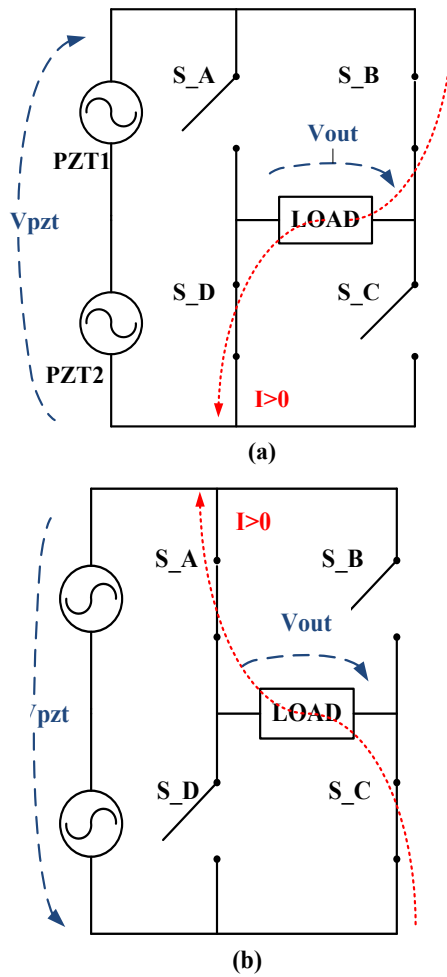
Fig. 48 - Electrical equivalent circuit of the system. The first beam touches the upper electrode while the second the lower (a) and vice versa (b). The current always flows in the same direction through the load.

the couplet [S_B, S_D] of switches will close. It should be noted that the polarity of the piezoelectric voltage is always coherent with the direction of displacement of the beam; moreover, the beam deflections are always in anti-phase and so are the voltages they produce. The two piezoelectric transducers are electrically connected in series but with opposite polarity so that they always generate the sum of each output voltage. Hence, a positive current will always flow from the piezoelectric generator to the load, thereby implementing the rectifying mechanism. This is schematized in Fig. 48.

Assuming that the cantilevers are identical, each one of them has been modeled as a second order mass (m) - spring (k) - damper (d) system. The repulsive magnetic forces and the relative couplings have been modeled via two nonlinear terms k_{nl} and k_{nlc}: the first is related to the single beam displacement, while the second takes into account the relative positions of the two cantilevers [**37**]. The resulting potential energy function of the system is bistable as shown in Fig. 49a.
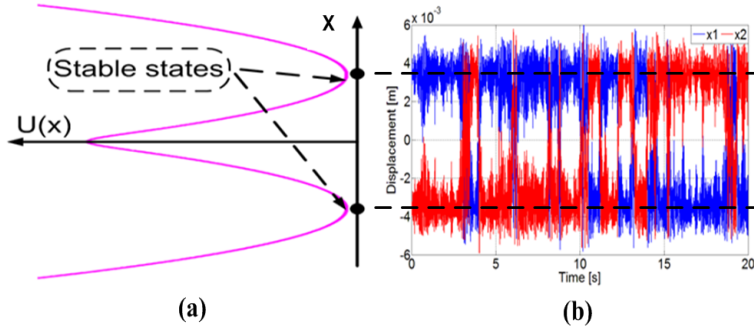
Fig. 49 - Bistable potential (a). Simulated displacement of the beams with a band limited (450 Hz) white noise input (b).

In order to account for the magnetic damping and the piezoelectric effect, two additional terms (with coefficients d_m and d_{pzt} respectively) have been introduced. Furthermore, two additional equations must also be introduced to take into account the piezoelectric transduction. Setting x_i to be the displacement, $\dot{x}_i$ the velocity (the overdot denotes the time derivative), and $\ddot{x}_i$ the acceleration of the *i-th* cantilever and with V_{x_i}, $\dot{V}_{x_i}$ and $\dot{\bar{s}}_i$ being the piezoelectric output voltage, its first derivative, and the first derivative of the strain [69] (according to Castigliano's Theorem [70]) of the *i-th* piezoelectric element respectively, the analytical model

for the electromechanical system can be written down:

$$\begin{cases} m\ddot{x}_1 + d\dot{x}_1 + kx_1 - k_{nl}x_1 + k_{nlc}(x_1 - x_2) + d_m(\dot{x}_1 - \dot{x}_2) + d_{pzt}V_{x_1} = F(t) \\ m\ddot{x}_2 + d\dot{x}_2 + kx_2 - k_{nl}x_2 + k_{nlc}(x_2 - x_1) + d_m(\dot{x}_2 - \dot{x}_1) + d_{pzt}V_{x_2} = F(t) \\ \dot{V}_{x_1} = k_{pzt}\dot{s}_1 - \Gamma V_{x_1} \\ \dot{V}_{x_2} = k_{pzt}\dot{s}_2 - \Gamma V_{x_2} \end{cases}$$

$$(3.1)$$

In equation (3.1), $k_{nl} = \alpha - \beta x_i^2$ and $k_{nlc} = \gamma - \delta(x_2 - x_1)^2$ with (i = 1,2), while k_{pzt} and Γ related to the piezoelectric material and its dynamical response. The parameters $\alpha, \beta, \gamma, \delta$ weight the effects of the magnetic and elastic forces. In order to perform the simulations necessary to understand the qualitative behavior of the device the parameters values, shown in Tab. 3, have been used. Finally, the (intermittent) contact between the beams and the stoppers has been modeled, in order to simulate the switching effect. Assuming $x = 0$ to be the plane where each mass should lie in the absence of the magnetic force, the stoppers have been modeled with two numerical thresholds (one positive and one negative, equidistant from $x = 0$) that represent the physical positions along the displacement direction x. In this specific case a value of x_{th} = 0.0035m has been used.

115

Tab. 3: Parameters. The labels "Estimated", "Calculated" and "Identified" mean that the value has been evaluated respectively through direct measurements, analytical formula, and the Nelder-Mead Simplex Method.

Name	Value	Units of measurement	Details
m	0.00082	kg	Estimated
k	44	N/m	Calculated
d	0.0044	Ns/m	Calculated
α	11	N/m	Identified
β	154270	N/m^3	Identified
γ	-15	N/m	Identified
δ	$-4.4997{\cdot}10^{-4}$	N/m^3	Identified
d_m	$1{\cdot}10^{-10}$	kg/s	Identified
d_{pzt}	$1{\cdot}10^{-7}$	N/V	Identified
k_{pzt}	$1.1299{\cdot}10^{9}$	V/m	Calculated
Γ	169.1580	s^{-1}	Calculated

Each switch has been considered in the ON-state when the position of the mass exceeds the threshold ($x_i > +x_{th}$ or $x_i < -x_{th}$). The electrical circuit is considered closed when both the two switches are in the ON-state at the same time. This model has been implemented in Simulink in order to evaluate the dynamical and electrical behaviors. The results of the simulations confirm the theoretical hypotheses, and the validity of the mechanical rectification

strategy. The simulations were carried out in the presence of a band limited (450 Hz) gaussian vibration source and, separately, an impulsive periodic (2 Hz) signal; the latter provides a good approximation to the mechanical vibrations generated during human walking.

It is instructive to define the "noise" in a more precise manner. The noise is considered to be Gaussian band-limited; it has zero mean value, and its two-point correlation function can be expressed via an Ornstein-Uhlenbeck process as [**71**]:

$$\tau_c \dot{y}(t) = -y(t) + \sigma\xi(t) \tag{3.2}$$

where $\xi(t)$ is Gaussian delta-correlated noise having zero mean. The "colored" noise *y(t)* thus has the correlation function:

$$\langle y(t)y(t^{'})\rangle = \frac{\sigma^2\tau_c}{2} exp\left[-\frac{|t-t^{'}|}{\tau_c}\right] \tag{3.3}$$

which, in the white limit ($\tau_c \rightarrow 0$) approaches the delta function correlation $\langle y(t)y(t^{'})\rangle = \sigma^2\delta(t - t^{'})$. The correlation time τ_c of the colored noise *y(t)* is the inverse of the noise bandwidth (450Hz in our simulations), and $\langle y^2(t)\rangle = \frac{\sigma^2\tau_c}{2}$ is the colored noise intensity. One readily
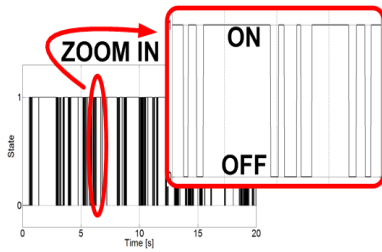
117

Fig. 50 - Simulated switches states..
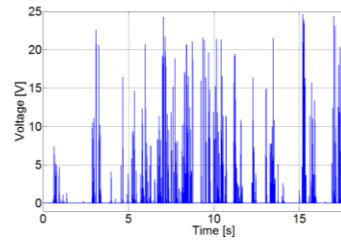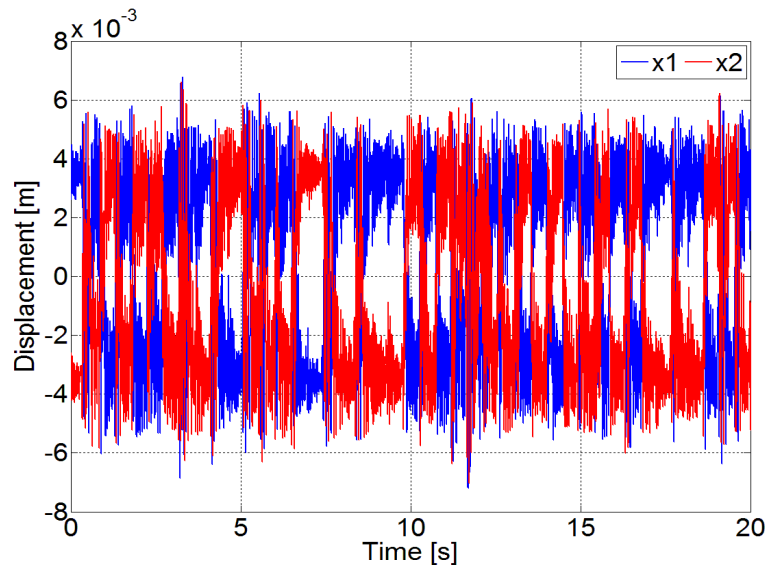

Fig. 51 - Simulated output voltage.

Fig. 52 - Simulated displacement of the beams with a human walk input [52].

verifies that the power spectral density of the colored noise has the form $\Xi(\omega) = \frac{\sigma^2}{1+\omega^2\tau_c^2}$ in the white noise limit this reduces to $\Xi_w(\omega) = \sigma^2$ as expected.

The response to the noisy vibrations is shown in Fig. 49b wherein the bistable dynamical behavior of the two beams is evident. In Fig. 50, the states of the two mechanical switches are shown: when the value is 1 the first/second beam touches the upper stopper and the second/first the lower. When the value is 0 the circuit is open and there is no current flow. In Fig. 51, the output voltage evaluated across a 390kΩ resistor is reported. Finally in Fig. 52, Fig. 53 and Fig. 54, the displacement of the beams, the rectified voltage output, and a comparison between the rectified output voltage and the PZT output are, respectively, shown for a pulse train input. It is worthwhile to compare the approach proposed in this paper and the classical full wave, diode bridge rectifier; to this end, several simulations have been carried out in order to evaluate the output voltages of both systems on a 390kΩ resistor (this has been estimated as the optimal
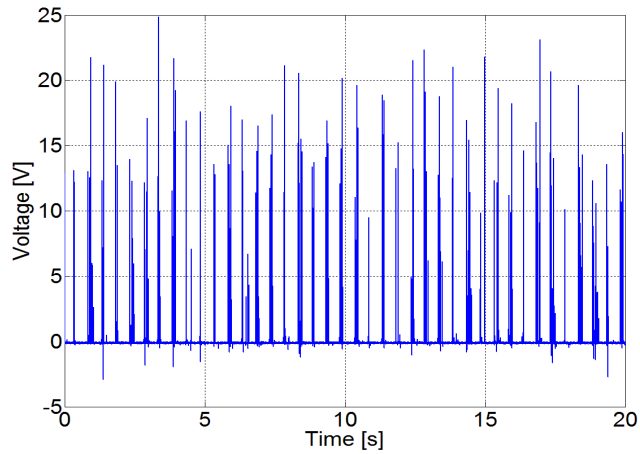
Fig. 53 - Simulated output voltage on a resistor with a human walk input [52**]. It can be seen that the voltage has negligible negative peaks.**
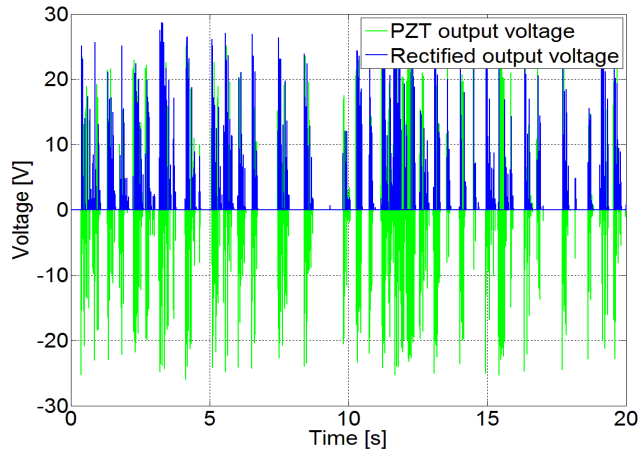

Fig. 54 - Simulated single PZT output voltage (green), and mechanically rectified output voltage (blue) with a human walk input [52].

load for power transfer in our system [**72**]). Four diodes, each having a 0.8V threshold voltage, have been used to substitute the mechanical switches in the system of Fig. 48. A noisy input, having a bandwidth of 450Hz, has been applied; its rms amplitude has been changed to explore the system behavior in different working regimes. The simulation results, shown in Fig. 55, demonstrate that the proposed solution provides better performances than the classical one for small input rms voltage, in fact with these signals the peak amplitude is lower than the diode threshold and the diode bridge cannot transfer any power to the load. When the input signal level increases the proposed H-Bridge remains advantageous, even if less efficient (as can be seen from the lower slope of the transduction curve in Fig. 55), for a range of input rms values up to the diode threshold. An experimental prototype of the mechanical H-bridge rectifier has been realized in order to validate the ideas presented here. Two brass cantilever beams (l = 40mm, w = 7mm, t = 0.2mm) have been used, together with two cylindrical permanent magnets, made of N_dF_eB and having diameters of 7mm,
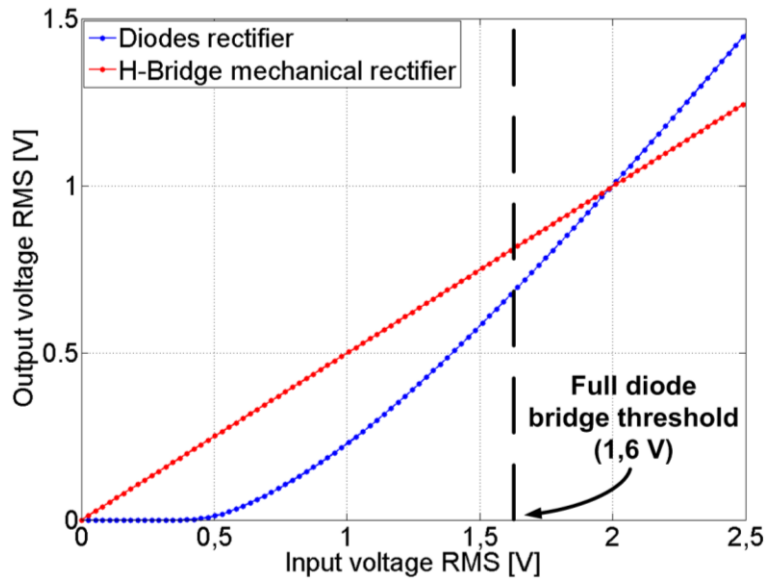
121

Fig. 55 - Output voltage from the proposed H-Bridge circuit (red) and classical, i.e. diode bridge based (blue) rectifying solutions. The input here is a nosy signal whose rms value is shown in the horizontal axis.

heights of 4mm; these magnets, weighing 0.00082kg each, are attached to the free tip of each cantilever. The magnets are placed with identical direction of magnetization; hence the reciprocal of their separation determines the repulsive force that generates the bistable behavior of the system. The experimental prototype is shown in **Errore. L'origine riferimento non è stata trovata.**. It is comprised of the PZT (Lead Zirconate Titanate) transducer bonded to the cantilever in the region of maximum strain and the electrical contacts, to realize the switches that are tunable in, both, the distance from the beam and their horizontal position. The system was stimulated by an electrodynamical shaker driven by a waveform generator, as shown in Fig. 57. An accelerometer MMA7361L has been used as feedback element in order to have an independent measurement of the acceleration applied to the system. Numerous experimental tests have been performed on the prototype by adjusting the positions of the electrical contacts, in search of the optimal performances for mechanical exciting input signals of

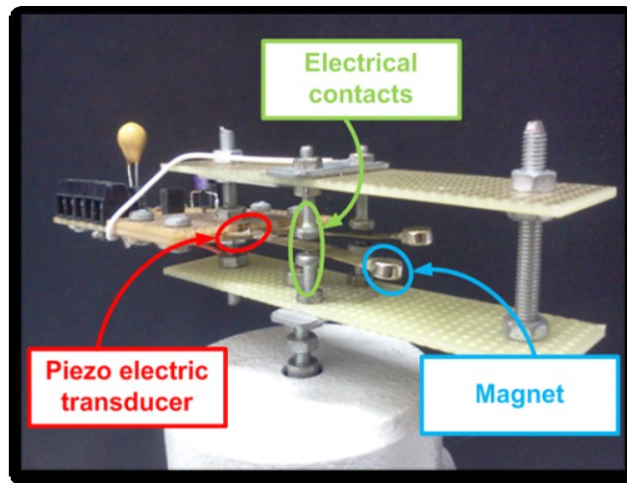various shape (e.g. sinusoidal, noisy, impulsive) and amplitude. The measurement results

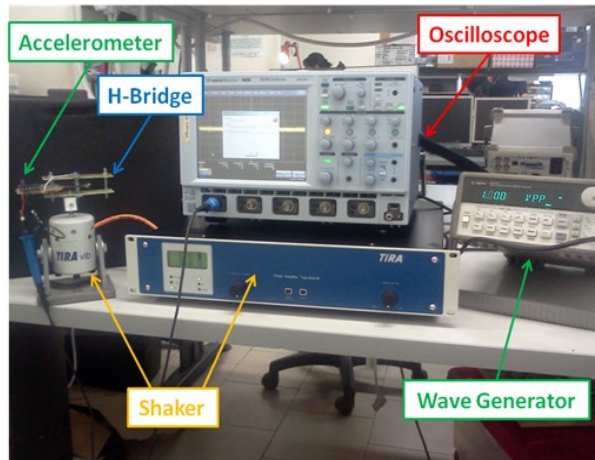**Fig. 56 - Experimental prototype.**

Fig. 57 - Experimental setup.

have demonstrated that the optimal configuration has the stoppers placed close to the middle of the beams with $L = 0.028$ m and $th = 0.001$ m. The parameter th represents the distance between the beam that lies in a stable state and the nearest stopper (see Fig. 58d.). A noisy input signal has been considered here having amplitude of 2.2 g and bandwidth of 450Hz. Fig. 58b and Fig. 58c show the output voltage measured in non optimal conditions where the stoppers are placed either too close (Fig. 58b) or too far (Fig. 58c) from the beam. The optimal positioning of

the stoppers gives a larger output signal as shown in Fig. 58d. Experiments were performed both on a resistive (390kΩ) and capacitive (47uF) load. While the resistive load has been used to demonstrate the voltage rectification working principle as shown in Fig. 58b-d, the capacitor has been used to demonstrate the validity of our approach for energy storing. This is, in fact, the main goal of this device: electrical energy must be collected and stored even with weak piezo electric voltages, thus avoiding the loss due to the diode threshold in conventional rectification schemes.

Configurations

(a)

(c)

127
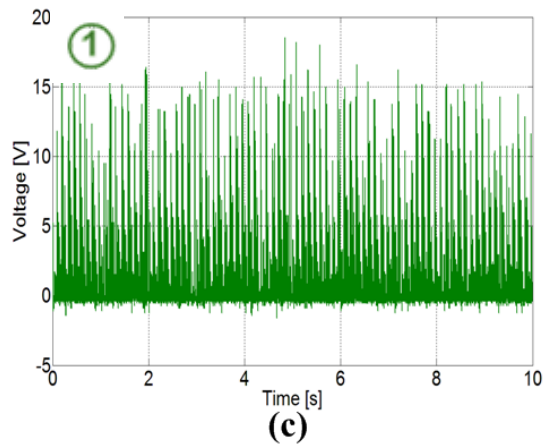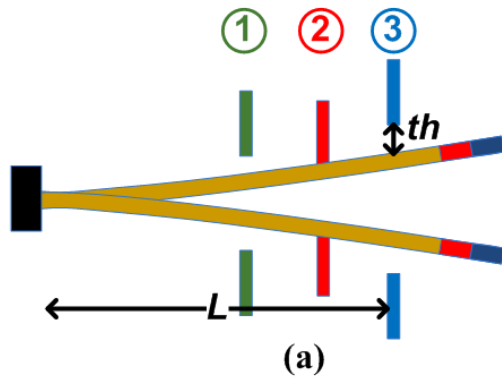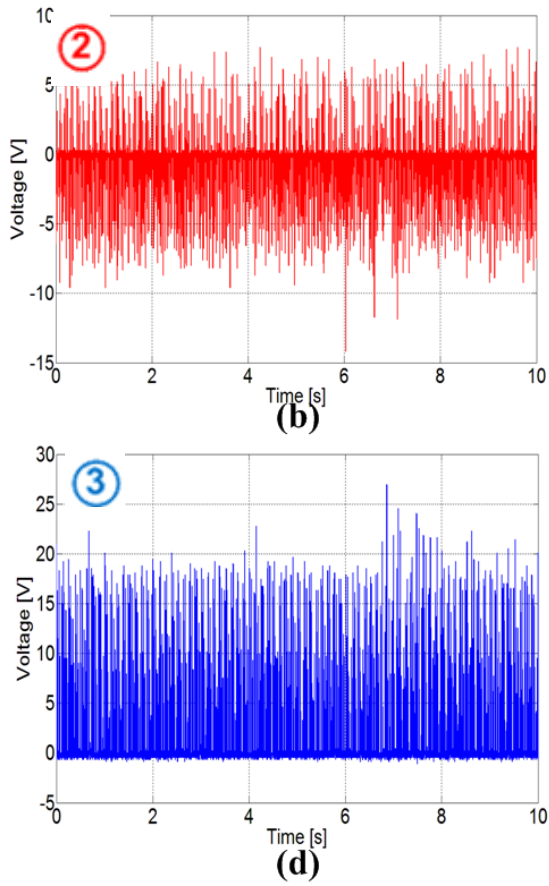
Fig. 58 - PZT output voltage for different placements of the stoppers(identified by the numbers and colors). The optimal placement of the stoppers is obtained in the case (d).
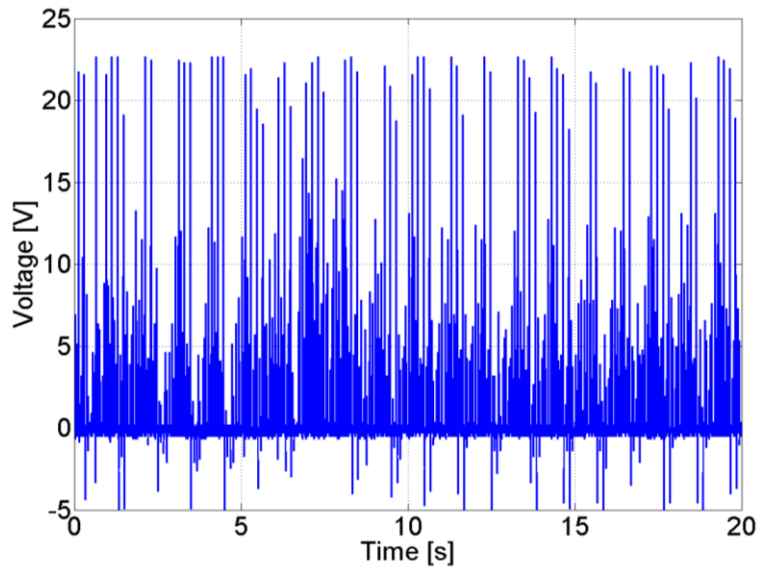
Fig. 59 - Rectified output voltage on a 390kΩ resistive load. Some negative voltage peaks are, clearly, visible.

The system was excited by a noisy vibration acceleration having a 3.03g rms value and 450Hz bandwidth, producing a 7V rms piezoelectric voltage. In Fig. 59 the output voltage is shown as a function of time for the experimental prototype: the experiments reveal some unwanted negative voltage peaks which, in the case of a capacitive load, would result in very little capacitor discharge with respect to the ideal rectified value.

129
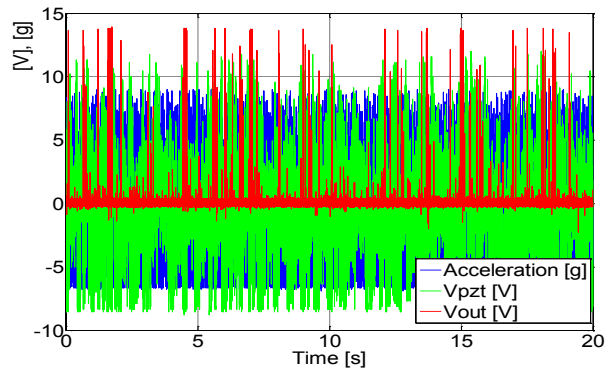
a)
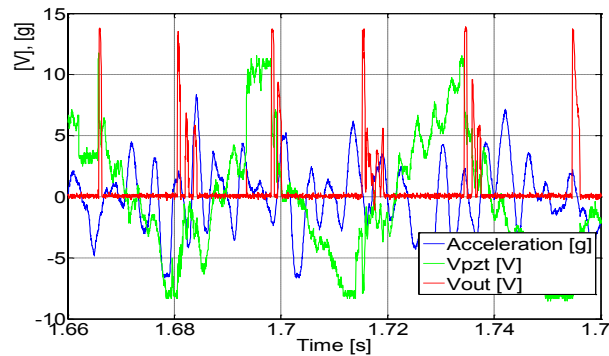
b)

Fig. 60 - Experimental measurements on the mechanical H-bridge rectifier. a) The external acceleration is reported together with the voltage produced by the series of piezoelectric transducers and the rectified output. b) Expanded view where the rectified output voltage (V_{out}) in response to the bistable switching of the coupled cantilever is more evident.

A closer look at the time evolution of signals in the experimental prototype is given in Fig. 60. In Fig. 60a the voltage appearing across the series of the two piezoelectric transducers (see Fig. 48) is shown together with external acceleration and the rectified output voltage across the load resistor. The same signal as in Fig. 60a is exploited in time in Fig. 60b, the working principle is clearly shown: the output voltage shows peaks corresponding to each simultaneous closure of the two switches. The rectifying mechanism shown here is also important whenever weaker signals are involved, as in the case of very small piezoelectric converters or weak vibrations. In these cases, the voltage produced may be well below the threshold represented by the diodes in a conventional rectifier. The approach proposed here, allows for rectifying these weak voltages, as well; in fact, no diodes are involved in our system. Fig. 61 shows that the rectified output voltage can be obtained, also, in the case of very weak piezoelectric voltages provided that the coupled cantilever switches are suitably crafted to allow switching between the two stable states even for small input vibrations. This justifies the

larger efficiency claimed for the mechanical H-bridge (and shown in the left region of Fig. 55) where the presence of diodes inhibit the rectification of weak voltages. The diode threshold will obviously depend on the technology considered, however a threshold will be necessarily always present, the strategy proposed here presents a zero threshold approach. The inserts in Fig. 61 show the voltage transferred by the mechanical H-bridge to the resistive load in the case of sub- threshold voltages; these low voltages would have been wasted with a traditional diode rectifier. Finally, in order to show the ability of the proposed circuit to store energy, a 47nF capacitor has been considered as "load" in the scheme shown in Fig. 48. The same working conditions as in the case shown in Fig. 59 were applied and the time evolution of the voltage across the storage capacitor is shown in Fig. 62. It should be noted that the steady state value is related to the rms value of the rectified piezoelectric output voltage when the circuit is closed: in fact when the circuit is open there is no current flow on the capacitor and the voltage across it can be considered constant.
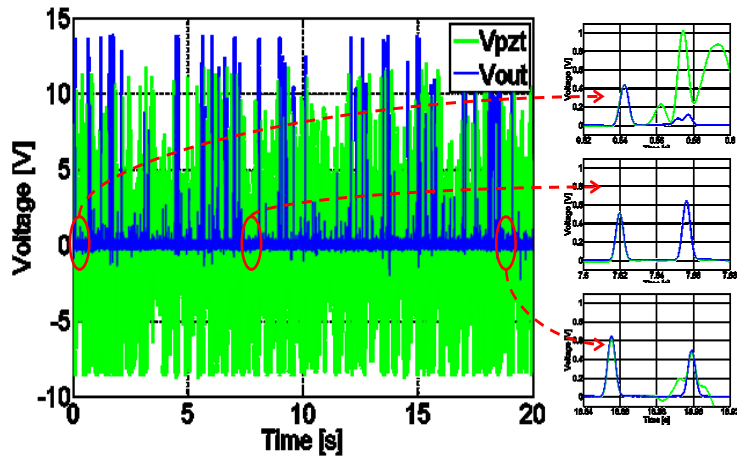
Fig. 61 - Experimental output voltage for the mechanical H-bridge. The inserts show expanded region where weak, sub-threshold voltages are collected and rectified. These sections of the input signal would have been lost in the case of a diode rectifier. The proposed mechanical H-bridge rectifier is, therefore, especially suitable for the use with weak voltages to be rectified provided that the bistable system is suitably crafted to switch with the input vibrations.

133
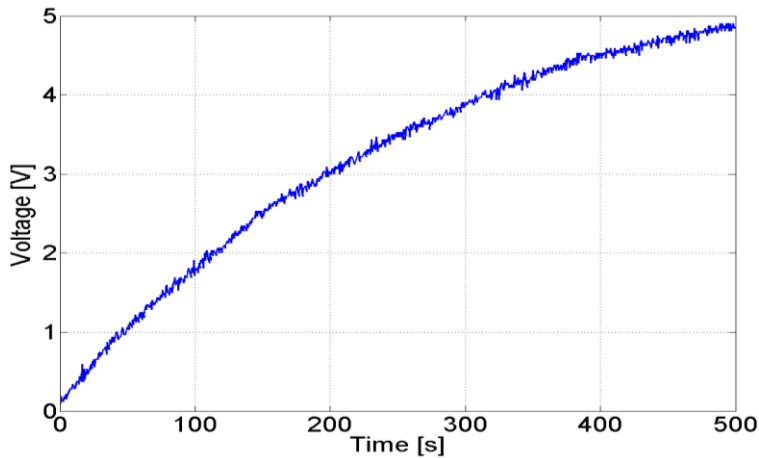
Fig. 62 - Voltage buildup on a 47uF capacitor connected as output load in the mechanical H-bridge rectifier. The trace shows the capacitor voltage when the with the same input as in the case shown in Fig. 60 for a resistive load.

Summarizing, a new energy harvester device is presented in this paragraph. It allows for the collection of energy from widespread random mechanical vibrations thanks to a nonlinear bistable mechanism and implements a rectifying strategy based on an opposite (i.e. anti-phase) configuration of mechanical switches driven by the same input vibrations that induce electric charges into the piezo electric beams. The H-Bridge idea avoids the use of diodes

and their voltage threshold limits. It is, therefore, suitable in affording a route to efficiently provide full wave signal rectification even for very low voltages which would be subthreshold in a diode-bridge underpinned harvester circuit. This is, in fact, the main issue that must be addressed with micro and nano energy harvesting systems in which the dimension shrinkage will, inevitably, result in a reduction in the output voltage. The working principle has been confirmed through extensive numerical simulations; in addition an experimental prototype has provided a validation of the model and its predictions. Further work is in progress in order to develop an integrated device in microsystems technology.

3.2. A diode-less mechanical voltage multiplier: a novel transducer for vibration energy harvesting.

Voltage rectification is one of the most important issues in a lot of microelectronics and micro-systems applications: usually, a simple voltage rectifying mechanism is not sufficient to satisfy the requirements, especially when a higher level than the simple rms (root means square) input value is required. Typically, capacitors and diodes suitably interconnected in networks are used in order to obtain the desired multiplication effect. An example is shown in Fig. 63, where a circuital configuration known as Villard Cascade is shown: these kind of solutions are limited by the presence of diode thresholds that must be overcome by the input signal in order to guarantee a correct work. It is clear that in the specific conditions characterized by input voltage signals under diode activation threshold, the classic Villard Cascade approach, based on diodes, is not able to provide any output voltage. Innovative solutions are needed to avoid the use of diodes: starting from this consideration the proposed approach has been developed and will be shown below.
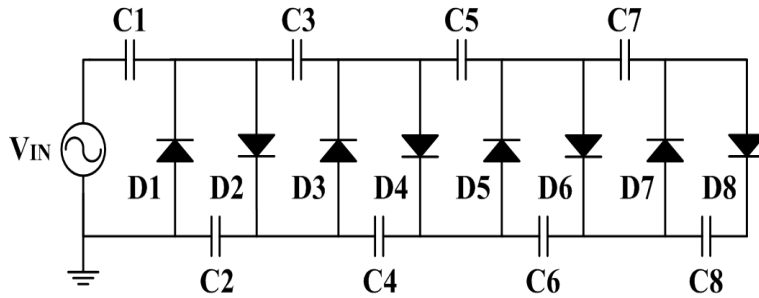
Fig. 63 - Electrical schematic of the classic diode based voltage multiplier, also called Villard cascade.
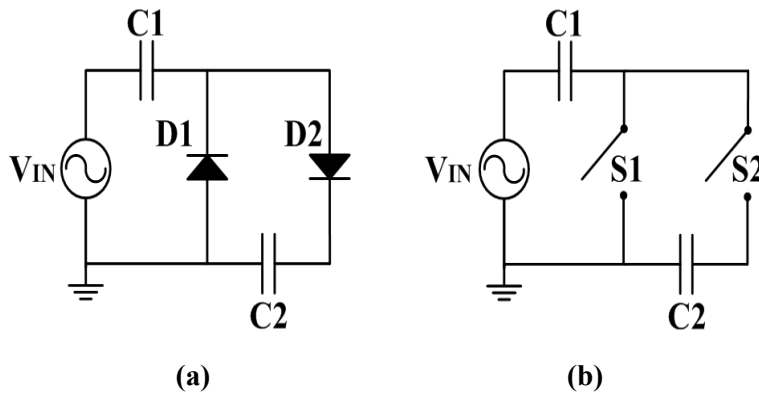

(a)   **(b)**

Fig. 64 - Comparison between the single cell of traditional voltage multiplier (a) and the proposed approach (b): the switches replace the diodes emulating their behavior, but no voltage threshold has to be overcome.

Let us consider a single cell (Fig. 64a) of the network shown in Fig. 63. The basic idea of the novel approach is to replace diodes with a couple of mechanical switches (Fig. 64). The working principle is based on the anti-phase behavior of the switches, according to the sign of the input voltage, thus emulating diodes behavior: specifically, considering Fig. 64, if V_{IN} is negative, S1 is closed and S2 open as it would be for D1 and D2, while if V_{IN} is positive the two switches will reverse their configuration. In electromechanical systems, vibrations are often used as energy source; there are several mechanisms used to transform mechanical energy to electrical, for example the piezoelectric transduction [73], according to which if a piezoelectric transducer is placed into an oscillating systems it provides an alternate voltage source as shown in Fig. 64.

Referring to Fig. 65, if there is no input acceleration the piezoelectric voltage is zero, the switches are open so no current flows through the circuit and no charge appears at the capacitors (Fig. 65a); when an input acceleration
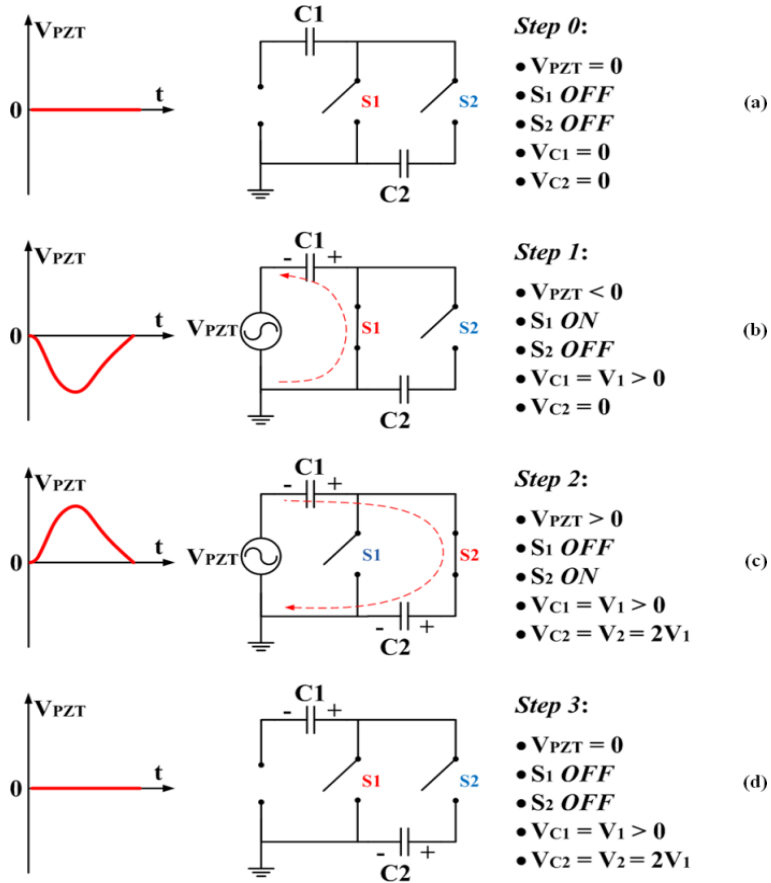
Fig. 65 - The circuital equivalent of the proposed system: (a) No piezoelectric input voltage is produced and the switches are open, C1 and C2 are discharged; (b) the piezoelectric voltage is negative, S1 is closed and S2 open so a current flows through C1 and V_{C1} is positive; (c) the piezoelectric voltage is positive, S1 is open and S2 closed so a current flows through C1 and C2 and V_{C2} is positive (close to $V_{PZT} + V_{C1}$); (d) V_{PZT} is zero and the switches are open again so the voltage across C2 is maintained.

139

occurs, providing a piezoelectric voltage negative, S1 is closed, S2 open and a positive current flows through C1 in the sense of the arrow so C1 is charged with a positive voltage V_{C1} (Fig. 65b). In the following step (Fig. 65c) the piezoelectric voltage is positive, S1 is open and S2 closed so C2 is charged with a positive voltage V_{C2} obtained adding V_{PZT} with V_{C1}; finally, in the last step, the input acceleration disappears, both of the switches are open, and a positive voltage is maintained across C2 (Fig. 65d). The maximum value achievable for V_{C1} is ideally the rms value of the piezoelectric voltage and V_{C2} is $2 \cdot V_{PZT}$ (rms): connecting *n* cells in cascade and repeating the same considerations as for the single cell, a $2 \cdot n \cdot V_{PZT}$ (rms) can be obtained (Fig. 66). The goal of the proposed approach is to realize a 4-stage mechanical voltage multiplier: it is based on the use of 4 cantilever beams with 4 couples of stoppers that implement the mechanical switches and another beam (together with a piezoelectric transducer) used for generating an alternate voltage where each cantilever can be modeled with a second order mass-spring-damper system.

140

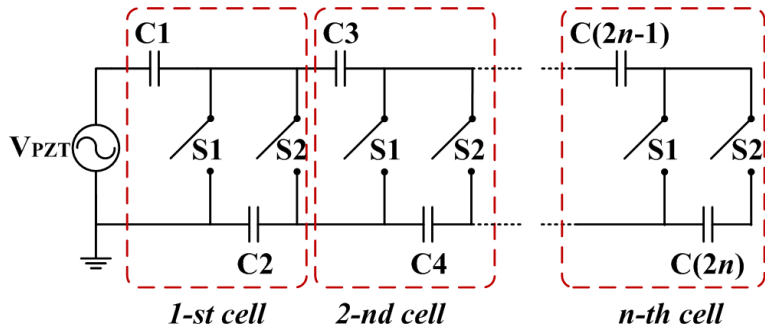**Fig. 66 - The system obtained connecting n cells of the single stage**
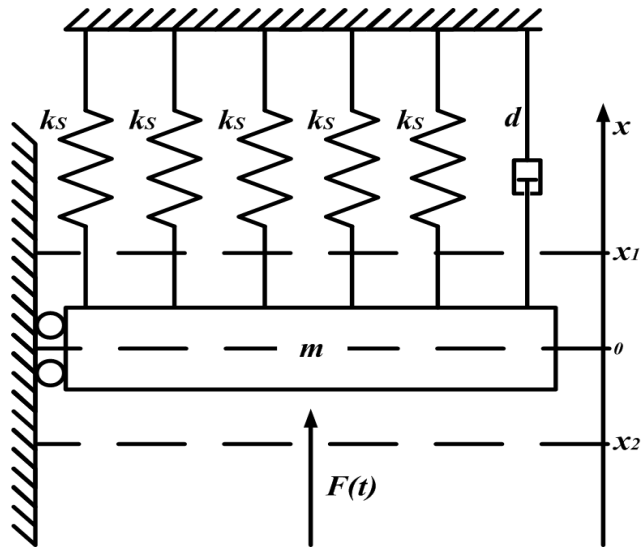

Fig. 67 - A second order mass-spring-damper system has been used to represent the mechanical part of the proposed system. Each cantilever beam is considered having an elastic constant k_S; since the springs are in parallel configuration, the whole of the system will have an elastic constant given by $k = 5 \cdot k_S$.

141

In order to implement the synchronization mechanism between every couple of switches (as better explained in Section III), the beams can be joined by a single mass on their free tips as the schematic system in Fig. 67 shows. In this case the beams can be considered as 5 parallel springs, each of them characterized by an elastic constant k_S, so that in the model it's possible to summarize the 5 beams with a single spring with $k=5 \cdot k_S$. Furthermore the system has been analytically modeled in order to evaluate both the mechanical and the electrical behavior through numerical simulations. As explained before a mass-spring-damper equation has been used to model the mechanical part of the system, capable to oscillate in response to an external mechanical stress (such as a vibrational input); an additional equation has been introduced to take into account the piezoelectric transduction effect, as shown in (3.4) [69]:

$$\begin{cases} m\ddot{x} + d\dot{x} + kx + d_{pzt} V_x = F(t) \\ \dot{V}_x = k_{pzt}\, \dot{s} - \Gamma V_x \end{cases} \qquad (3.4)$$

x, $\dot{x}$ and $\ddot{x}$ represent displacement, velocity and acceleration of the mass m respectively while k and d the elastic constant and the damping coefficient, V_x and $\dot{V}_x$ are the piezoelectric voltage and its first derivate, d_{pzt}, k_{pzt}, Γ, take into account the transduction and in particular are related to the piezoelectric damping effect, the material, the dynamic response respectively, $F(t)$ and $\dot{\bar{s}}$ are the external input mechanical force and the derivate of the strain according to Castigliano's Theorem [**70**]. In absence of external mechanical input, the mass m lies in the x = 0 plane, all the switches are open (OFF) and the piezoelectric transducer doesn't produce any output voltage; when an external input with sufficient amplitude occurs the mass starts oscillating and a piezoelectric output voltage is generated in accordance to eq. (3.4). The switching mechanism is implemented taking into account the mass position: it is assumed that the switches S1 and S2 close (get ON) when the mass reaches a well defined positive and negative position respectively. The parameter values used in simulations are shown in Tab. 4.

Tab. 4 - System parameters; the labels "Estimated", "Calculated" and "Identified" mean that the value has been evaluated respectively through direct measurements, analytical formula, and the Nelder-Mead Simplex Method.

Name	*Value*	*Units of measurement*	*Details*
m	*0.00511*	*kg*	*Estimated*
k	*59*	*N/m*	*Calculated*
d	*0.0024*	*Ns/m*	*Calculated*
d_{pzt}	$1 \cdot 10^{-7}$	*N/V*	*Identified*
k_{pzt}	$1.1299 \cdot 10^{9}$	*V/m*	*Calculated*
Γ	*2030*	s^{-1}	*Calculated*

The implemented model refers to a four stages voltage multiplier. Simulations have been carried out in Simulink. In order to evaluate the dynamical behavior, the system has been stimulated with a sinusoidal input acceleration having amplitude of 1.06 g (rms) and frequency of 15.6 Hz (Fig. 68); a 0.92 V (rms) piezoelectric voltage (Fig. 69) has been obtained and used as input for the mechanical multiplier; moreover it has been chosen a capacitance values of 1 μF to realize the voltage multiplication and a resistance values of 3.95MΩ to take into account the losses due to the contacts of the switches and the read-out set-up.
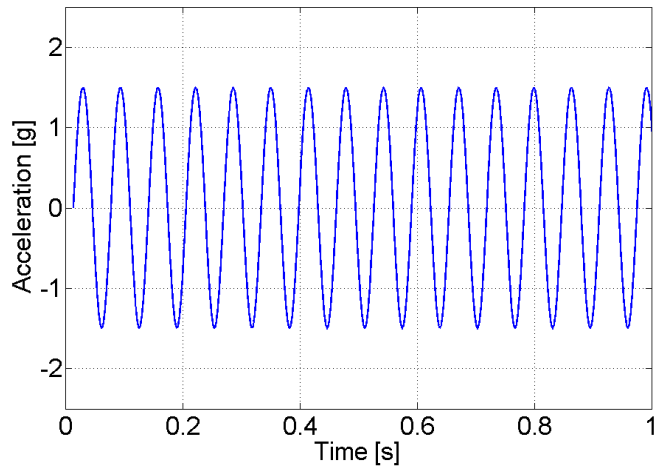
Fig. 68 - The simulated input acceleration.
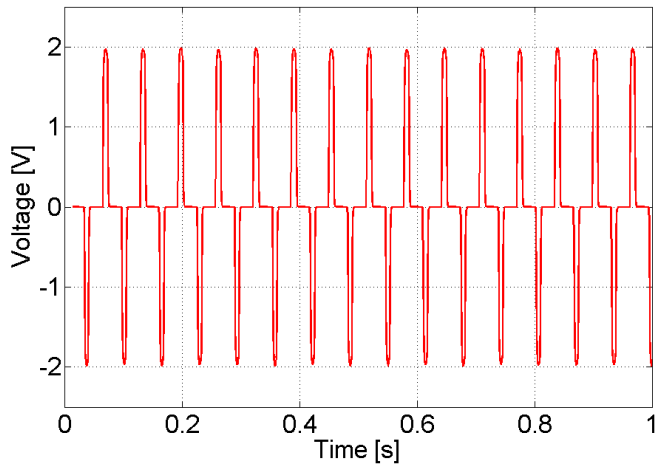
Fig. 69 - The simulated piezoelectric voltage obtained exciting the system with the input acceleration described in the previous figure.

145
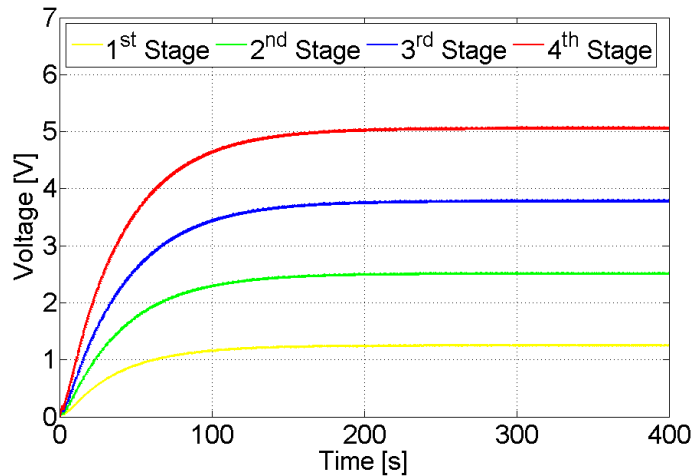
Fig. 70 - The simulated output voltages of a 4-stage mechanical voltage multiplier; results are shown for 400 seconds with 1µF capacitors.

The simulated output voltages are shown in Fig. 70. Some simulations have been carried out to show the current flowing through the capacitors, in order to analyze the differences between the proposed approach and the classical voltage multiplier based on diodes: these simulations have highlighted that the currents flow in the same direction in both the approaches, except for a little contribution due to the not unidirectional behavior of the mechanical switch unlike diodes (Fig. 71).
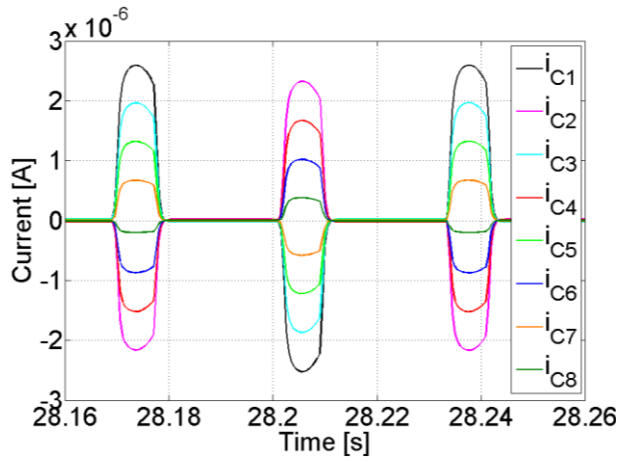
(a)
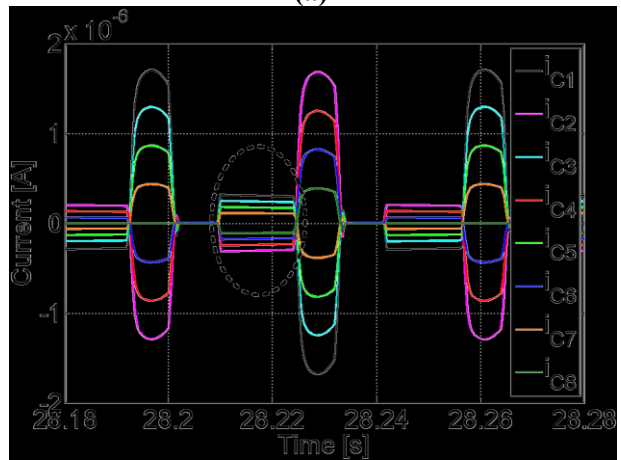
(b)

Fig. 71 - (a) Simulated currents flowing through the capacitors in the classical diode based voltage multiplier, having 0.8 diode threshold and 1μF capacitors. (b) Simulated currents flowing through the capacitors in the proposed mechanical voltage multiplier, having 1μF capacitors.

There isn't a way to reduce the reverse current because the mechanical switches (differently from diodes) are not unidirectional and the open and close phases depends on the geometrical configuration of the system and from the vibrational external input. The presence of these reverse currents explains why the steady-state values for DC output voltages of every single stage are obtained by multiplying the RMS value of the input voltage rather than its peak value as it would be into a standard Villard Cascade circuit.

A laboratory prototype of the presented system has been fabricated in order to experimentally demonstrate the validity of the proposed approach: it is composed of five cantilever beams having their own free tips constrained to the same proof mass m of 0.00511 kg (Fig. 72) in order to guarantee an univocal and synchronized motion direction. The beams are made of brass, and each one has the following dimensions: length of 77 mm, width of 4 mm, thickness of 0.2 mm. The piezoelectric transducer, made of a PZT (Lead Zirconate Titanate), has been placed in the maximum strain region of the central beam in order to
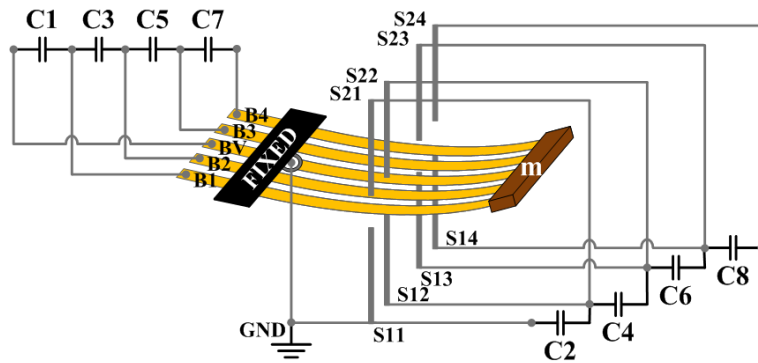
Fig. 72 - The schematic representing the whole of the electro-mechanical system.
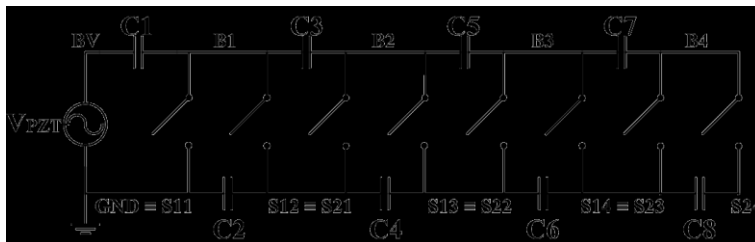
Fig. 73 - The electrical schematic of the proposed 4-stage mechanical voltage multiplier, with the correspondence of each electric junction with respect to the mechanical scheme of the previous figure.

optimize the output amplitude voltage; all the cantilevers, except the central one, are employed to implement the switching mechanism, each one together with a couple of conductive stoppers while the central cantilever is electrically connected with the piezoelectric transducer in order to generate an alternate voltage coherent with the switching phases. Assuming x=0 the rest position, the output voltage is positive (negative) when the cantilevers get up (down), S2i (S1i) are closed and S1i (S2i) open.

Fig. 72 and **Errore. L'origine riferimento non è stata trovata.** show the electrical schematic of the whole of the system and how beams, stoppers, transducer and capacitors have been connected in the prototype.

The fabricated prototype is shown in Fig. 74. The experimental setup used in order to carry out measurements and to validate the proposed multiplying strategy is shown in Fig. 75: it includes an electro dynamical shaker driven by a signal generator used to give the vibrational input, an accelerometer MMA7361L used as feedback element in order to independently estimate the

applied acceleration, two digital oscilloscopes used to show and acquire the signals of interest.
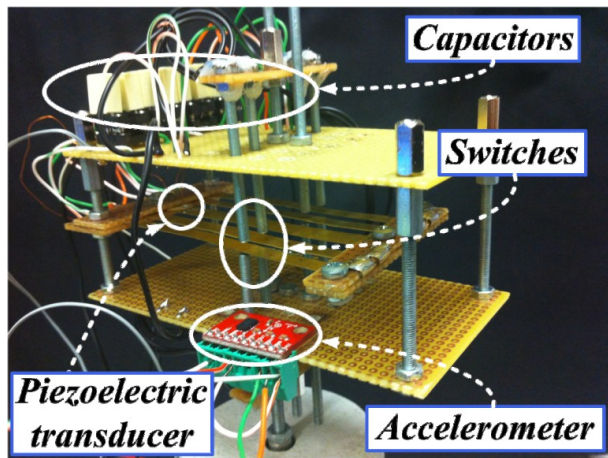
Fig. 74 - The experimental prototype.
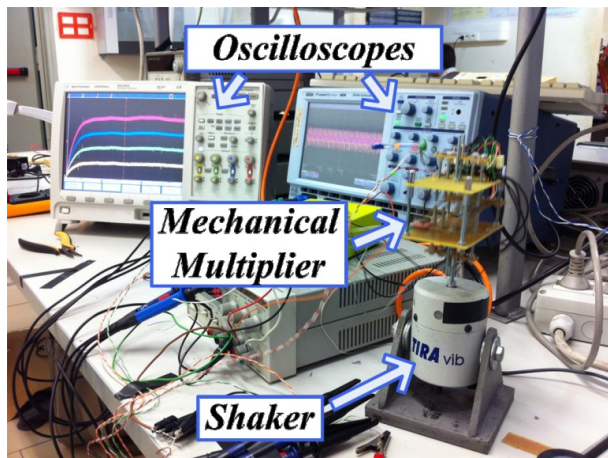
Fig. 75 - The experimental setup.

Some preliminary tests have been carried out in order to verify that the switches close at the same time as it has been previously described: DC voltages of 5 and -5 V have been forced to the stoppers S2i and S1i respectively and the voltage on the beams acquired. Experimental results (continuous colored lines), compared with simulations (dashed black lines), shown in Fig. 76, have confirmed the correct behavior of the mechanical switches: as it can be seen, Fig. 76 shows the presence of a lot of glitches; this effect is due to the realization of the prototype, and in particular to a little misalignment between the stoppers and the plain where cantilevers lie and to the rebounds during cantilever-stopper contact too. Therefore this effect, how it can be seen, does not significantly affect the overall device performances.

The experimental results are shown in Fig. 77, Fig. 78 and Fig. 79. Experimental results demonstrate that the novel multiplication mechanism here proposed shows very good performance, confirming hypothesis and simulations as it

can be seen in the comparisons shown in Fig. 79, Fig. 80 and Fig. 81.
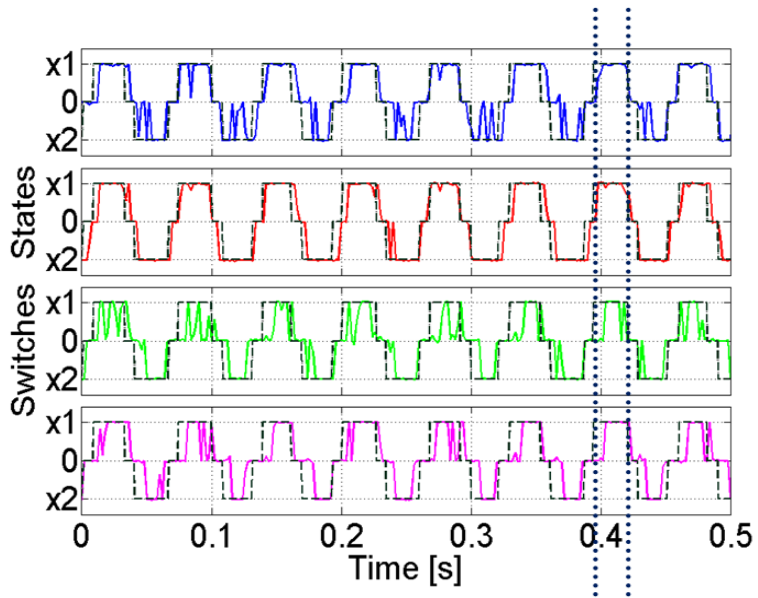
Fig. 76 - Experimental results showing the switching phases for every couple of switch. The correct behaviour of the system can be demonstrated thanks to the observed contemporary of the contacts. The figure shows also a comparison between experimental (continuous colored lines for each switch) and simulations (dashed black lines).
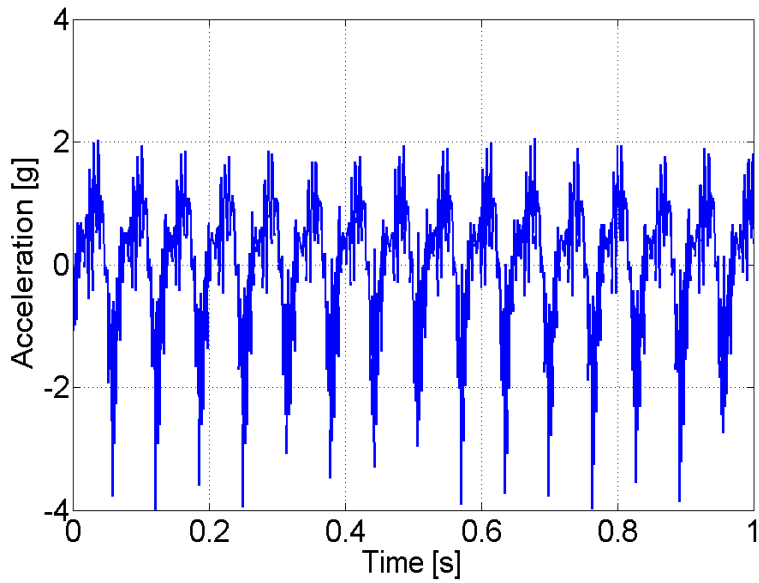
Fig. 77 - Experimental acceleration: the driving signal set to the shaker is a sinusoid with a frequency of 15.6 Hz and an amplitude of 1.06 g(rms), while the noisy signal shown is the feedback measured by the accelerometer MMA7361L.
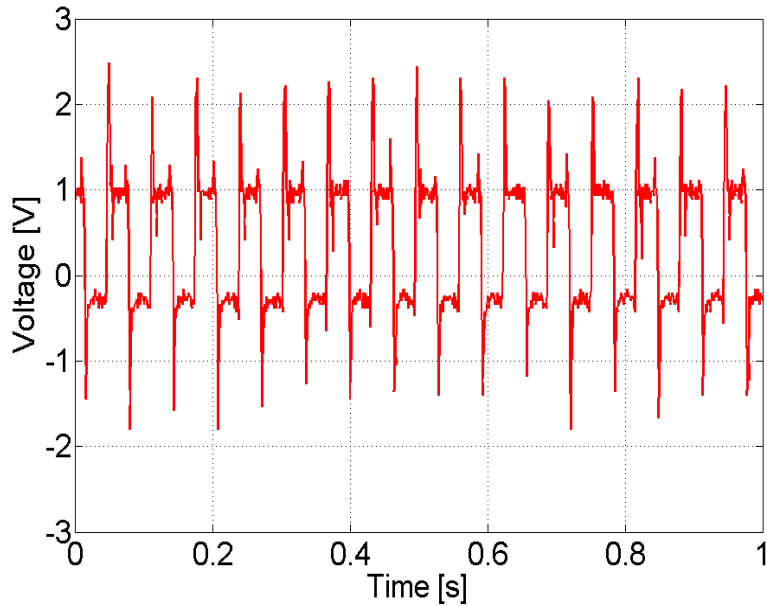
Fig. 78 - The experimental piezoelectric voltage obtained exciting the system with the input acceleration described in the previous figure. The impulsive behaviour caused by the impacts is observed here, as in the simulation tests. The rms value is 0.87 V(rms). The offset in the signal is due to the deformation of the beams (on which the piezoelectric layer is placed) caused by the impact with the mechanical stoppers that are not perfectly symmetric.
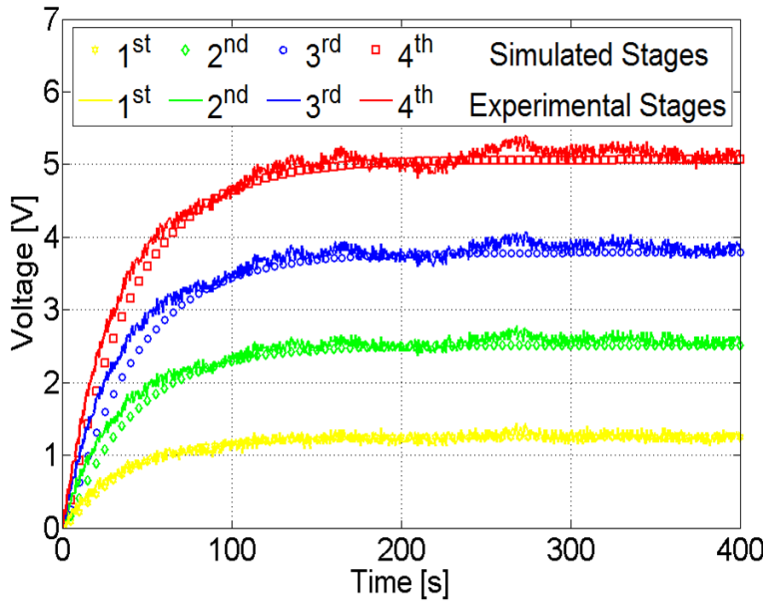
Fig. 79 - Comparison between experimental (colored shapes) and simulated (colored continuous lines) output voltages. The experimental output voltages of the 4-stage prototypal mechanical voltage multiplier; results are shown for 400 seconds with 1µF capacitors. The 4th stage capacitor is charged with a voltage level higher than the input one. The multiplication effect is demonstrated.
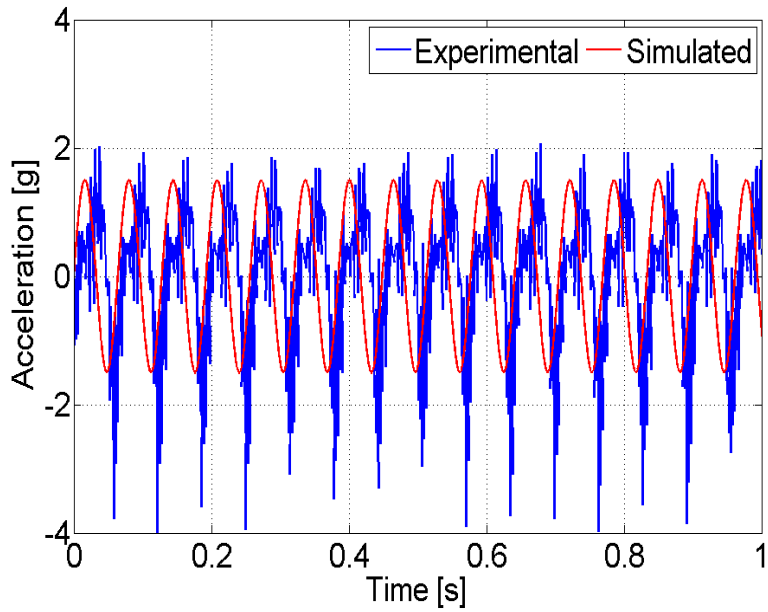
Fig. 80 - Comparison between experimental (blue line) and simulated (red line) input acceleration.
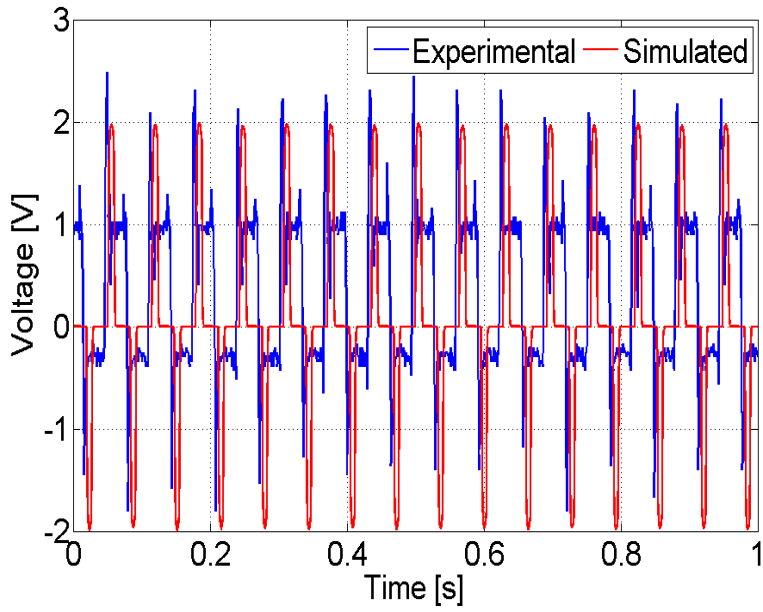
Fig. 81 - Comparison between experimental (blue line) and simulated (red line) piezoelectric voltage.
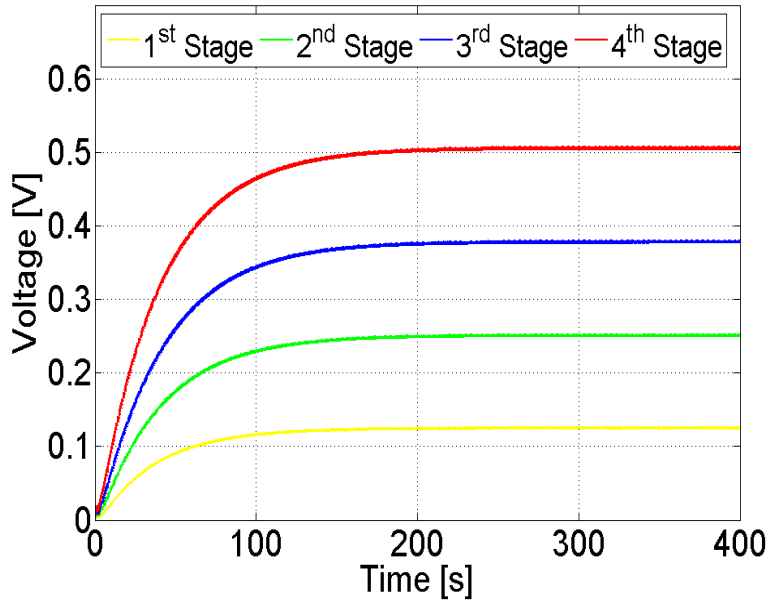
Fig. 82 - The simulated output voltages of a 4-stage mechanical voltage multiplier when PZT voltage is under diode threshold (peak value of about 0.2 V and RMS value of about 0.1 V). Results are shown for 400 seconds with 1μF capacitors.

As already discussed at the end of section II, the RMS value of the voltage produced by the piezoelectric transducers must be taken into account: this voltage has been measured in our prototype being equal to 0.87 V. Each voltage multiplication stage should produce therefore a DC output voltage equal to 2*n*Vin (RMS), that is

159

ideally 1.74 V for the first multiplication stage (n=1) and 6.96 V for the 4-th one (n=4). During the measurements campaign losses occurred due to the readout setup, to the parasitic resistive effects of the contacts cantilever/stoppers, so the measured output voltages at the first and the 4-th stages resulted into lower values than expected (respectively 1.25 V and 5 V). These losses are proportional with both the number of multiplication stages and the input voltage, it has been modeled therefore as a resistive loss in the device model. The piezoelectric transducer used in order to fabricate the macro-scale laboratory prototype allows obtaining output voltages over the classical diode threshold (0.7 - 0.8 V) as shown in Fig. 78. However the method proposed in this paper can be adopted even in the case of very low voltage multiplication, where the classical diode based approach doesn't work because the diode activation threshold has to be overcome; this latter case has been investigated and simulation results are shown in Fig. 82.

In conclusion, this paragraph concerns the development of a novel solution for vibration energy harvesting: in particular here a strategy for multiplying voltages based on mechanical switch instead of diodes is presented. This issue of avoiding the use of diodes is one of the most important addressed in scientific community because the reduction of devices sizes inevitably results in a drop of voltage levels. The system has been designed, modeled, simulated and experimentally tested using a laboratory prototype which has confirmed the validity of the working principle; moreover, the case of very weak voltages has been successfully studied through numeric simulations. Further efforts are in progress to study an integrated solution in order to fabricate a device in MEMS technology.

3.3. "Vibration driven" mechanical switches: a novel transduction methodology with applications to DC-DC "diode-less" voltage multipliers.

The main goal of the proposed device is to multiply DC voltages in order to obtain desired and suitable levels. The system has a DC input voltage and *n* DC output voltages, where *n* represents the multiplication factor. Each stage is composed of cantilever beams and stoppers, together with capacitors connected in a suitable way, that allow the system to provide the desired effect. Fig. 83 shows the diagram of the proposed system with respect to the classical approach. The second block (the multiplication stage, composed of diodes and transistors in the typical techniques) is replaced by a fully mechanical vibration driven system, also including storage capacitors. In Fig. 84 a complete schematic representation of the designed system, has been reported: this figure shows the details of the designed system including the connections between stoppers, capacitors and DC input voltage source (the number of stage can be increased).

162
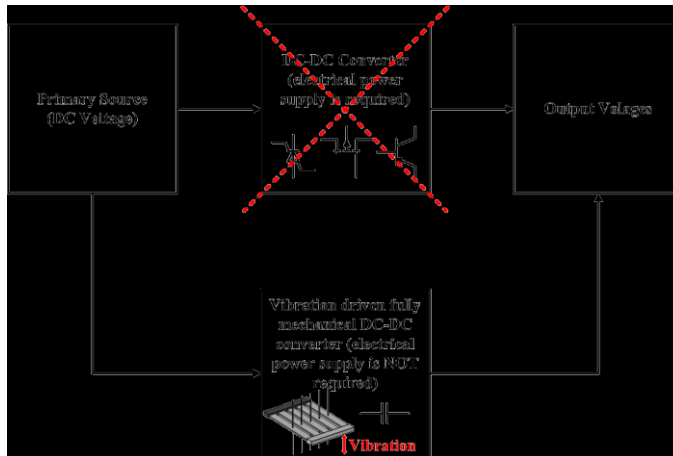
Fig. 83 - Block diagram of the presented system with respect to the classical approaches, based on diodes and transistors.
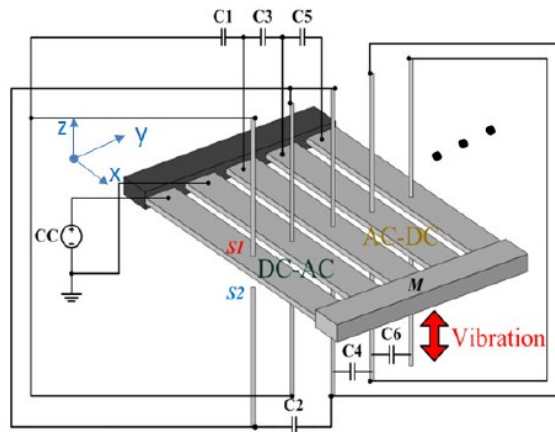
Fig. 84 - Generic electromechanical scheme of the system. The switch mechanism is implemented by using the contact between a conductive beam and two stoppers in orthogonal position with respect to the plane xy.

163
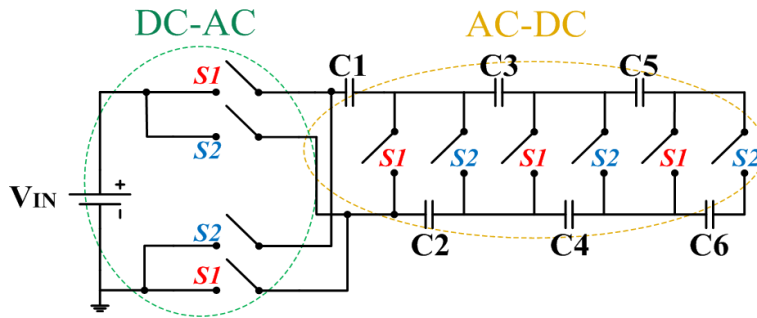
Fig. 85 - Generic electrical scheme (the number of stage can be increased): the switches are driven by two different alternating phases, S1 and S2. The first two couple of switches implement the DC-AC conversion while the remaining three couples realize the AC-DC conversion and the voltage rise. Typically the capacitors C1, C2…. have the same capacitance value, in order to maintain the same multiplication factor.

The corresponding circuital configuration of the DC-DC converter is shown in Fig. 85.

As it can be seen, the entire converter can be divided into two main sections: the first is a DC-AC converter that transforms the DC input voltage into a square wave through the alternation between S1 and S2 phases, the second one is composed of mechanical switches and capacitors useful to multiply the AC voltage coming from the first section and in order to obtain the DC transduction. The working principle of the transducer can be
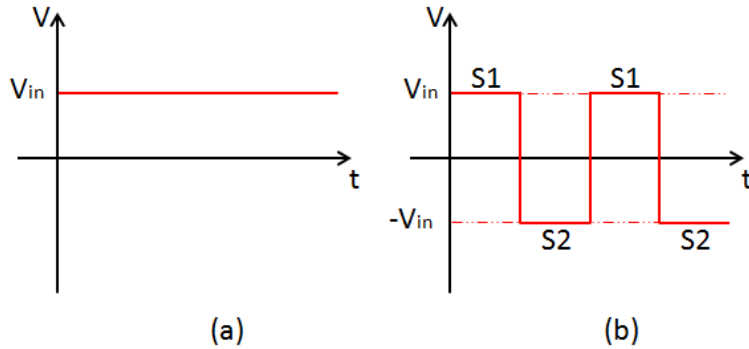
Fig. 86 - Ideal behavior of DC-AC section in the DC-DC proposed solution. (a) DC voltage input, and (b) square wave.

summarized as follows: in absence of external vibrations (absence of displacement), all the cantilever-stopper contacts are open; the output voltage provided at the outputs of the converter is zero. When external vibrations occur, the cantilevers begin to oscillate along the z axis; as consequence the stoppers will alternatively bump on the top and on the bottom of the plane xy; the corresponding electrical contacts are closed in phase opposition (S1 and S2 are used here to identify the two phases). The first two mechanical switches (two cantilevers and the four corresponding stoppers) are exploited in order to realize

the DC-AC conversion: during S1 phase, the DC input voltage presents positive sign while during S2 the polarity is exchanged (the sign is negative). The obtained effect is a similar to a square-wave voltage signal (see Fig. 86). The voltage can be multiplied in order to obtain the desired levels exploiting the rest of the mechanical switches. It must be observed that traditional voltage multiplier [74] [75] are based on diodes and capacitors connected in a suitable way. However these kind of solutions have limits due to the presence of diodes threshold to be overcome in order to obtain an output voltage. The approach here proposed do not require diodes and it exploits vibration energy in order to realize a fully mechanical voltage multiplication effect [76]: in the proposed solution, in fact, the AC voltage multiplication is also fully mechanically obtained. Always taking into the account the phase of S1 and S2 previously introduced: the first two mechanical switches provide the conversion of the input voltage fro DC to AC, while the rest of the switches provides to rectify and multiply the voltage [76]. The novel approach proposed is suitable to realize

vibration driven mechanical DC-DC transducers based on mechanical switches (passive elements) addressed to implement low power device (i.e. WSNs, disseminated and autonomous measurement systems) and low leakage voltage multipliers. Furthermore, the DC voltage source to be multiplied, can be under diodes threshold in fact here no diodes are required. The system proposed has been analytically modeled by using a second order mass-spring-damper system, see equations (3.5).

Each cantilever has a spring constant k_c, furthermore the beams are connected in parallel. A common inertial mass (*m*) has been located at the tip of the oscillating structure in order to synchronize the open and closed phases, so that the entire system has a spring constant equal to $k = 5k_c$. Assuming a damping constant *d*, an external vibration source *F(t)*, the equation of the motion of the system has been modeled as follows:

$$\begin{cases} m\ddot{x} + d\dot{x} + kx = F(t) \\ \quad V(i)_{out} = 2iV_{in} \end{cases} \tag{3.5}$$

Tab. 5 - System parameters; the labels "Estimated" and "Calculated" mean that the value has been evaluated respectively through direct measurements, analytical formula.

Name	Value	Units of measurement	Details
m	*0.0376*	*kg*	*Estimated*
k	*333.6*	*N/m*	*Calculated*
d	*0.0024*	*Ns/m*	*Calculated*

Where *i* represents the *i-th* multiplication stage. The switching mechanism is implemented taking into account the mass position, in particular it has been assumed that the switches S1 and S2 are closed/open when the mass reaches a well defined positive and negative position respectively, neglecting bump, transient effects and nonlinear contribution of the stoppers. The parameter values used in simulations are shown in **Errore. L'origine riferimento non è stata trovata.**, while Fig. 87 shows simulations results obtained implementing equations (3.5) through matlab simulink and considering a four stage structure has been considered. The prototype used is composed of a four stages DC-DC voltage multiplier

useful to describe and demonstrate the basic working principle, however an *n* stages multiplier can be
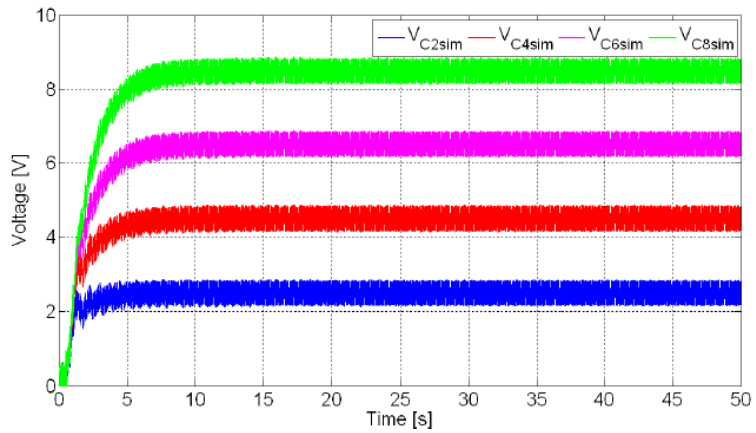
Fig. 87 - Simulated voltages obtained by numerical simulations.
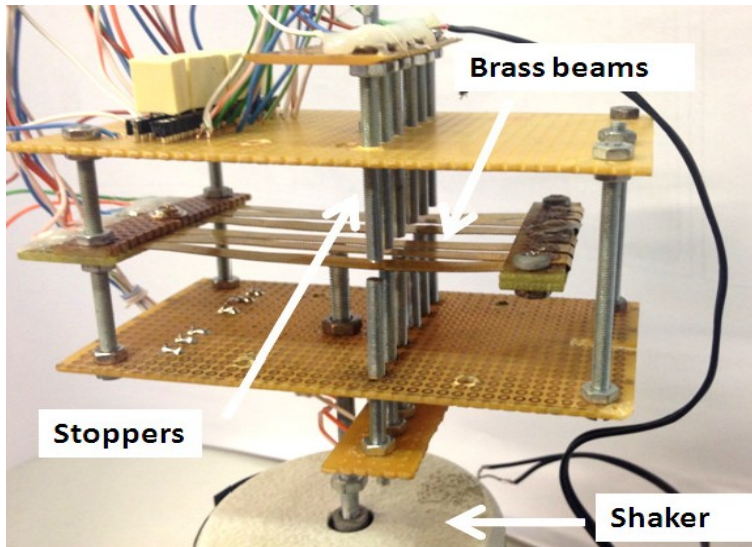
Fig. 88 - Laboratory prototype.

**easily obtained assuming *n* stages cascaded [76]. The laboratory
prototype has been fabricated in order to validate the model and the
desired behavior. The DC-DC converter consists of 6 brass beams with an
inertial mass located at the tip. A pair of conductive stoppers for each
cantilever have been placed along the oscillation direction. A capacitor of
A capacitor of 1µF has been used as output load (C1…C8). The prototype
(C1…C8). The prototype has been shown in**

Fig. 88. Several input amplitudes have been considered, in
particular Fig. 89 shows the measured performed using a
DC voltage of 1V while an harmonic vibration of about
15Hz (that corresponds to the mechanical resonant

frequency of the oscillating system) has been imposed as mechanical stimulus through an electro-dynamic shaker. Summarizing, a novel solution for the multiplication of DC voltages based on vibration driven mechanical switches have been designed, modeled, simulated and experimentally tested. Here, the vibrational energy is exploited to open and close a series of mechanical switches composed of cantilever and stoppers.
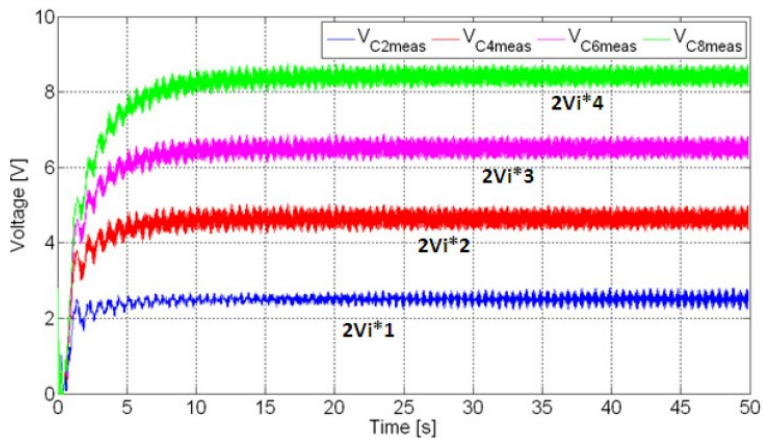
Fig. 89 - Experimental results considering an input voltage Vi=1V. As it can be seen tests validated the expected working principle.

A laboratory prototype has been fabricated in order to validate the working principle and experiments have shown good performance and agreement with the model.

The proposed device is fully passive, in fact no transistors have been used, and furthermore it is able to correctly work with input voltages under the diode threshold because no diodes are required. All these features make the proposed solution suitable for micro and nano low power systems. The future activities will include an exhaustive characterization of the proposed mechanical transducer.

Chapter 4

Devices miniaturization: technologies for piezoelectric MEMS

In this chapter two technologies to fabricate linear and bistable piezoelectric devices will be introduced. Then, rapid prototyping solutions for nanotechnology devices and centimeter size components based on FIB milling will be proposed. The acronym MEMS means Micro Electro Mechanical Systems; it is referred to the whole of technologies for the integration and the miniaturization of electro-mechanical elements. Usually, MEMS physical dimensions go under the millimiter. Various type of MEMS can be found in literature: sensors, actuators, etc. MEMS with mechanical moving elements are the most interesting in energy harvesting applications because they are potentially able to oscillating in response to a vibrational mechanical input. This characteristic is very important because it represents the first step in the energy conversion from mechanical to electrical, as explained in

the chapter above. At first, MEMS have been fabricated by adapting microelectronics technologies (for example CMOS); however the wide diffusion of micro devices, the good performances showed, and the progresses in engineering, physics and chemistry have induced researchers and companies to modify some process and also to develop custom technologies for MEMS fabrication (for example BESOI, MetalMUMPS, ThELMA). In nonlinear piezoelectric energy harvesting from vibrations there are two main issues: the nonlinearity of the mechanical structures and the need of a piezoelectric layer. As regard mechanical structures, several strategies can be employed in order to obtain the desires nonlinearity (for example axial preload, permanent magnets, etc.); for the piezoelectric layer, fabrication processes have to be properly engineered in terms of materials, sequence of material etc. Two processes, PiezoMUMPS® and Radiant pMEMs®, will be briefly described here because they have been investigated in the research activity described in this work.

4.1. PiezoMUMPS® process

PiezoMUMPs® is a multi-user process provided by MEMSCAP® under the program MUMPs (Multi-User MEMS Processes). PiezoMUMPs® process has been introduced by MEMSCAP® during the 2013 and is designed for general purpose micromachining of piezoelectric devices in a Silicon-On-Insulator (SOI) framework for sensors, actuators and energy harvesters [**77**]. The cross-section of this process is showed in the schematic in Fig. 90. A silicon-on-insulator wafer, having the following characteristics, is used as the starting substrate:

- silicon layer thickness: 10μm

- oxide layer thickness: 1μm

- handle wafer (Substrate) thickness: 400μm

The Substrate can be patterned and etched from both the top and the bottom side, so that suspended structures can be fabricated. The silicon layer can be also used for mechanical structures; furthermore it can be employed for fabricate resistors and, as it is doped, for electrical routing too.

175

🟥 Silicon	🟦 Substrate	🟩 Bottom Oxide	⬜ Pad Metal
⬛ Oxide	🟦 PiezoMaterial	🟨 Pad Oxide	
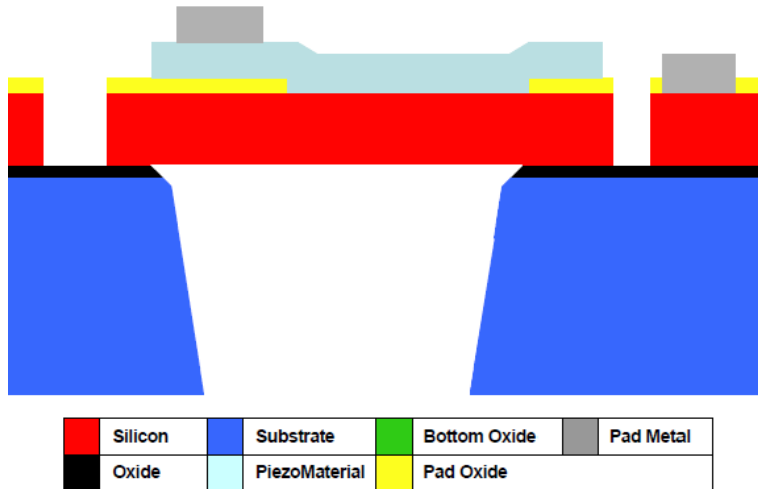
Fig. 90 - Cross section of the PiezoMUMPS® process.
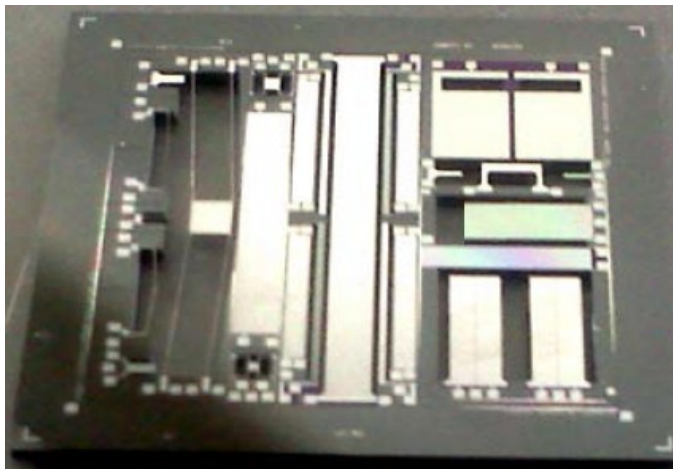
Fig. 91 - PiezoMUMPS® process die with several linear and nonlinear devices.

176

A piezoelectric layer, made of aluminum nitride (AlN), allows for the development of piezoelectric sensors. A 1μm thick aluminum layer deposited and patterned on the top of the aluminum nitride layer acts as top electrode of the piezoelectric layer (the bottom electrode is represented by the 10μm thick silicon layer) and electrical routing layer. A 0.2μm thick silicon dioxide layer is used as electrical isolating layer. Further details about process flow and design rules are described in [**77**]. In **Errore. L'origine riferimento non è stata trovata.** a picture of a PiezoMUMPS® process die with several linear and nonlinear devices is shown; the die has been designed at the Nanotechlab of the University of Catania (Italy)
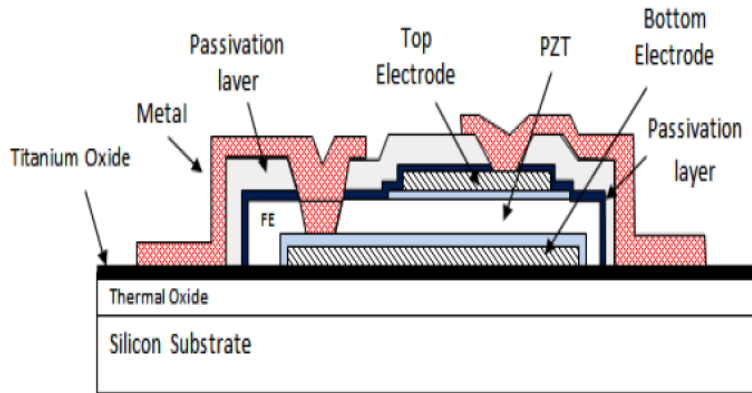
Fig. 92 - Schematic representation of the RTI 5µ® process
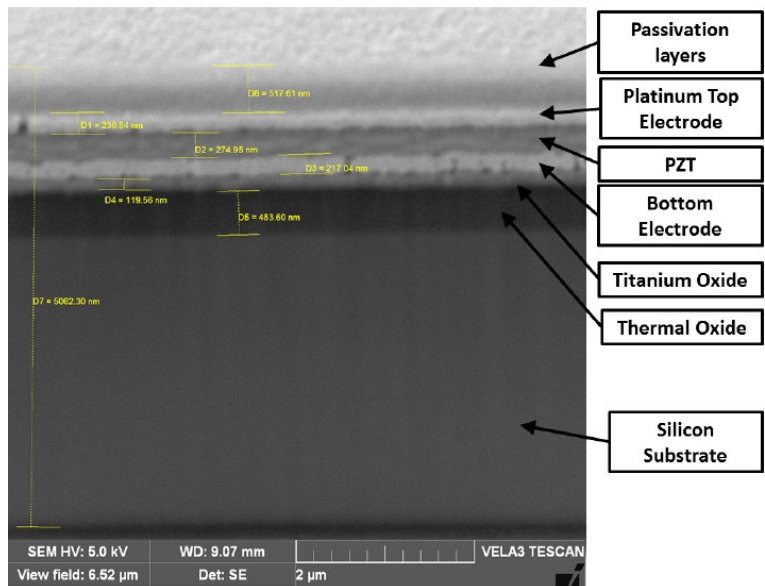
Fig. 93 - SEM picture of a RTI 5µ® process.

178

4.2. Radiant pMEMs® process

Radiant is an American company specialized in the fabrication of integrated ferroelectric devices. Radiant has developed a specific fabrication process named "RTI 5μ®" in order to fabricate integrated ferroelectric capacitors. In RTI 5μ® a thin film (about 250 nm) of Lead Titanate Zirconate (PZT) as dielectric material, has been placed between two platinum layers (each one of about 150 nm of thickness), as electrodes [78]. The silicon substrate has been electrically and thermally isolated from the piezoelectric stack described above by using a 500 nm thick silicon dioxide layer. Furthermore, a very thin (about 40 nm) buffer layer like titanium oxide has been used between oxide and piezoelectric stack in order to encourage their adhesion. A passivation layer has been employed on the top of the piezoelectric stack to protect the device instead, metal pads for electrical interconnections have been implemented by using an alloy of chromium and gold. In Fig. 92 and Fig. 93 a schematic representation of the RTI 5μ® process cross section and a SEM picture are respectively shown.

In this work, the ferroelectric capacitors just described have been used for rapid prototyping of piezoelectric cantilevers, thanks to the presence of the PZT layer and the electrodes. Rapid prototyping has been carried out by using a focused ion beam (FIB) lithography based approach. An example of realized device is shown in Fig. 94 and

Fig. 95: it has been fabricated by using the Tescan Vela3 SEM-FIB of the Nanotechlab of Catania (Italy).

SEM HV: 30.0 kV	WD: 8.81 mm		VELA3 TESCAN
View field: 166 µm	Det: SE	50 µm	
Felice Maiorca	Date(m/d/y): 09/25/13		
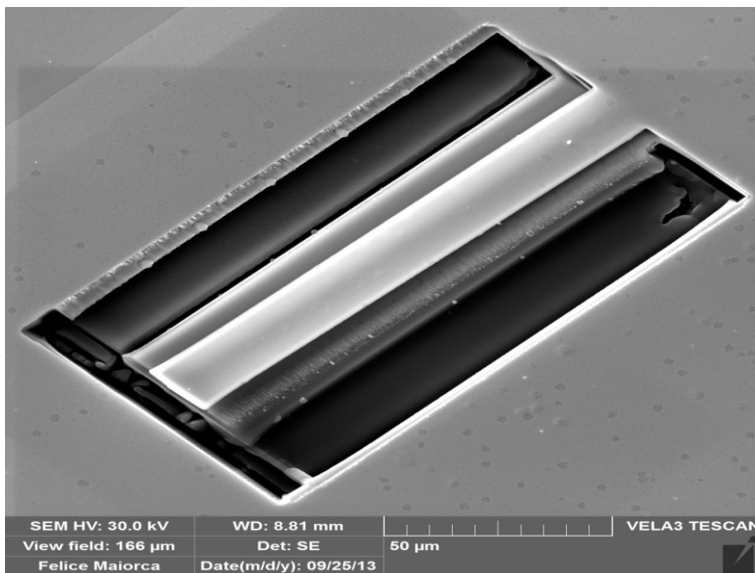
Fig. 94 - Cantilever beam fabricated by using the Tescan Vela3 SEM-FIB of the Nanotechlab of Catania (picture 1).

SEM HV: 30.0 kV	WD: 9.00 mm		VELA3 TESCAN
View field: 168 µm	Det: SE	50 µm	
Felice Maiorca	Date(m/d/y): 09/25/13		
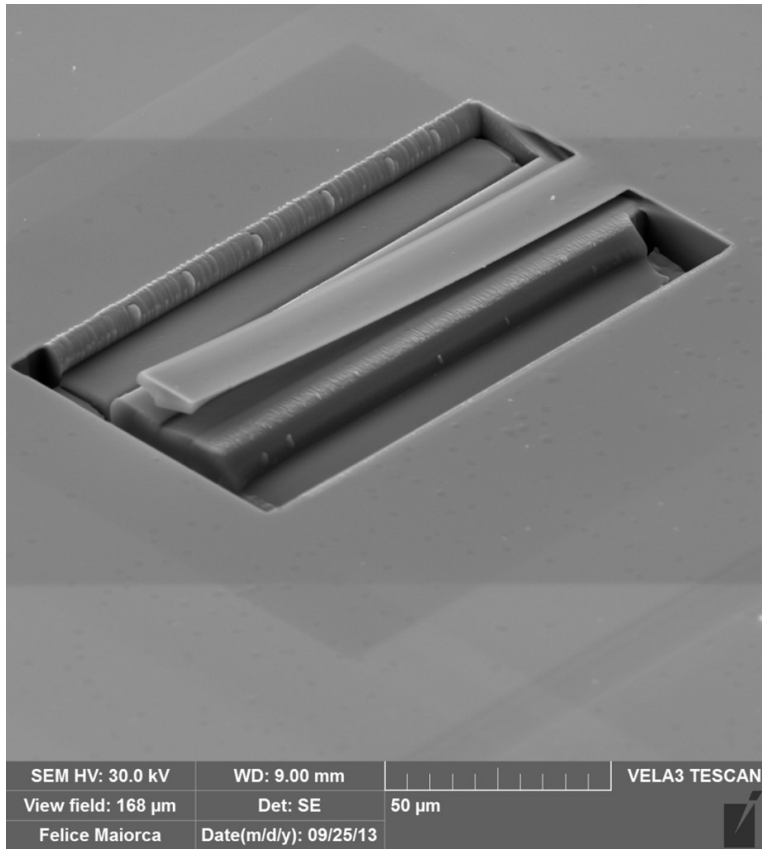
Fig. 95 - Cantilever beam fabricated by using the Tescan Vela3 SEM-FIB of the Nanotechlab of Catania (picture 2).

Conclusions and future trends

The most important results of three years of research activity have been described in this work. Environmental vibration energy harvesting has been the main focus of all the activities and innovative strategies have been developed to recover energy with very good results.

Nonlinear oscillating systems and piezoelectric transducers have been widely investigated and employed, in order to transform the kinetic energy in electric, maximizing the energy harvested.

The "magnetically coupled cantilevers with antiphase bistable behavior for kinetic energy harvesting" has been the starting point; once consolidated, the working principle has been extended to the "multiple nonlinear oscillators". The "two dimensional bistable vibration energy harvester" has been successfully developed in order to investigate the possibility to harvest energy coming from any direction, while the goal of the "tristable system" has been to study the possibility of reducing the potential barrier to be

overcome in order to encourage the cantilevers' switching mechanisms.

In order to rectifying, multiplying and, in general, managing the piezoelectric output voltages coming from vibration energy harvesters, mechanical switches have been introduced. In this way, diodes have been successfully replaced by "vibration driven mechanical switches" in order to avoid issues related to the voltage threshold.

The H-Bridge device, described in this work, have represented an interesting example of bistable, mechanical switches based, voltage rectifiers, while the AC-DC and the DC-DC converters have also achieved the goal of the voltage multiplication.

Macro scale prototypes of all the devices mentioned above have been designed, fabricated and tested. Simulations and experiments have been compared with excellent results.

MEMS technologies, PiezoMUMPS and Radiant, have been taken into account in order to investigate the

possibility to fabricate micro scale devices; very simple laboratory prototype have been fabricated with very encouraging results.

The fabrication of the most of the device described in this work in micro scale will be surely an intriguing future trend.

Activities during Ph.D. Course

Training

- In 2014 I attended the LTC - Electron beam Lithography Training Course.

  The main goal of this course was to learn about the basics of electron beam lithography. In particular, during the training course I was teached about both theoretical and practice notions of electron beam lithography. The Raith GmbH eLine plus has been used as working station during the practical sessions. I successfully attended the course in Dortmund (Germany) at the headquarters of Raith GmbH, and I obtained the relative certification.

- In 2014 I attended about 90 hours of lectures regarding micro and nano systems analysis, fabrication technologies, materials (chemical and physical behaviors) .

- In 2014 I attended about 20 hours of lecture held by Ing. Florinda Schembri about microfluidics.

- In 2014 I attended the following seminars held by Prof. Philipp Hoevel (Technical University of Berlin):

  o "Chimera states in systems of nonlocally coupled oscillators - Part I Theory"

  o "Chimera states in systems of nonlocally coupled oscillators - Part II Experiments"

- In 2014 I attended 10 hours of lessons held by Prof. Skandar Basrour (INPG, Grenoble) about PiezoMEMS and biosensors.

- In 2014 I attended the following seminar held by Prof. Seeram Ramakrishna (Centre for Nanofibers & Nanotechnology, National University of Singapore):

  o "Functional Nanomaterials by Electrospinning & Electrospraying"

- In 2014 I attended the following seminar held by Dott. Dario Motta:

  o "Full-scale investigation of sail pressure and shapes to understand how they produce forces"

- In 2013 I attended the Ph.D. summer school "Italo Gorini" organized by "Gruppo Misure Elettriche ed Elettroniche (GMEE)" and "Gruppo Misure Meccaniche e Termiche (GMMT)". The school was held in Padova, Italy.

- In 2013 I attended the "XXX Congresso Nazionale Gruppo Misure Elettriche ed Elettroniche" in Trento, Italy.

-

List of publications

[1] B. Ando, S. Baglio, A. Beninato, F. Maiorca, C. Trigona, *"“Vibration driven” mechanical switches: A novel transduction methodology with applications to DC-DC “diode-less” voltage multipliers"*, 2015 IEEE International Instrumentation and Measurement Technology Conference (I2MTC), 1779-1782, IEEE, 2015.

[2] C. Trigona, A. Algozino, F. Maiorca, B. Andò, S. Baglio, *"Design and Characterization of PiezoMUMPs Microsensors with Applications to Environmental Monitoring of Aromatic Compounds via Selective Supramolecular Receptors"*, Procedia Engineering 87, 1190-1193, Elsevier, 2015.

[3] F. Maiorca, F. Giusa, C. Trigona, B. Andò, S. Baglio, S. Graziani, *"H-Bridge: vibration energy harvester e raddrizzatore meccanico a soglia zero"*, GMEE 2014, Ancona.

[4] F. Giusa, F. Maiorca, A. Noto, C. Trigona, B. Andò, S. Baglio, *"A diode-less mechanical voltage*

multiplier: A novel transducer for vibration energy harvesting"*, Sensors and Actuators A: Physical 212, 34-41, Elsevier, 2014.

[5] C. Trigona, F. Maiorca, F. Giusa, A. Noto, B. Ando, S. Baglio, *" Performance characterization of different nonlinear-transduction mechanisms for piezoelectric energy harvesting"*, 2014 IEEE International Instrumentation and Measurement Technology Conference (I2MTC) Proceedings, 1148-1151, IEEE, 2014.

[6] C. Trigona, F. Giusa, F. Maiorca, A. Noto, B. Ando, S. Baglio, *" Anti-phase coupled bistable transducers: A review of recent progress"*, Sensors Applications Symposium (SAS), 166-169, IEEE, 2014.

[7] B. Andò, S. Baglio, F. Maiorca, C. Trigona, *"Analysis of two dimensional, wide-band, bistable vibration energy harvester "*, Sensors and Actuators A: Physical 202, 176-182, Elsevier, 2013.

[8] F. Maiorca, F. Giusa, C. Trigona, B. Andò, A.R. Bulsara, S, Baglio, *" Diode-less mechanical H-bridge rectifier for "zero threshold" vibration energy*

harvesters", Sensors and Actuators A: Physical 201, 246-253, Elsevier, 2013.

[9] C. Trigona, F. Maiorca, B. Andò, S. Baglio, *" Tristable behavior in mechanical oscillators to improve the performance of vibration energy harvesters"*, 2013 Transducers & Eurosensors XXVII: The 17th International Conference on, 458-461, IEEE, 2013.

[10] B. Andò, S. Baglio, F. Maiorca, C. Trigona, *" Multiple nonlinear oscillators for autonomous Wireless Sensor Nodes"*, Instrumentation and Measurement Technology Conference (I2MTC), 2013 IEEE International, 1311-1314, IEEE, 2013.

[11] B. Andò, S. Baglio, G. L'Episcopo, F. Maiorca, C. Trigona, *" Autonomous bistable microsensors for noninvasive AC electrical current measurements"*, Instrumentation and Measurement Technology Conference (I2MTC), 2013 IEEE International, 93-97, IEEE, 2013.

[12] B. Andò, S. Baglio, F. Giusa, S. Graziani, F. Maiorca, C. Trigona, *"Studio e caratterizzazione di sistemi*

bistabili accoppiati per recupero di energetico da vibrazioni ambientali", GMEE 2013, Trento.

[13] B. Andò, S. Baglio, G. L'Episcopo, F. Maiorca, C. Trigona, *"Un sensore autonomo e bistabile per la misura non invasiva di correnti elettriche alternate"*, GMEE 2013, Trento.

[14] B. Andò, S. Baglio, L. Latorre, F. Maiorca, P. Nouet, C. Trigona, *"Magnetically-coupled cantilevers with antiphase bistable behavior for kinetic energy harvesting"*, Procedia Engineering 47, 1065-1068, Elsevier, 2012.

[15] B. Andó, S. Baglio, F. Maiorca, C. Trigona, *" Two dimensional bistable vibration energy harvester"*, Procedia Engineering 47, 1061-1064, Elsevier, 2012.

[16] S. Baglio, C. Trigona, B. Andò, F. Maiorca, G. L'Episcopo, A. Beninato, *" Energy Harvesting from weak random vibrations: Bistable strategies and architectures for MEMS devices"*, Circuits and Systems (MWSCAS) 2012 IEEE 55th International Midwest Symposium on, 154-157, IEEE, 2012.

References

[1] Kelly N.A. and Gibson T.L., "Increasing the solar photovoltaic energy capture onsunny and cloudy days," *Solar Energy*, vol. 85, pp. 111-125, 2011.

[2] T. Ackermann, "Wind Power in Power Systems, 2nd ed.," 2012.

[3] Thiam A.G. and Pierce A.D., "Electromechanical transduction system design for optimal energy harvesting from ocean waves," *Journal of the Acoustical Society of America*, vol. 130, no. 2504, 2011.

[4] Monfray S. et al., "Innovative thermal energy harvesting for zero power electronics," *Proceedings of Silicon Nanoelectronics Workshop*, pp. 1-4, 2012.

[5] Buratti C., Martalò M., Verdone R., and Ferrari G., "Sensor Networks with IEEE 802.15.4 Systems," *Springer*, pp. 3-28, 2011.

[6] Oudenhoven J.F.M., Vullers R.J.M., and Van Schaijk R., "A review of the present situation and future developments of micro-batteries for wireless autonomous sensor systems," *Int. J. of Energy*

Research, vol. 36, pp. 1139–1150, 2012.

[7] Silva A., Liu M., and Moghaddam M., "Power-Management Techniques for Wireless Sensor Networks and Similar Low-Power Communication Devices Based on Nonrechargeable Batteries," *Journal of Computer Networks and Comm.*, pp. 1-10, 2012.

[8] Wang J. and Gao W., "Nano/Microscale Motors: Biomedical Opportunities and Challenges," *ACS nano*, 2012.

[9] Song W., Yu H., Liang Ce., and Wang Q., "Body monitoring system design based on android smartphone," *Information and Communication Technologies (WICT), 2012 World Congress on*, pp. 1147-1151, 2012.

[10] Khan T.H. and A Wahi K., "An advanced physiological data logger for medical imaging applications," *Journal on Embedded Systems*, vol. 10, 2012.

[11] Letcher T.M. and Vallero D., *Waste: A Handbook for Management*.: Academic Press, 2011.

[12] Harb A., "Energy harvesting: state-of-the-art," *Renewable Energy*, vol. 36, pp. 2641–2654, 2011.

[13] Renno J., Daqaq M.F., and Inman D.J., "On the optimal energy harvesting from a vibration source," *Journal of Sound and Vibration*, vol. 320, pp. 386-405, 2009.

[14] Fauzi Bin M., Rahman A., and Leong K.S., "Investigation of useful ambient vibration sources for the application of energy harvesting," *Proceedings of Student Conference on Research and Development,* pp. 391–396, 2011.

[15] Thomson W., "Theory of vibration with applications ," *Taylor & Francis*, 2004.

[16] Naruse Y., Matsubara N., Mabuchi K., Izumi M., and Suzuki S., "Electrostatic micro power generation from low-frequency vibration such as human motion," *Journal of Micromechanics and Microengineering*, vol. 19, pp. 1-5, 2009.

[17] Zorlu Ö., Topal E.T., and Külah H., "A vibration-based electromagnetic energy harvester using mechanical frequency up-conversion method," *IEEE Sensor Journal*, vol. 11, pp. 481-488, 2011.

[18] A. Erturk and D.J. Inman, *Piezoelectric Energy Harvesting*.: John Wiley & Sons, Ltd., Pubblication, 2011.

[19] Meninger S., Mur-Miranda J.O., Amirtharajah R., Chandrakasan A., and Lang J., "Vibration-to-electric energy conversion," *proceedings of the 1999 international symposium on Low power electronics and design*, p. 53, 1999.

[20] S.M. Shahruz, "Design of mechanical band-pass filters for energy scavenging," *Journal of Sound and Vibration*, vol. 292, no. 3-5, pp. 987–998, 2006.

[21] Roundy S., Leland E.S., Baker J., and Carleton E., "Improving power output for vibration-based energy scavengers," *IEEE Pervasive Computing*, vol. 4, no. 1, pp. 28-36, 2005.

[22] Anton S.R. and Sodano H.A., "A review of power harvesting using piezoelectric materials," *Smart Materials and Structures*, vol. 16, no. 3, 2007.

[23] Roundy S. and Zhang Y., "Toward self-tuning adaptive vibration-based microgenerators," *Proceedings of SPIE*, vol. 5649, p. 373, 2005.

[24] Mossi K., Green C., Ounaies Z., and Hughes E., "Harvesting Energy Using a Thin Unimorph Prestressed Bender: Geometrical Effects," *Journal of Intelligent Material Systems and Structures*, vol. 16, no. 3, pp. 246-261, 2005.

[25] Tadesse Y., Zhang S., and Prya S., "Multimodal Energy Harvesting System: Piezoelectric and Electromagnetic," *Journal of Intelligent Material Systems and Structures*, vol. 20, no. 5, pp. 625-632, 2009.

[26] Opdahl P.G., Jensen B.D., and Howell L.L., "AN INVESTIGATION INTO COMPLIANT BISTABLE MECHANISMS," *Proceedings of DETC'98*, 1998.

[27] Bulsara A.R. and L. Gammaitoni, "Tuning in to noise," *Physycs Today*, vol. 49, no. 3, p. 39, 1996.

[28] Gammaitoni L. and A.R. Bulsara, "Noise Activated Nonlinear Dynamic Sensors," *Phys. Rev. Lett.*, vol. 88, no. 23, 2002.

[29] M. Ferrari et al., "Improved energy harvesting from wideband vibrations by nonlinear piezoelectric converters," *Sensors and Actuators A: Physical*, vol. 162, no. 2, pp. 425-431, 2010.

[30] B. Andò et al., "Nonlinear mechanism in MEMS devices for energy harvesting applications," *Journal of Micromechanics and Microengineering*, vol. 20, no. 12, p. 125020(12), 2010.

[31] Prya S. and Inman D.J., "Energy Harvesting Technologies," *Springer*, 2008.

[32] F. Cottone, H. Vocca, and L. Gammaitoni, "Nonlinear energy harvesting," *Phys. Rev. Lett.*, vol. 102, no. 8, p. 080601(4), 2009.

[33] Andò B. et al., "Nonlinear behaviour of a micromachined SOI device for energy harvesting application," *Proc. of DTIP*, 2010.

[34] Trigona C. et al., "Exploiting Benefits of a Periodically-Forced Nonlinear Oscillator for Energy Harvesting from Ambient Vibrations," *Proc. of Eurosensors 2011*, pp. 1-4, 2011.

[35] Vullers R.J.M., Schaijk R., Visser H.J., Penders J., and Van Hoof C., "Energy Harvesting for Autonomous Wireless Sensor Networks," *IEEE Solid-State Circuits Magazine*, pp. 29-38, 2010.

[36] Zivanovic S., Pavic A., and Reynolds P., "Probability-based prediction of multi-mode

vibration response to walking excitation," *Engineering Structures*, vol. 29, no. 6, pp. 942-954, 207.

[37] Andò. B. et al., "Magnetically-Coupled Cantilevers with Antiphase Bistable Behavior for Kinetic Energy Harvesting," *Procedia Engineering*, vol. 47, pp. 1065-1068, 2012.

[38] Andò B., Baglio S., Maiorca F., and Trigona C., "Multiple nonlinear oscillators for autonomous Wireless Sensor Nodes," *Instrumentation and Measurement Technology Conference (I2MTC)*, pp. 1311-1314, 2013.

[39] Bartsch U., Gaspar J., and Paul O., "Low-frequency two-dimensional resonators forvibrational micro energy harvesting," *Journal of Micromechanics and Micro-engineering*, vol. 20, 2010.

[40] Zhu Y., Moheimani S.O.R., and Yuce M.R., "A 2-DOF wideband electrostatic trans-ducer for energy harvesting and implantable applications," *IEEE Sensors Conference*, pp. 1542-1545, 2009.

[41] Park J.C. and Park J.Y., "A two-dimensional vibration energy harvester usingan piezoelectric

bimorph cantilever with an asymmeteric inertial mass," *Proceedings of Power MEMS*, pp. 281-284, 2011.

[42] Andò B., Baglio S., L'Episcopo G., and Trigona C., "Investigation on mechanicallybistable MEMS devices for energy harvesting from vibrations," *IEEE Journal ofMicroelectromechanical Systems*, vol. 21, pp. 779-790, 2010.

[43] Ferrari M. et al., "Improvedenergy harvesting from wideband vibrations by nonlinear piezoelectric converters," *Procedia Chemistry*, vol. 1, no. 1, pp. 1203-1206, 2009.

[44] Vandemeer J.E., Kranz M.S., and Fedder G.K., "Nodal simulation of suspended MEMSwith multiple degrees of freedom," *DSC*, vol. 354, pp. 1-7, 1997.

[45] Lagarias J.C., Reeds J.A., Wright M.H., and Wright P.E., "Convergence properties of theNelder–Mead simplex method in low dimensions," *Journal on Optimization*, vol. 9, pp. 112-147, 1998.

[46] Andò B. et al., "A BE-SOIMEMS for inertial measurement in geophysical applications," *IEEE Transactionson Instrumentation & Measurement*,

vol. 99, pp. 1-8, 2011.

[47] Calvo M., J.I. Montijano, and Randez L., "A fifth-order interpolant for the Dormandand Prince Runge–Kutta method," *Journal of Computational and Applied Mathematics*, vol. 29, pp. 91-100, 1990.

[48] Okamoto S., "Experimental Study of Flow-Induced Vibrations and Scatteringof Roof Tiles by Wind Tunnel Testing," *InTech, Available from: http://www.intechopen.com/books/wind-tunnels/experimental-study-of-flow-induced-vibrations-and-scattering-of-roof-tiles-by-wind-tunnel-testing*, 2011.

[49] Priya S. and Inman D.J., "Energy Harvesting Technologies," *Springer Science*, 2010.

[50] S.P. Beepy, M.J. Tudor, and N.M. White, "Energy harvesting vibration sources for microsystems applications," *Measurement Science and Technology*, vol. 17, no. 12, pp. 175-195, 2006.

[51] M. Rahman and K. Leong, "Investigation of useful ambient vibration sources forthe application of energy harvesting," *IEEE Student Conference on Researchand Development*, 2011.

[52] I. Neri et al., "A real vibration database for kinetic energy harvesting application," *Journal of Intelligent Material System and Structures*, vol. 23, no. 18, pp. 2095-2101, 2012.

[53] N.A. Khovanova and I.A. Khokanova, "The role of excitations statistic and nonlinearity in energy harvesting from random impulsive excitations," *Applied Physycs Letters*, vol. 99, no. 14, pp. 144101-144103, 2011.

[54] M. Ferrari, M. Baù, M. Guizzetti, and V. Ferrari, "A single-magnet nonlinear piezoelec-tric converter for enhanced energy harvesting from random vibrations," *Sensorsand Actuators A: Physical* , vol. 172, no. 1, pp. 287-292., 2011.

[55] A. Tabesh and L. Fréchette, "A low-power stand-alone adaptive circuit for harvesting energy from a piezoelectric micropower generato," *IEEE Transaction onIndustrial Electronics* , vol. 57 , no. 3, pp. 840-849, 2010.

[56] D. Marinkovic, A. Frey, I. Kuehne, and G. Scholl, "A new rectifier and trigger circuit fora piezoelectric microgenerator," *Procedia Chemistry*, vol. 1, no. 1, pp. 1447-1450, 2009.

201

[57] J. Quiu, H. Jiang, H. Ji, and K. Zhu, "Comparison between four piezoelectric energyharvesting circuits," *Frontiers of Mechanical Engineering in China*, vol. 4, no. 2, pp. 153-159, 2009.

[58] M. Sarker, S. Ali, M. Othman, and M. Islam, "Designing a low voltage energy harvesting circuits for rectified storage voltage using vibrating piezoelectric," *IEEEStudent Conference on Research and Development*, 2011.

[59] S. Cheng, Y. Jin, Y. Rao, and D. Arnold, "A bridge voltage doubler ad/dc converter forlow-voltage energy harvesting applications," *Proceedings of PowerMEMS*, 2009.

[60] J. Handwerker, D. Maurath, Y. Manoli C. Peters, "A sub-500 mV highly efficientactive rectifier for energy harvesting applications," *IEEE Transaction on Circuitsand Systems*, vol. 58, no. 7, pp. 1542-1550, 2011.

[61] Y. Lam, W. Ki, and C. Tsui, "Integrated low-loss CMOS active rectifier for wirelesslypowered devices," *IEEE Transaction on Circuits and Systems* , vol. 53, no. 12, pp. 1378-1382, 2006.

[62] T. Lehmann and Y. Moghe, "On-chip active power rectifiers for biomedical appli-cations," *IEEE International Symposium on Circuits and Systems*, 2005.

[63] Lee et al., "Deformable carbon nanotube-contact pads for inertial microswitch to extend contact time, ," *IEEE Transactionson Industrial Electronics*, vol. 59, no. 12, pp. 4914-4920, 2012.

[64] G. Stemme, J. Oberhammer, "Passive contact force and active opening force elec-trostatic switches for soft metal contact materials," *19th IEEE InternationalConference on Micro Electro Mechanical Systems*, 2006.

[65] H. Kai et al., "Design, simulation and fabrication of a novel contact-enhanced MEMS inertial switch with a movablecontact point," *Journal of Micromechanics and Microengineering* , vol. 18, no. 11, 2008.

[66] S. Nagasawa, T. Suzuky, Y. Takayama, K. Tsuji, and H. Kuwano, "Mechanical rectifierfor microelectric generators ," *IEEE 21st International Conference on MicroElectro Mechanical Systems*, 2008.

[67] K. Tsuji, H. Okamoto, S. Nagasawa, and H. Kuwano,

"Rectifier of vibration-drivenmicro energy harvesting system," *PowerMEMS*, 201.

[68] F. Giusa et al., ""'Random Mechan-ical Switching Harvesting on Inductor": a novel approach to collect and storeenergy from weak random vibrations with zero voltage threshold," *Sensor and Actuators* , vol. 198, 2013.

[69] B Andò, S Baglio, F Maiorca, and C Trigona, "Analysis of two dimensional, wide-band, bistable vibration energy harvester," *Sensors and Actuators A: Physical*, vol. 202, pp. 176 - 182, 2013.

[70] William Riley, Leroy Sturges, and Don Morris, *Mechanics of Materials, 6th Edition*.: Wiley, 2006.

[71] C. Gardiner, "Handbook of Stochastic Methods," *Springer Verlag*, 1983.

[72] B. Andò, S. Baglio, F. Maiorca, and C. Trigona, "Tri-stable behaviour in mechanical oscillators to improve the performance of vibration energy harvesters," *Proceedings of Transducers* , 2013.

[73] Xudong Wang, "Piezoelectric nanogenerators - Harvesting ambient mechanical energy at the nanometer scale," *Elsevier, Nano Energy*, vol. 1, no.

1, pp. 13-24, 2012.

[74] T.J. Lin, J.F. Chen, and Y.P. Hsieh, "A novel high step-up DC-DC converterwith coupled-inductor," *1st International Future Energy Electronics Conference (IFEEC)*, pp. 777-782, 2013.

[75] A.I. Bratcu, I. Munteanu, S. Bacha, D. Picault, and B. Raison, "Cascaded dc–dc converter photovoltaic systems: Power optimization issues," *IEEE Transactions on Industrial Electronics*, vol. 58, pp. 403-411, 2011.

[76] F. Giusa et al., "A diodeless mechanical voltage multiplier: A novel transducer for vibration energy harvesting," *Sensors and Actuators A: Physical*, vol. 212, pp. 34-41, 2014.

[77] A. Cowen, G. Hames, K. Glukh, and B. Hardy. (2014) PiezoMUMPs Design Handbook. [Online]. http://www.memscap.com/__data/assets/pdf_file/0020/5915/PiezoMUMPs.DR.1.3a.pdf

[78] B. Andò, S. Baglio, A.R. Bulsara, V. Marletta, and N. Savalli, "E-field ferroelectric sensors: Modeling and simulation [Instrumentation Notes]," *Instrumentation & Measurement Magazine, IEEE*, vol. 12, no. 2, pp.

31-37, 2009.